Constitutive Parameters of Metamaterial Structures
Used for Invisible Cloak Realization

Zvonimir Sipus
Dario Bojanjac
Marko Bosiljevac

**Fakultet Elektrotechnike I
Racunarstva
Unska 3
Zagreb 10000
Croatia**

Report Date: October 2013

Final Report for 18 July 2012 to 17 July 2013

**Air Force Research Laboratory
Air Force Office of Scientific Research
European Office of Aerospace Research and Development
Unit 4515 Box 14, APO AE 09421**

REPORT DOCUMENTATION PAGE

1. REPORT DATE *(DD-MM-YYYY)* 13 October 2013	2. REPORT TYPE Final Report	3. DATES COVERED *(From – To)* 18 July 2012-17 July 2013

4. TITLE AND SUBTITLE	5a. CONTRACT NUMBER
Constitutive Parameters of Metamaterial Structures Used for Invisible Cloak Realization	FA8655-12-1-2080
	5b. GRANT NUMBER
	Grant 12-2080
	5c. PROGRAM ELEMENT NUMBER
	61102F

6. AUTHOR(S)	5d. PROJECT NUMBER
Zvonimir Sipus Dario Bojanjac Marko Bosiljevac	
	5d. TASK NUMBER
	5e. WORK UNIT NUMBER

7. PERFORMING ORGANIZATION NAME(S) AND ADDRESS(ES) Fakultet Elektrotechnike I Racunarstva Unska 3 Zagreb 10000 Croatia	8. PERFORMING ORGANIZATION REPORT NUMBER N/A

9. SPONSORING/MONITORING AGENCY NAME(S) AND ADDRESS(ES) EOARD Unit 4515 BOX 14 APO AE 09421	10. SPONSOR/MONITOR'S ACRONYM(S) AFRL/AFOSR/IOE (EOARD)
	11. SPONSOR/MONITOR'S REPORT NUMBER(S) **AFRL-AFOSR-UK-TR-2013-0045**

12. DISTRIBUTION/AVAILABILITY STATEMENT

Distribution A: Approved for public release; distribution is unlimited.

13. SUPPLEMENTARY NOTES

14. ABSTRACT

The realization of structures that do not scatter electromagnetic fields ("cloaking devices") has been envisioned since the 1960s; recent advances in metamaterial research has shifted cloaking possibilities to this new field through transformation optics, creating a shell which effectively cloaks the space inside the shell by diverting EM radiation around it. The author finds such a cloak unfeasible in practice but investigates a simplified cloak design for one specific polarization of incident plane waves in an effort to improve the scattering properties of the realized cloaks. The proposed procedure attempts to characterize a planar structure, examine its realization using planar metamaterials, and then attempt to curve the metamaterials to obtain the desired geometry. The research proposes to develop this method, estimate parameters of planar multilayer periodic structures, and then estimate parameters of curved multilayer periodic structures.
The main realized outcomes of the project are that the investigators proposed a four-step procedure to design metamaterial structures, investigated procedures to extract constitutive parameters of cloaks, showed design examples of structures containing different types of periodic-cell elements, and developed algorithms/programs for characterizing metamaterial structures including extensions of algorithms which calculate Green's functions of anisotropic multilayer structures.

15. SUBJECT TERMS

EOARD, Metamaterials, Invisible Cloak Realization

16. SECURITY CLASSIFICATION OF:			17. LIMITATION OF ABSTRACT	18, NUMBER OF PAGES	19a. NAME OF RESPONSIBLE PERSON Victor Putz
a. REPORT UNCLAS	b. ABSTRACT UNCLAS	c. THIS PAGE UNCLAS	SAR	83	19b. TELEPHONE NUMBER *(Include area code)* +44 (0)1895 616013

FINAL REPORT FOR CONTRACT **FA8655-12-1-2080**

Constitutive Parameters of Metamaterial Structures Used for Invisible Cloak Realization

by

Zvonimir Sipus
Dario Bojanjac
Marko Bosiljevac

SUBMITTED BY: Prof. Zvonimir Sipus
Faculty of Electrical Engineering and Computing
University of Zagreb
Unska 3
Zagreb, HR-10000, Croatia

13 October 2013

TABLE OF CONTENTS

1   INTRODUCTION

Introduction

The realization of structures that do not scatter electromagnetic field, i.e. structures that appear invisible to EM waves, is a concept that has been investigated theoretically since the 1960s when the possibility of a plane wave passing without distortions through a structure with anisotropic filling was investigated [1]. Hard surfaces have been used in the design of supporting struts of reflector antenna feeds, i.e. it was experimentally demonstrated that it is possible to considerably reduce the scattered field for one angle of incidence and for both polarizations of the incident wave [2]. In [3]-[6] it was shown that the scattered field of a two-layer dielectric ellipsoid is zero for certain combinations of permittivities. To obtain that at least one of the layers should have relative permittivity smaller than one (i.e. local negative polarizability, which is inherent to plasmonic materials and plasma-like ENG metamaterials). Several other concepts for obtaining invisible scatterers were proposed, like minimum scattering antennas and active scatterers ([7], [8]).

The focus has recently shifted to the possibility of cloaking objects using a metamaterial cover ([8]-[15]). The main principle of metamaterial cloaking approach arises from coordinate transformations which transform the volume (in particular, cylindrical one) into a shell (cloak), making the space inside the shell concealed. The required cloak material is fully anisotropic and, in addition, the constitutive parameters (tensors ε and μ) are functions of radial coordinate. Such cloak design is not feasible in practice, however the simplified cloak designs were proposed in [16] and [17] which claim to work for one specific polarization of the incident plane wave (TM_z and TE_z polarizations, respectively). These specific cloaks benefit from simplifications of constitutive parameters, since only radial component of permeability [16] or permittivity [17] needs to have radial variation, which is obtainable by using split-ring resonators or metal wires in dielectric host, respectively.

Experimental results ([16], [19] and [20]) reveal that the measured scattered field was reduced compared to the object without a cloak (i.e. the cloak working principle was proved), however the level of scattered field was much larger compared to the desired one. The realized metamaterial structures were quite complicated, and the lack of "really good" experimental results has raised the question where are the problems – in the non-perfect general electromagnetic solver, in the non-perfect realization of a very complex structure, or in some hidden (physical) limitations that are not so obvious. Therefore, there is a need to understand the real essence of the problem.

The purpose of this report is to give a contribution to the design of metamaterial structures that will have good scattering properties. In doing so, we will avoid to simply press the button "optimization" in some electromagnetic solver. We will try to develop a procedure that will start with the physical picture of how our structure should look like (in the cloak case first design will be made through transformation optics), and in several steps we will arrive to the actual realization. It should be noted that it is extremely difficult to design curved periodic structures, i.e. it is much easier to design planar periodic structure (in this case, it is only necessary to design a unit cell). Therefore, the proposed procedure will first characterize an equivalent planar structure, its realization using planar metamaterials, and in the last step will include the effect of curving the metamaterials needed to obtain the desired geometry.

2   PROJECT OBJECTIVE AND REALIZED OUTCOMES

Project objective and realized outcomes

The work in the project has been divided in the following tasks:

- Development of the method - systematic approach for characterizing metamaterial structures. The method should use results of test cases calculated by a general electromagnetic solver, and the selected test cases will depend on the geometry of the considered structure. Two types of parameters will result from the analysis: (a) reflection and transmission coefficients of the considered structure, and (b) permeability and permittivity material tensors of the considered periodic structure (homogenization approach – needed for designing the first prototype where the desired constitutive parameters are determined by the program that can analyze multilayer anisotropic homogeneous structure). Furthermore, the rigorous full-wave parameters of the considered structure will be also determined.

- Estimation of parameters of planar multilayer periodic structures. The considered structures will be periodic in two dimensions, and it will have finite number of layers (all the layers will be the same). Two basic configurations will be investigated – configurations in free-space and configurations that are part of some transmission line (e.g. a planar or cylindrical waveguide). It will be discussed how the number of layers influences the constitutive parameters of the structure. Furthermore, it will be investigated is it possible to treat each layer separately, or is it necessary to analyze the whole structure (which is much more complex electromagnetic problem).

- Estimation of parameters of curved multilayer periodic structures. It will be investigated how the radius of curvature influences the constitutive parameters. In particular, the cylindrical waves will be analyzed in details.

The main realized outcomes of the project are:

- We have proposed the procedure for designing metamaterial structures. The procedure consists of four steps. In the first step a device is designed using some physical method (like transformation optics) and then it is realized using layers with homogeneous anisotropic materials. In the second step an equivalent planar multilayer structure is characterized using reflection & transmission coefficient method. In the third step a metamaterial periodic structure is designed (using some general

electromagnetic solver) which has the same scattering properties like multilayer homogeneous structure from the second step. In the last step the designed metamaterial structure is curved, and the curvature effects are taken into account using e.g. conformal mapping approach.

- We have investigated properties of different procedures for extracting effective constitutive parameters. It was shown that the method is quite accurate (and the extracted effective parameters quite useful in the design procedure) if the metamaterial elements are not resonant. However, for frequencies around resonant the structure becomes narrow-banded, and it is almost impossible to predict its behavior.

- We have made a detailed investigation of the procedure that connects the considered curved structure and the equivalent planar structure. It is shown that with the method based on conformal mapping it is possible to accurately predict the curvature effects. Furthermore, with the Bloch theory for cylindrical structures it is possible to efficiently analyze multilayer cylindrical periodic structures.

- We have given several design examples of metamaterial structures containing different types of periodic-cell elements. In all cases the results indicate that the proposed design procedure is quite accurate and enables fast design of the desired metamaterial structure.

- We have developed several algorithms and programs needed for characterization of metamaterial structures. First, we have developed an extension of the G1DMULT algorithm, which calculates Green's functions of planar, cylindrical and spherical multilayer structures, to calculate Green's functions of anisotropic multilayer structures as well. Theoretical formulation is given in the Appendix, and the algorithm was used in designing "ideal" metamaterial structures built from homogeneous anisotropic layers. Furthermore, we have developed moment-method based programs for analyzing planar and cylindrical periodic structures. Their description is also given in the Appendix.

We sincerely hope that this report will help researchers in understanding where are the critical points when designing metamaterial structures, and will result in an efficient and successful designing procedure.

3   DESIGN OF METAMATERIAL STRUCTURES

Design of metamaterial structures

3.1. EXAMPLE: CLOAK DESIGN USING TRANSFORMATION OPTICS

The possibility of cloaking objects using a metamaterial cover has extensively been studied in the last several years (see e.g. [9]-[15]). In the metamaterial cloak approach, material has been used to render a volume effectively invisible to incident radiation, i.e. to squeeze space from a volume into a shell surrounding the concealment volume. Coordinate transformations that are used for cloak design do not influence the form of Maxwell's equations, but they affect permittivity and permeability tensors ($\boldsymbol{\varepsilon}$ and $\boldsymbol{\mu}$, respectively), making the needed materials spatially varying and anisotropic. When viewed externally, the concealed volume and the cloak both appear to have the propagation properties of free space, i.e. they appear invisible to electromagnetic waves.
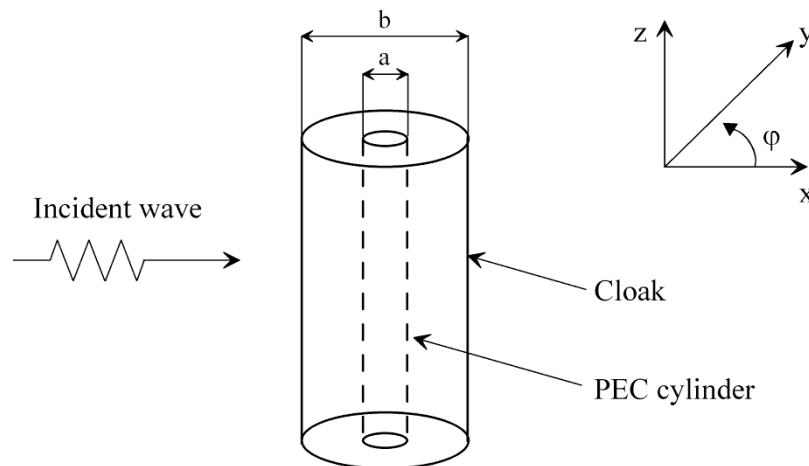
Figure 3.1. A sketch of the analyzed structure.

As an example we consider a circular-cylindrical cloak oriented with the axis in z-direction as shown in Fig. 3.1. The inner and outer radii of the cloak are denoted by a and b. The permeability and permittivity tensors in the cylindrical coordinate system are given with

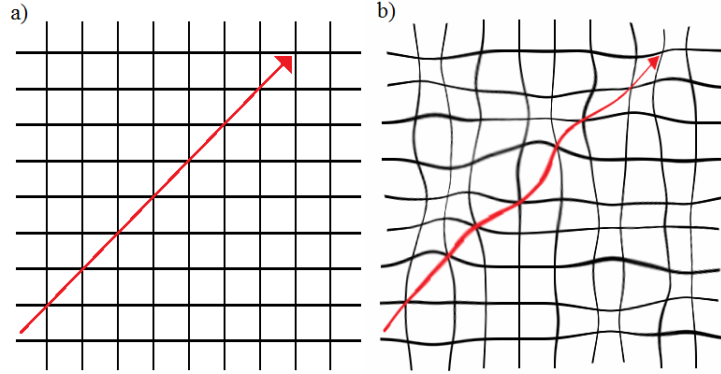$$\underline{\mu} = \mu_0 \begin{vmatrix} \mu_{\rho\rho} & 0 & 0 \\ 0 & \mu_{\phi\phi} & 0 \\ 0 & 0 & \mu_{zz} \end{vmatrix}, \tag{3.1}$$

$$\underline{\varepsilon} = \varepsilon_0 \begin{vmatrix} \varepsilon_{\rho\rho} & 0 & 0 \\ 0 & \varepsilon_{\phi\phi} & 0 \\ 0 & 0 & \varepsilon_{zz} \end{vmatrix}. \tag{3.2}$$

Figure 3.2. (a) a field line in free space with the Cartesian coordinate grid in the background, (b) the distorted field line with the background coordinates distorted in the same manner.

For the cloak design, a coordinate transformation which compresses free space from the cylindrical region $0 < r < b$ into the concentric cylindrical shell $a < r' < b$ is applied, where a and b represent the cloak inner and outer radius, respectively (the constitutive structure parameters are considered in the cylindrical coordinate system). Presuming that electromagnetically inhomogeneous metamaterials offer more freedom in design than regular materials found in nature, it is possible to imagine for electromagnetic fields to be controlled and redirected at will. The design of a cloaking structure is based on the transformation of space, i.e. the stretching and the pulling of a Cartesian coordinate system as shown in Figure 3.2. The Maxwell's equations are invariant under spatial transformations, i.e. they take the same form in the transformed coordinate system:

$$\nabla' \times \mathbf{E}' = -j\omega\mu' \mathbf{H}', \qquad \nabla' \times \mathbf{H}' = j\omega\varepsilon' \mathbf{E}' \tag{3.3}$$

The permeability and permittivity tensors $\boldsymbol{\mu}'$ and $\boldsymbol{\varepsilon}'$ are related to the tensors $\boldsymbol{\mu}$ and $\boldsymbol{\varepsilon}$ in the original space via equations:

$$\mu' = \frac{\mathbf{A}\mu\mathbf{A}^T}{\det \mathbf{A}}, \qquad \varepsilon' = \frac{\mathbf{A}\varepsilon\mathbf{A}^T}{\det \mathbf{A}}, \tag{3.4}$$

where A is the Jacobi matrix of the spatial transformation

$$\mathbf{A} = \begin{bmatrix} \partial x'/\partial x & \partial x'/\partial y & \partial x'/\partial z \\ \partial y'/\partial x & \partial y'/\partial y & \partial y'/\partial z \\ \partial z'/\partial x & \partial z'/\partial y & \partial z'/\partial z \end{bmatrix}. \tag{3.5}$$

In the considered case the circular annular cloak is obtained using the following transformation:

$$\rho' = a + \frac{b-a}{b}\rho, \qquad \phi' = \phi, \qquad z' = z, \tag{3.6}$$

and the Jacobi matrix is given by

$$\mathbf{A} = \begin{vmatrix} \dfrac{b-a}{b} & 0 & 0 \\ 0 & \dfrac{\rho'}{\rho} & 0 \\ 0 & 0 & 1 \end{vmatrix} = \begin{vmatrix} \dfrac{b-a}{b} & 0 & 0 \\ 0 & \dfrac{\rho'}{\rho'-a}\dfrac{b-a}{b} & 0 \\ 0 & 0 & 1 \end{vmatrix}. \tag{3.7}$$

This transformation allow us to design a 2D cylindrical electromagnetic invisibility cloak by compressing all the fields from the region $\rho < b$ into the region $a < \rho < b$ so that the permittivity and permeability of the medium located within the cloaking shell are free to take any value without contributing to electromagnetic scattering. For $a < \rho < b$ the permittivity and permeability values are [9]:

$$\varepsilon_{\rho\rho} = \mu_{\rho\rho} = \frac{\rho-a}{\rho}$$

$$\varepsilon_{\phi\phi} = \mu_{\phi\phi} = \frac{\rho}{\rho-a} \tag{3.8}$$

$$\varepsilon_{zz} = \mu_{zz} = \left(\frac{b}{b-a}\right)^2 \frac{\rho-a}{\rho}$$

Note that all components of the tensors are functions of radius, which implies a very complicated metamaterial design. Such a cloak is referred to as an ideal cloak that has not yet been realized. However, several cloak designs have been reported which claim to work properly when illuminated with a normal incident plane wave of specific polarization [16], [17], that is, with either the electric field or the magnetic field parallel to the z-axis (TM$_z$ polarization or TE$_z$ polarization, respectively).

The metamaterial cloak, designed by Schurig *et al.* [16], is intended for use with TM$_z$ polarization of the incident wave at microwave frequencies. It is clear that only ε_{zz}, $\mu_{\rho\rho}$ and $\mu_{\phi\phi}$ components are relevant in this case. Therefore, it is possible to vary the values of permeability and permittivity tensors as long as the products $\varepsilon_{zz}\cdot\mu_{\rho\rho}$ and $\varepsilon_{zz}\cdot\mu_{\phi\phi}$ are kept the same. A significantly simplified design can be achieved by fixing values of ε_{zz} and $\mu_{\phi\phi}$ (ε_{zz} is determined by supporting dielectric material and $\mu_{\phi\phi}$ is simply equal to 1), and letting only $\mu_{\rho\rho}$ to vary along the radial direction:

$$\mu_{\rho\rho} = \left(\frac{\rho-a}{\rho}\right)^2$$

$$\mu_{\phi\phi} = 1 \tag{3.9}$$

$$\varepsilon_{zz} = \left(\frac{b}{b-a}\right)^2$$

The metamaterial reported in [16] used the unit cell of approximately cubic shape, filled with one split-ring resonator. The realized cloak consisted of ten concentric cylinders, each of which was three unit cells tall (see Figure 3.3).

(a)   (b)
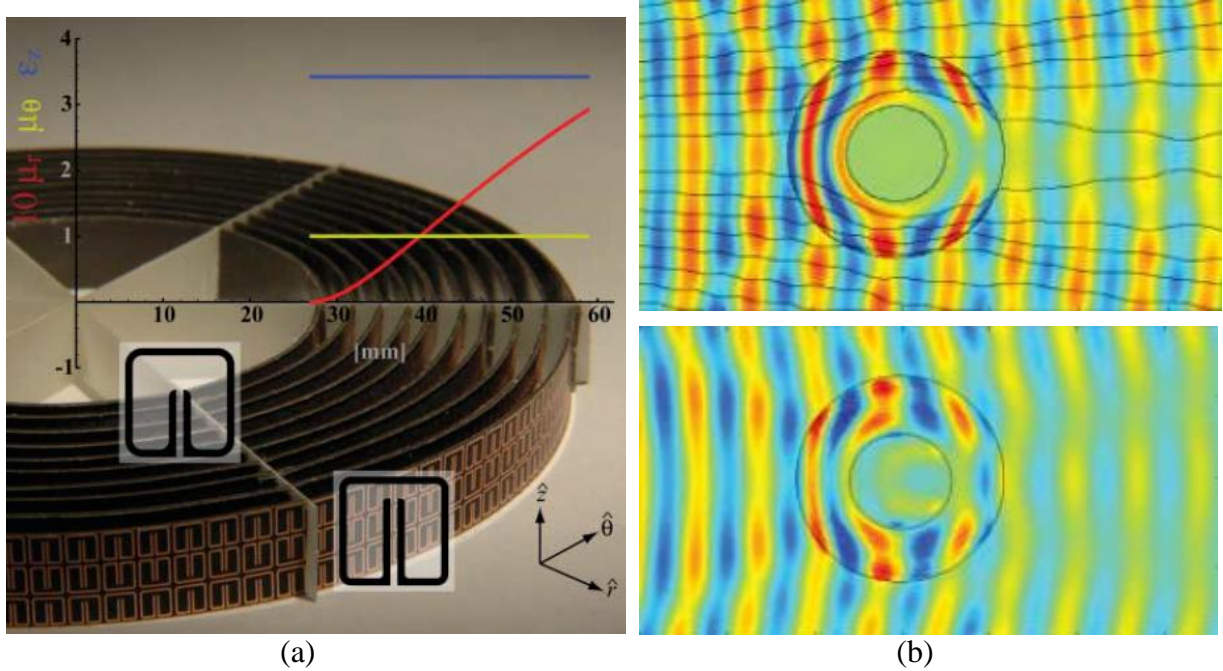
Figure 3.3. (a) sketch of the first experimentally developed cloak, (b)calculated and measured scattered field (Schurig *et al*, 2006 [16]).

The described cloak was prototyped and embedded into scattering chamber. The distribution of the vertical component of the electric field around the cloak was scanned, and the obtained results showed some decrease of the scattered field (see Fig. 3.3.b). Although this experiment proved the basic idea of cloaking, the level of scattered field has not been quantified.

Similarly to the realization of a so-called TM$_z$ cloak, there is another realization of metamaterial cloak by Cai *et al.* [17]. This cloak is intended to work with TE$_z$ polarized wave at optical frequencies. In TE$_z$ cloak only components μ_{zz}, $\varepsilon_{\rho\rho}$ and $\varepsilon_{\phi\phi}$ are relevant, thus it is again possible to simplify the metamaterial design by allowing only $\varepsilon_{\rho\rho}$ to vary in radial direction:

$$\varepsilon_{\rho\rho} = \left(\frac{b}{b-a}\right)^2 \left(\frac{\rho-a}{\rho}\right)^2$$

$$\varepsilon_{\phi\phi} = \left(\frac{b}{b-a}\right)^2 \tag{3.10}$$

$$\mu_{zz} = 1.$$

Again, the products $\varepsilon_{\rho\rho}\cdot\mu_{zz}$ and $\varepsilon_{\phi\phi}\cdot\mu_{zz}$ are kept the same. The required distribution of $\varepsilon_{\rho\rho}$ can be realized using metal wires embedded in a dielectric material, i.e. with a thin wire plasma-like metamaterial. Here, the effective permittivity varies in radial direction and its real part

has to exhibit the required behavior ($0 < \mathrm{Re}\{\varepsilon_{\rho\rho}\} < 1$) with negligible imaginary part (i.e with negligible losses) [17]. First practical realization in microwave frequency range has used split-rings to obtain required permittivity distribution (see Fig. 3.4 and references [18] and [19] for details).
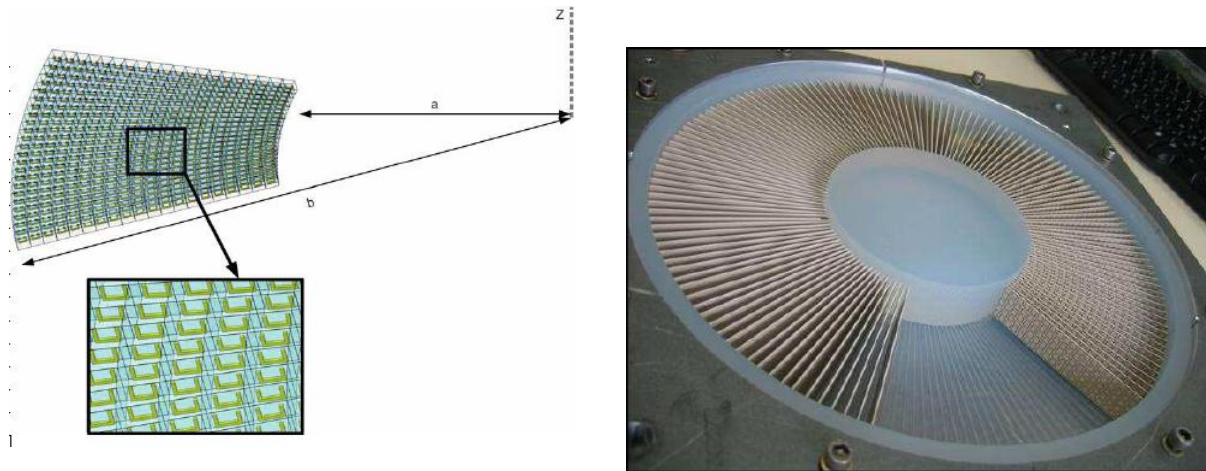
Figure 3.4. Sketch of the experimentally developed TE$_z$ cloak ([18], [19])
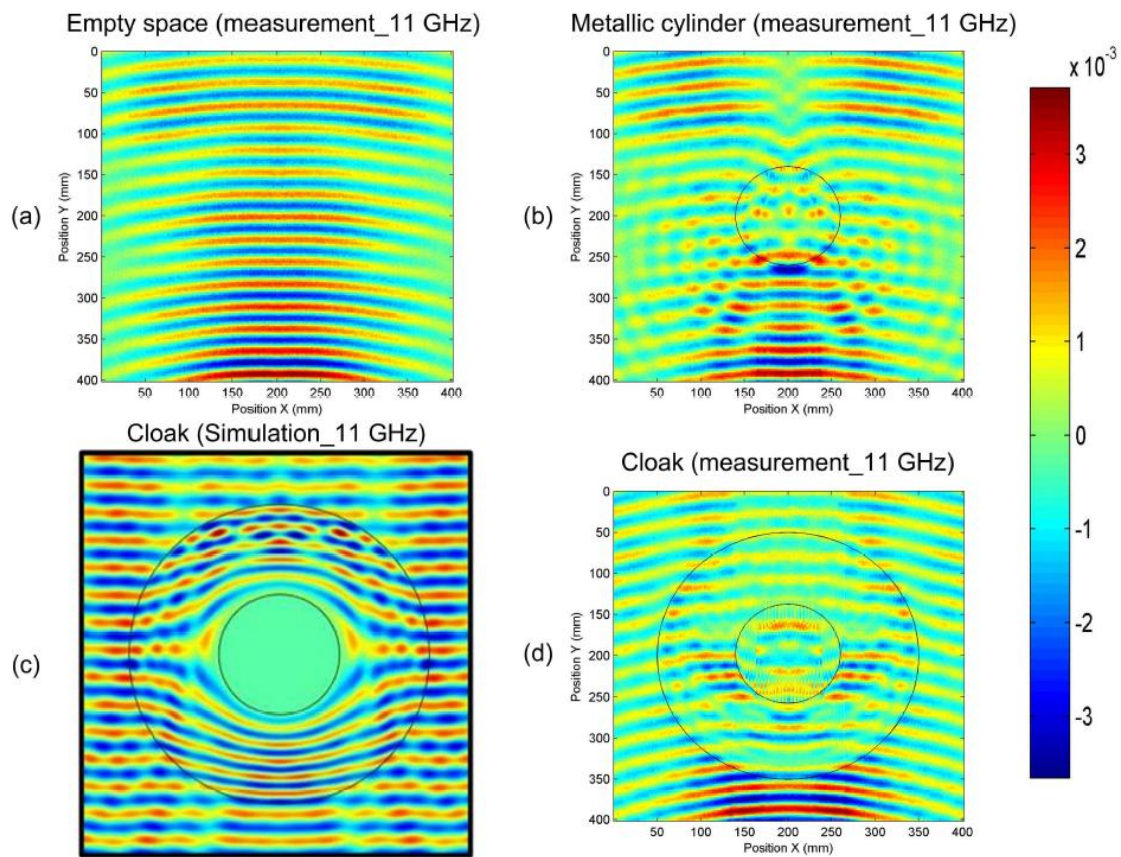
Figure 3.5. Experimental demonstration of the TEz cloak.

Table 3.1 gives the comparison of the permeability and permittivity values of the ideal, TM_z and TE_z cloaks. It should be noted that for some of the proposed cloak designs there is no need to use metamaterial structures. For example, hard surfaces have been used in the design of supporting struts of reflector antenna feeds [6], and parallel-plate waveguide structures have been used to reduce scattering from dielectric or metallic obstacles [21], [22].

TABLE 3.1. THE VALUES OF PERMEABILITY AND PERMITTIVITY TENSORS OF THE CONSIDERED CLOAKS (a AND b REPRESENT THE INNER AND OUTER RADIUS OF THE CLOAK, AND ρ IS THE RADIAL COORDINATE)

| Ideal cloak [9]	TM cloak [16]	TE cloak [17]
$\varepsilon_{\rho\rho} = \mu_{\rho\rho} = \dfrac{\rho - a}{\rho}$	$\mu_{\rho\rho} = \left(\dfrac{\rho - a}{\rho}\right)^2$	$\varepsilon_{\rho\rho} = \left(\dfrac{b}{b-a}\right)^2 \left(\dfrac{\rho - a}{\rho}\right)^2$
$\varepsilon_{\phi\phi} = \mu_{\phi\phi} = \dfrac{\rho}{\rho - a}$	$\mu_{\phi\phi} = 1$	$\varepsilon_{\phi\phi} = \left(\dfrac{b}{b-a}\right)^2$
$\varepsilon_{zz} = \mu_{zz} = \left(\dfrac{b}{b-a}\right)^2 \dfrac{\rho - a}{\rho}$	$\varepsilon_{zz} = \left(\dfrac{b}{b-a}\right)^2$	$\mu_{zz} = 1$

In last several years different versions of cylindrical cloaks are experimentally realized, both in microwave and optical frequency ranges. Unfortunately, for some realizations (like Schurig cloak [16] or TE_z cloak [19]) there are no published data in open scientific literature which will give information about the level of scattered field or about the obtained frequency bandwidth. In other words, these experiments have only proved the basic idea of cloaking.

There is only one experimentally realized metamaterial-based cloak for which data about the obtained invisibility and bandwidth are available [20]. It was realized at Duke University and the cloak is nearly identical to the cloak realized by Schurig et al [16]. The central frequency was 10 GHz, and the total scattering width (of the bare PEC cylinder) was reduced in the frequency range 9.91 to 10.14 GHz. In other words, the obtained bandwidth was 230 MHz or 2.3% (which corresponds well to theoretical predictions). The reduction of total scattering width was 24% (i.e. the invisibility gain was only 1.32), and from the measurement report [20] it is not clear if such small obtained invisibility gain was consequence of losses or imperfections in the experimental realization. The experimentally measured total scattering width is given in Figure 3.6.
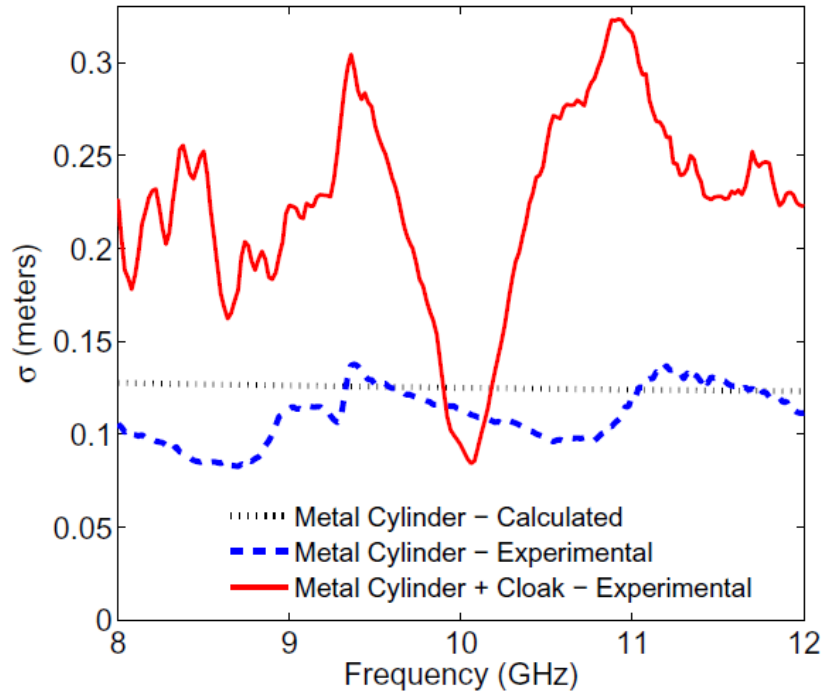
Figure 3.6. The measured total scattering width σ_T of an experimentally realized TM_z cloak [20]. For comparison, σ_T of an uncloaked metal cylinder is also given.

The experimental results give rise to a natural question, why the realized cloak has such poor performance. There are two basic reasons for that (additionally to the problem of tolerances and of the accuracy of electromagnetic solvers), as described below. In previous work we have developed a program that analyses multilayer uniaxial cylinders (see [EOARD]), which enabled us to analyze the "ideal" realization of the Schurig cloak. We have selected the same dimensions and the working frequency as in the experimental model realized by Schurig *et al*. [16] (see Tables 3.1 and 3.2).

TABLE 3.2. DIMENSIONS OF THE CYLINDRICAL CLOAK

	dimension (cm)	Dimension (wavelength)
Inner diameter 2*a*	5.42	1.44
Outer diameter 2*b*	11.78	3.34
Thickness of one layer (10-layer case)	0.318	0.09

First we have investigated the influence of the stepwise approximation of the continuous variation of constitutive parameters. The required has been approximated by 1- to 10- steps piecewise constant functions in order to analyze how the subtlety of the approximation of radial anisotropy influences the total scattering width, i.e. "the invisibility". The normalized total scattering width is given in Fig. 3.7, and it can be seen that for structures with more than 5 layers there is practically no improvement of the obtained invisibility – the obtained total scattering width reduction is around 3. The main reason for such a small gain was the reflection of the incident wave from the cloak surface due to the impedance mismatch. The level of scattered power can be approximated by

$$\frac{\left(\sigma_T^{Cloak}/2b\right)_{CLOAK}}{\left(\sigma_T^{PEC}/2a\right)_{PEC}} \approx \left|\frac{\eta-1}{\eta+1}\right|^2 = \left|\frac{\sqrt{\mu_{\phi\phi}/\varepsilon_{zz}}-1}{\sqrt{\mu_{\phi\phi}/\varepsilon_{zz}}+1}\right|^2 = \left(\frac{a}{2b-a}\right)^2. \tag{3.11}$$

Here *CLOAK* and *PEC* denotes the total scattering width of the cloaked and uncloaked cylinder, respectively. If we compare the calculated value (0.15) and approximated value (0.09) we can conclude that the impedance mismatch is the main reason why Schurig cloak always scattered large amount of power. The angular variation of scattered electric-field and the field distribution in the vicinity of the cloaked object is given in Fig. 3.8. and it can be seen that the reflection from the cloak surface causes ripples in the electric-field distribution.
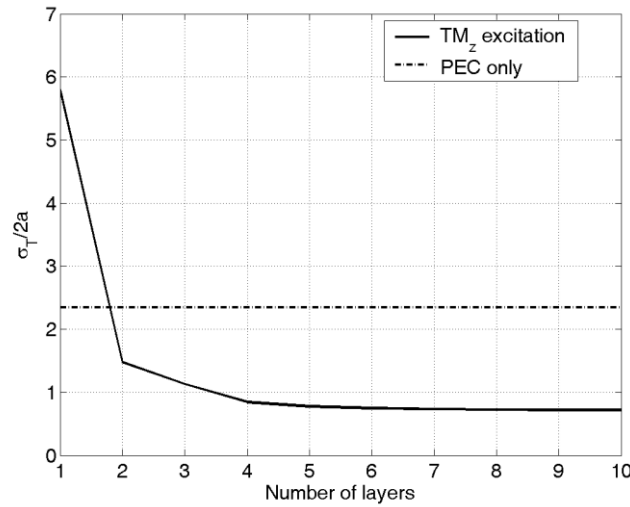
Figure 3.7. Normalized total scattering width vs. number of layers for TM_z cloak (TM_z polarization).


| (a) | (b) |
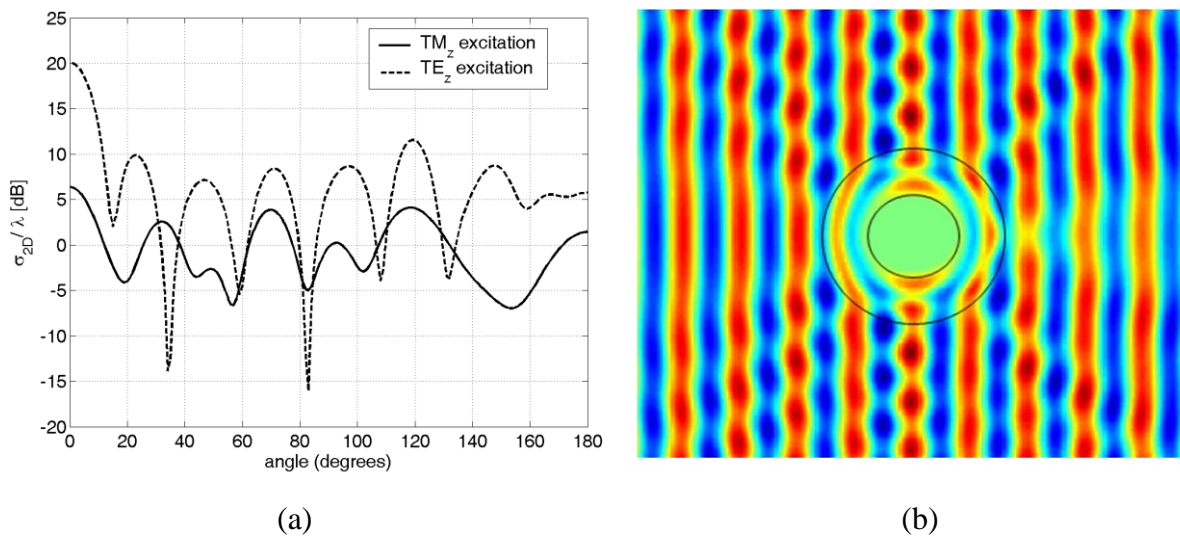
Figure 3.8. (a) Normalized bistatic scattering width (TM_z and TE_z polarizations) and (b) electric field distribution in the vicinity of the cloaked object (TM_z polarization) of 10-layers realization of TM_z cloak.

Next we have investigated the bandwidth of the cloak. The frequency dependence of the magnetic permeability (realized with some kind of split rings) is given by the so-called Lorentz model [23]:

$$\mu_{eff} = 1 - \frac{f_{mp}{}^2 - f_0{}^2}{f^2 - f_0{}^2 - j\gamma f}.$$

(3.12)

Here f is the frequency of the signal, f_{mp} denotes the frequency at which $\mu_{eff}=0$ for the lossless case (null-point of the function), f_0 is the frequency at which μ_{eff} diverges (the pole of the function), while the factor γ represents the losses.

In an attempt to approximate the experimental Schurig cloak we have to select one free parameter. The bandwidth results of the TM_z cloak strongly depend on the ratio between the frequencies f_{mp} (the frequency at which $\mu_{eff}=0$ for the lossless case) and f_0 (the frequency at which μ_{eff} diverges for the lossless case). Since this ratio depends on the particular realization of the split-ring resonator, we have investigated the dependence of the cloak bandwidth on that ratio. In Figure 3.9 we have illustrated this dependence. It can be seen that the bandwidth is between 0.24% and 2.4 %, depending on this ratio. Therefore, one can conclude that if the cloak is made from resonant type of elements the bandwidth will be quite narrow, typically several percent (as it was demonstrated in [20]). However, if we decide to select non-resonant elements (like wires that are used in TE_z cloak realization), the bandwidth can be much larger (at least one order of magnitude).
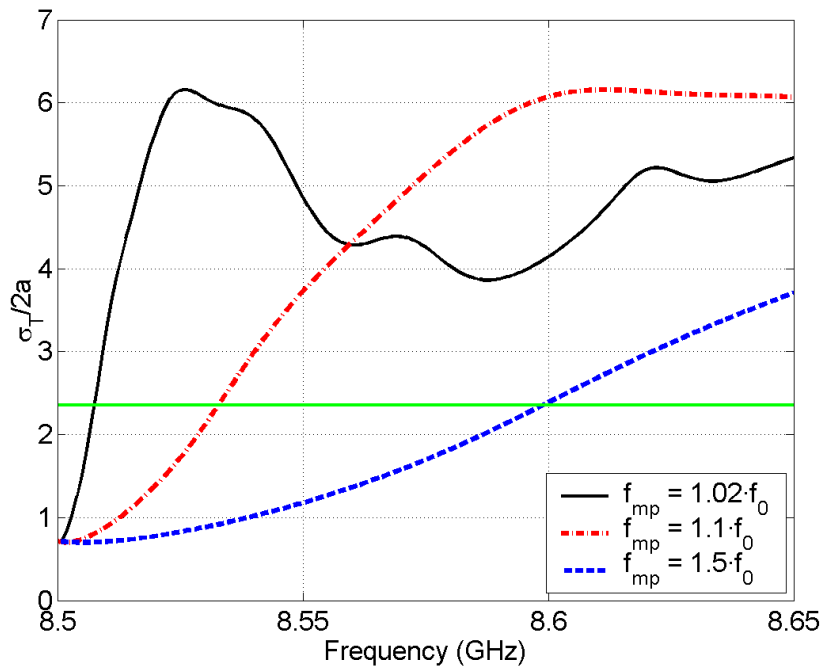
Figure 3.9. Normalized total scattering width as a function of ratio f_{mp} / f_0 for TM_z cloak (TM_z polarization).

3.2. EXTRACTION OF PARAMETERS

Previous work in invisibility gives rise to several questions:

1. Why the developed cloak with the reduced variation of constitutive parameters (i.e. cloaks made from uniaxial materials) scatters the electromagnetic field, even in the ideal case?
2. Is it possible to realize a cloak with the reduced variation of constitutive parameters that is entirely invisible (at least at the central frequency)?
3. Is it possible to realize a cloak with the reduced variation of constitutive parameters that works for oblique direction of incident wave?
4. What is the bandwidth of a cloak that is built using metamaterial layers? Is it possible to enlarge the bandwidth of such a cloak?
5. Is it possible to realize a cloak that is invisible to pulse excitation (i.e. to radar)?

We believe (and we will try to demonstrate that in this report) that with smart designing procedure it is possible to avoid most of possible failures, i.e. designing decisions that will result in a developed structure with poor electromagnetic performance (the explanation of the phenomena resulting in the first question is already given in section 3.1).

Before starting we should note that metamaterial structures are extremely hard to design since they have a lot of small details (small compared to the wavelength) which results in a large computation time when analyzing such structures using general electromagnetic solvers. Therefore, it is not possible simply to connect the electromagnetic solver with a optimization routine and press the button "Optimize".

All these lead to conclusion that the first design should be made using (anisotropic) homogeneous materials. This could be done using e.g. transformation optics (as described in section 3.1) or simply by connecting the fast electromagnetic solver with the optimization routine (homogeneous structures can be analyzed very quickly). We believe (due to complexity of possible realizations) that the design obtained in such a way is actually the best possible design. In other words, the practical realization will always have worse performance compared to this ideal model.

In order to connect the ideal design (based on homogeneous multilayer anisotropic structure) and "real" metamaterial structure we should somehow connect the considered periodic structure with effective constitutive parameters, i.e. with parameters that describe the scattering properties of the considered structure.

Extraction of parameters or homogenization is a procedure in which complex periodic structure is represented with a simpler structure. Usually that simpler structure can be described with several numbers, i.e. constitutive parameters. Procedure deals with equations in heterogeneous materials, with a periodic pattern, in which dimensions of a unit cell tend to zero. Method is based on the consideration of two length scales associated with the microscopic and macroscopic phenomena. Constitutive parameters of homogeneous materials do not depend on spatial variable. On the other hand, if the material is not homogeneous, parameters of the material effectively depend on the position in space. Parameters of material with periodic pattern are periodic functions of space variables. In certain cases the period is very small with respect to other dimensions appearing in the problem. In those cases solution is approximately the same as the solution for a homogeneous material with corresponding

constitutive parameters [24]. The homogenization procedure in electromagnetic theory introduces constitutive parameters of a discrete media as a result of averaging of the Maxwell equations for microscopic fields. The procedure makes sense if its result can be used for solving boundary problems of electrodynamics where a discrete set of scattering particles are replaced by a sample of continuous media [25]. The necessity for a good homogenization procedure is related with the request for a fast electromagnetic solver, i.e. within procedure of metamaterial design.

The constitutive parameters can be obtained by numerical calculations or by some approximate analytical model. In numerically based methods we simply calculate the ratio of electromagnetic field components. Approximate analytical methods are based on geometrical properties of periodic structure so there are some practical problems with implementing this for complicated metamaterial structures. Furthermore, due to complex geometrical pattern, some unit cells of periodic structures exhibit bianisotropic behavior.

3.2.1 Extraction based on reflection and transmission coefficient

In paper [26] the method for extraction of constitutive parameters from measured S parameters is presented. The idea is to extract constitutive material parameters from reflection and transmission coefficients for a unit cell in all three spatial directions. In all those directions our unit cell is illuminated by a normal incident plane wave. We have six incidences on a unit cell (see Figure 3.10). Three of them are TE, and three are TM modes. S parameters are defined in terms of the electric and magnetic fields for the TE and TM incidences. In every direction unit cell can display bianisotropic properties or it behaves as isotropic material. In directions for which the unit cell behaves as isotropic material we can use formulas from [27]. For all these directions the retrieval equations are the same.
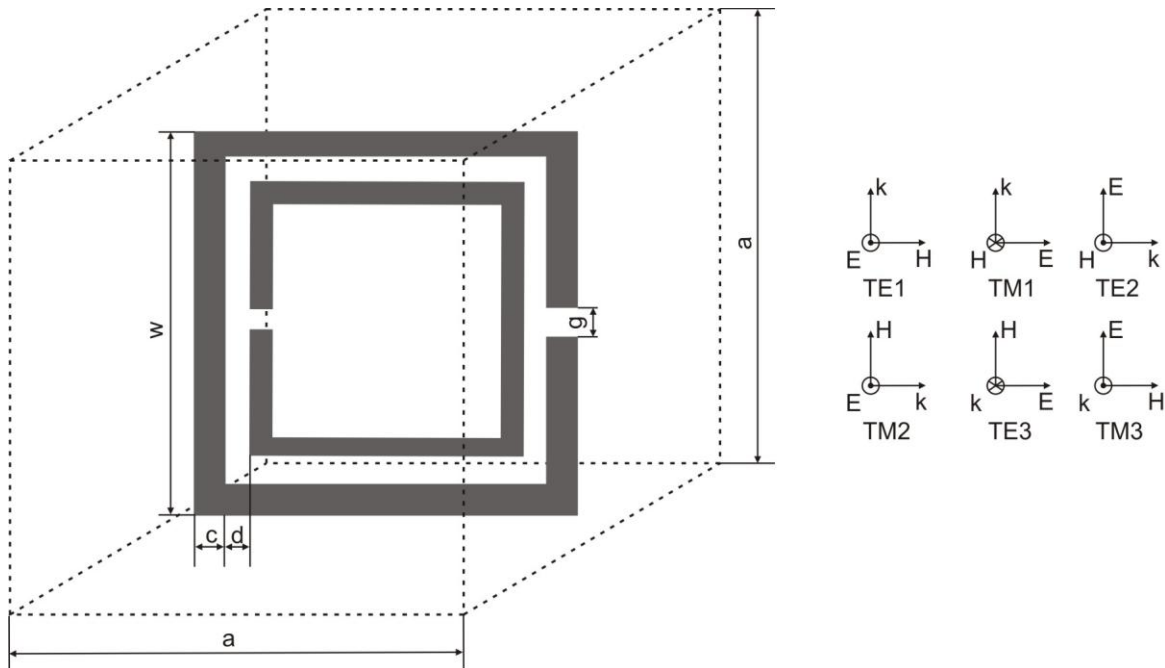
Figure 3.10. S-matrix approach for determining constitutive parameters. The method is based on measuring or calculating S_{11} and S_{21} for six test cases.

Elements of the S matrix can be found from the elements of the T matrix as follows. The transfer matrix for a section of a transmission line is defined as:

$$\mathbf{F'} = \mathbf{T} \cdot \mathbf{F} \tag{3.13a}$$

$$\mathbf{F} = \begin{vmatrix} E \\ j\omega\mu H \end{vmatrix} \tag{3.13b}$$

$$T = \begin{vmatrix} \cos(nk_0 d) & -\dfrac{Z}{k_0}\sin(nk_0 d) \\ \dfrac{k_0}{Z}\sin(nk_0 d) & \cos(nk_0 d) \end{vmatrix} \tag{3.13c}$$

In [28] there is a connection between S and T matrices:

$$S_{11} = \frac{T_{11} - T_{22} + (jk_0 T_{12} - \dfrac{T_{21}}{jk_0})}{T_{11} + T_{22} + (jk_0 T_{12} + \dfrac{T_{21}}{jk_0})} \tag{3.14.a}$$

$$S_{21} = \frac{2}{T_{11} + T_{22} + (jk_0 T_{12} + \dfrac{T_{21}}{jk_0})} \tag{3.14.b}$$

$$S_{12} = \frac{2\det(T)}{T_{11} + T_{22} + (jk_0 T_{12} + \dfrac{T_{21}}{jk_0})} \tag{3.14.c}$$

$$S_{22} = \frac{T_{22} - T_{11} + (jk_0 T_{12} - \dfrac{T_{21}}{jk_0})}{T_{11} + T_{22} + (jk_0 T_{12} + \dfrac{T_{21}}{jk_0})} \tag{3.14.d}$$

For a homogeneous slab $T_{11} = T_{22}$ and $\det(T) = 1$. Furthermore, S matrix is symmetric:

$$S_{11} = \frac{\dfrac{1}{2}(\dfrac{T_{21}}{jk_0} - jk_0 T_{12})}{T_{11} + \dfrac{1}{2}(jk_0 T_{12} + \dfrac{T_{21}}{jk_0})}$$

$$S_{21} = \frac{1}{T_{11} + \dfrac{1}{2}(jk_0 T_{12} + \dfrac{T_{21}}{jk_0})} \tag{3.15}$$

Using the analytic expression for T matrix elements we get:

$$S_{11} = S_{22} = \frac{j}{2}(\frac{1}{Z} - Z)\sin(nk_0 d)$$

$$S_{21} = \frac{1}{\cos(nk_0 d) - \frac{j}{2}(\frac{1}{Z} + Z)\sin(nk_0 d)} \tag{3.16}$$

Here k_0 denotes the wave number of the incident wave in free space, d is the thickness of the slab, n is the refractive index, R is the half space reflection coefficient. From these two equations we can get expressions for index of refraction n and characteristic impedance Z:

$$n = \frac{1}{kd}\arccos\left(\frac{1}{2S_{21}}(1 - S_{11}^2 + S_{21}^2)\right) \tag{3.17.a}$$

$$Z = \sqrt{\frac{(1 + S_{11}^2) - S_{21}^2}{(1 - S_{11}^2) - S_{21}^2}} \tag{3.17.b}$$

Note that signs in equations (3.17) are determined from conditions for passive media. Effective parameters are calculated from:

$$\mu = nZ \tag{3.18.a}$$

$$\varepsilon = \frac{n}{Z} \tag{3.18.b}$$

Table 3.3 describes the proposed method with the six test cases. It can be seen that each component of the $\boldsymbol{\mu}$ and $\boldsymbol{\varepsilon}$ tensors is calculated twice. Comparison of two cases gives an indication how accurate the constitutive parameters are calculated (in particular, this is critical around resonant frequencies of metamaterial elements).

If in some direction material behaves as a bianisotropic material then other methods have to be used. Some of those methods are explained in [29]. Those formulas are not enough to determine constitutive parameters because in some situations we will get two roots of some parameters and from theory we cannot conclude which one is the physical one. Recommendation from the paper is to use one which gives better match between calculated and simulated or measured S parameters.

TABLE 3.3. EXTRACTION OF PARAMETERS BY S-MATRIX APPROACH (SIX TEST CASES INCLUDED).

Case	Z	n	Solved components
TE1	$\sqrt{\mu_x/\varepsilon_y}$	$\sqrt{\mu_x\varepsilon_y}$	μ_x, ε_y
TM1	$\sqrt{\mu_y/\varepsilon_x}$	$\sqrt{\mu_y\varepsilon_x}$	μ_y, ε_x
TE2	$\sqrt{\mu_y/\varepsilon_z}$	$\sqrt{\mu_y\varepsilon_z}$	μ_y, ε_z
TM2	$\sqrt{\mu_z/\varepsilon_y}$	$\sqrt{\mu_z\varepsilon_y}$	μ_z, ε_y
TE3	$\sqrt{\mu_z/\varepsilon_x}$	$\sqrt{\mu_z\varepsilon_x}$	μ_z, ε_x
TM3	$\sqrt{\mu_x/\varepsilon_z}$	$\sqrt{\mu_x\varepsilon_z}$	μ_x, ε_z

3.2.2 Extraction based on Bloch theory

In this it is assumed that the interactions among adjacent frequency selective surfaces (in the normal direction) are well described by the dominant Floquet mode, and that other modes have negligible coupling effects. From this assumption equivalent transmission line model is adopted in which every FSS layer is represented by an equivalent admittance matrix. In general, the admittance of FSS layer depends on frequency and on direction of arrival of electromagnetic wave. In order to determine the FSS admittance the full-wave analysis is adopted. Isolated FSS is illuminated by a plane wave with a given frequency and incident direction. If propagation vector is in the principle plane of the FSS, the equivalent admittance is a diagonal matrix. That means that interaction of the plane wave and FSS could be modeled with decoupled equivalent transmission lines, one for TM and one for TE polarization. The whole device, which is made as a multilayer structure, is modeled as a couple of periodically loaded transmission lines that are analyzed with Bloch theory [30]. From that procedure we get propagation constant and characteristic impedance of the supported modes. Then, a homogeneous medium supporting the same scattered field distribution is defined.

One of the problems with the described procedure is that the solution is not unique. Since the transmission line model only provides information on the transverse field components, there are infinite media that satisfy the boundary conditions of the solution. All those media provide the same dispersion relation and scattering coefficients of the fundamental modes of the periodic pattern but they are characterized by different constitutive parameters, so all those solutions are externally equivalent. In order to uniquely determine the effective constitutive parameters it is necessary to find additional information on the longitudinal field components inside periodic structure. It is assumed that electromagnetic field inside material is very well approximated by the dominant Bloch mode only. Under this assumption, a closed form expression of the longitudinal field can be obtained as a function of the FSS equivalent admittances. That step provides the complete characterization of the homogenized material. The largest weakness of this method lays in the assumption that only dominant mode is needed. That is not true for FSS layers which are close to each other because in that situation we need more modes, i.e. we need to consider evanescent modes as well.

In the first step we calculate the reflection coefficient of a considered FSS using some general electromagnetic solver. Equivalently, we consider the network from Fig.3.11.
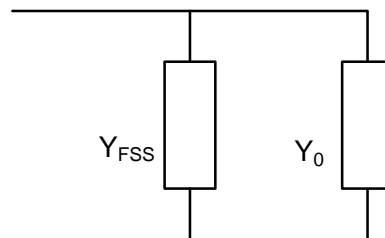
Figure 3.11. Equivalent network of FSS in free-space.

From reflection coefficient Γ we calculate the normalized FSS admittance:

$$\bar{Y}_{FSS}^{TE,TM} = \frac{Y_{FSS}^{TE,TM}}{Y_0^{TE,TM}} = \frac{-2\Gamma}{1-\Gamma} \tag{3.18}$$

The Bloch theory, described in [30], gives the parameters of the equivalent transmission line:

$$\cos(k_{z_B}^{TE,TM}d) = \cos(k_{z_0}d) + j\frac{\bar{Y}_{FSS}^{TE,TM}}{2}\sin(k_{z_0}d) \tag{3.19.a}$$

$$\frac{Z_B^{TE,TM}}{Z_0^{TE,TM}} = \bar{Z}_B^{TE,TM} = \pm\left[\frac{2\sin(k_{z_0}d) - j\bar{Y}_{FSS}^{TE,TM}\cos(k_{z_0}d) + j\bar{Y}_{FSS}^{TE,TM}}{2\sin(k_{z_0}d) - j\bar{Y}_{FSS}^{TE,TM}\cos(k_{z_0}d) - j\bar{Y}_{FSS}^{TE,TM}}\right] \tag{3.19.b}$$

From procedure described in [31] we get:

$$\mu = \begin{bmatrix} \dfrac{k_{z_B}^{TE}Z_B^{TE}}{\omega} & 0 & 0 \\[2ex] 0 & \dfrac{k_{z_B}^{TM}Z_B^{TM}}{\omega} + \dfrac{k_\rho^2}{\omega^2\varepsilon_{zz}} & 0 \\[2ex] 0 & 0 & \mu_{zz} \end{bmatrix} \tag{3.20}$$

$$\varepsilon = \begin{bmatrix} \dfrac{k_{z_B}^{TM}}{\omega Z_B^{TM}} & 0 & 0 \\[2ex] 0 & \dfrac{k_{z_B}^{TE}}{\omega Z_B^{TE}} + \dfrac{k_\rho^2}{\omega^2\mu_{zz}} & 0 \\[2ex] 0 & 0 & \varepsilon_{zz} \end{bmatrix}, \tag{3.21}$$

where k_ρ is a propagation constant in ρ direction. As mentioned above, z components of constitutive parameters are not determined in this procedure. To determine them we need additional information, longitudinal components of the electromagnetic fields. The longitudinal fields are constructed by properly averaging the corresponding components of the microscopic fields [32]. The final expressions for z-components of constitutive parameters are:

$$\varepsilon_{zz} = -\frac{\dfrac{k_\rho}{d_x d_y} \displaystyle\int\limits_{-\frac{d_x}{2}}^{\frac{d_x}{2}} \int\limits_{\frac{d_y}{2}}^{\frac{d_y}{2}} h_\alpha(x,y,0)e^{j(k_x x + k_y y)}dxdy}{\dfrac{\omega}{d} \displaystyle\int\limits_{-\frac{d}{2}}^{\frac{d}{2}} e_z(0,0,z)e^{jk_{zB}z}dz} \tag{3.23.a}$$

$$\mu_{zz} = \frac{\dfrac{k_\rho}{d_x d_y} \displaystyle\int\limits_{-\frac{d_x}{2}}^{\frac{d_x}{2}} \int\limits_{\frac{d_y}{2}}^{\frac{d_y}{2}} e_\alpha(x,y,0)e^{j(k_x x + k_y y)}dxdy}{\dfrac{\omega}{d} \displaystyle\int\limits_{-\frac{d}{2}}^{\frac{d}{2}} h_z(0,0,z)e^{jk_{zB}z}dz} \tag{3.23.b}$$
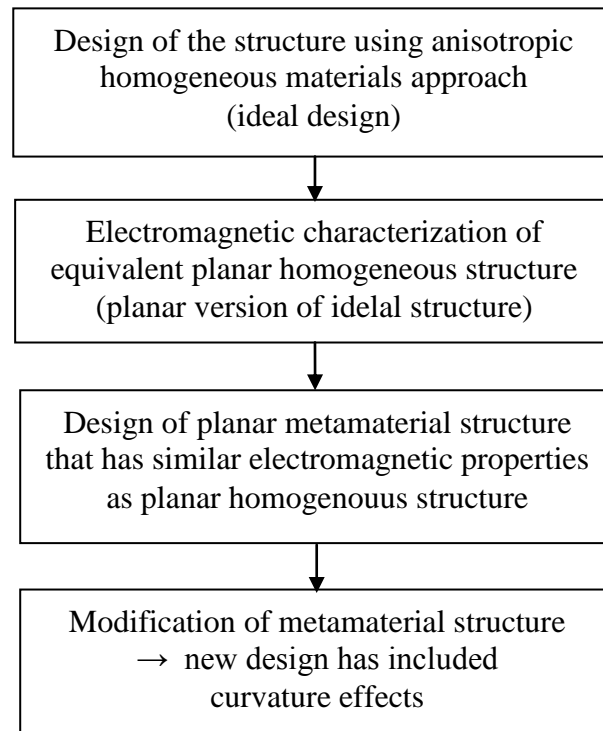
where *h* and *e* are microscopic fields. With these two expressions we have obtained expressions for all components of the constitutive parameters. The problems with practical implementation lie mostly in evaluation of microscopic fields, i.e. the accuracy of the Bloch method mostly depends on the accuracy of calculating microscopic near-fields.

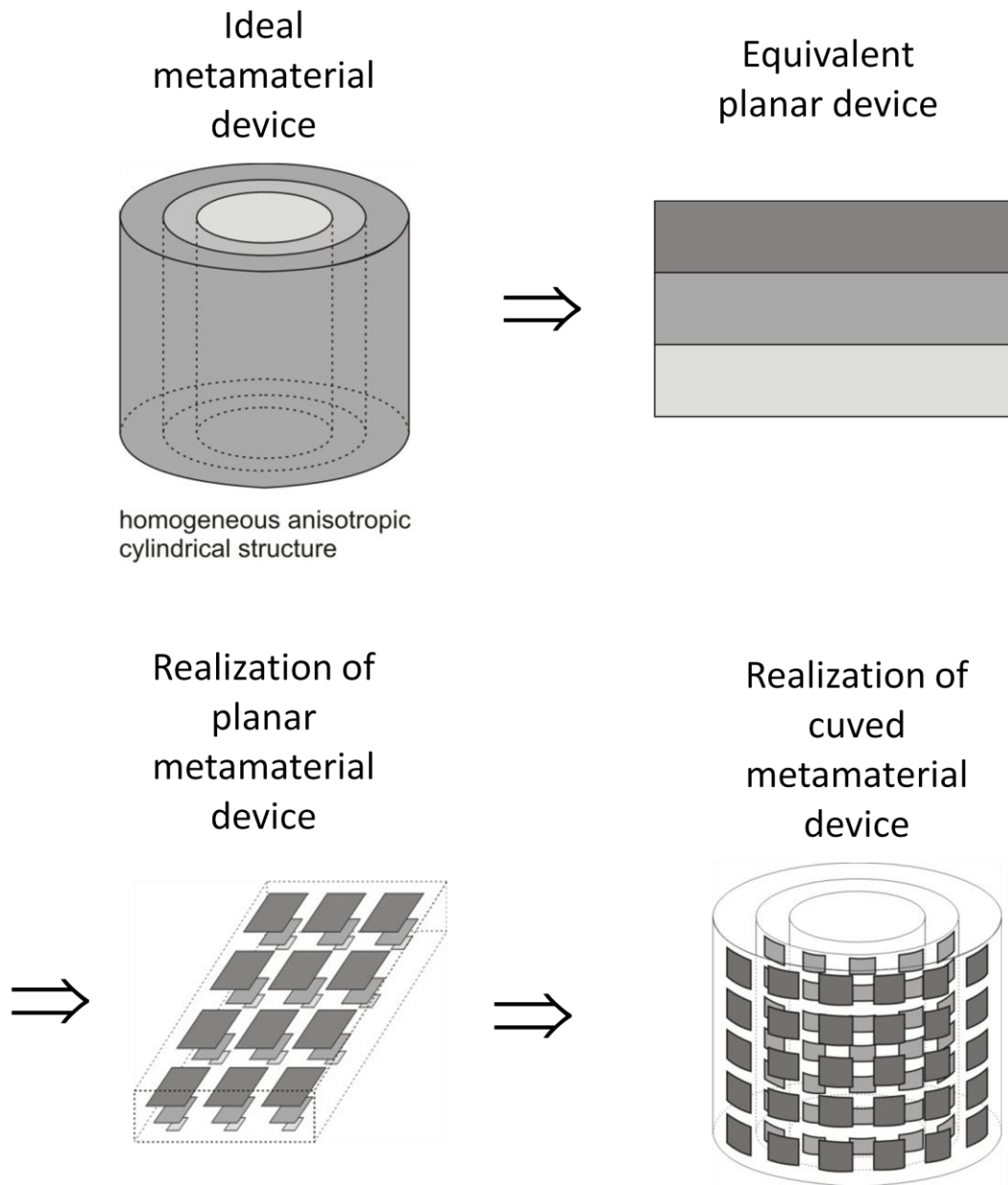### 3.3. PROCEDURE FOR DESIGNING METAMATERIAL STRUCTURES

When designing novel type of structures that contain metamaterial layers it is quite tedious and complicate to arrive from basic idea (obtained for example using transformation optics) to „real" structure that will be produced in some workshop. The main obstacle is that these novel structures (in the basic design) contain layers of materials that have permeability or permittivity smaller than one, i.e. such materials that are not possible to find in nature. Therefore, we need to "cheat" the nature, i.e. to use periodic structures with period much smaller than the wavelength, i.e. we need to implement the layers of metamaterials. Therefore, the straightforward path is to design a structure which will have effective constitutive parameters equal to the designed ones. However, this is simple only for some structures. At least two problems appear when one starts to design structures using this approach. In more details, in the first design (i.e. in the design that reflects the ideal structure obtained e.g. with ray approach) one would like to obtain material with specific either permeability or permittivity. However, the practical realization will also introduce variation of other quantity, the one that is usually kept constant. The larger problems appear from the resonance nature of elements used in metamaterial realization. It is shown [29] that around resonances there are frequency intervals in which it is not possible to accurately define effective constitutive parameters, i.e. parameters that will accurately predict the behavior of the electromagnetic waves that travel through such a structure.

So, the natural question arise that if is not possible to accurately characterize metamaterials using effective constitutive parameters, how metamaterial structures should be designed. Most often, the ideal structure is described using (anisotropic) permeability and permittivity, so we should not completely forget tensors ε and μ. But what we actually consider is how the waves are propagating through such a structure. Therefore, the description that is more practical from the design point of view is description of transmitted and reflected electromagnetic waves.

We will describe this principle on one example, i.e. how to design circular-cylindrical cloak (Figure 3.13). In the ideal design cylindrical layers with specific permeability and permittivity are obtained using transformation optics (see previous section). These layers we would like to obtain using cylindrical periodic structures. From CPU time and memory requirements it is much faster and easier to analyze planar periodic structures. Therefore, we will actually design planar multilayer metamaterial structure and then we will band it. In designing planar structure we will start with ideal homogeneous multilayer structure with desired (anisotropic) permeability and permittivity and then we will calculate reflection and transmission coefficients for set of incidence angles of incidence (and for polarization of incoming wave of interest). This dependency of reflection and transmission coefficient will be our cost function in optimization procedure, i.e. we will search for a periodic structure that have the same response to incoming waves as the desired ideal structure. This is now not a difficult task since we need to analyze only one periodic cell (multilayer in perpendicular direction), which is quite fast for all nowadays commercial electromagnetic solvers. This designing procedure is illustrated in Figure 3.12.

Figure 3.12. The proposed designing procedure of metamaterial structures

Ideal
metamaterial
device

Equivalent
planar device

homogeneous anisotropic
cylindrical structure

Realization of
planar
metamaterial
device

Realization of
cuved
metamaterial
device

Figure 3.13. Illustration of the proposed designing procedure: circular-cylindrical cloak

3.3.1 Characterization of a planar metamaterial layer

As a first step let us characterize planar multilayer anisotropic structures. The "real" structures usually are not planar, but this first step in designing procedure will give accurate starting point for final design, i.e. for final optimization with general electromagnetic solver. For example, the cylindrical cloak is actually circular-cylindrical multilayer anisotropic structure. The second step in the design process (Fig. 3.12) solves the sub-problem how to realize equivalent planar multilayer structure using metamaterial approach.

From mathematical point of view the question is how to characterize planar multilayer structure and to use this characterization as a cost function in optimizing metamaterial structure. The original structure is shown in Figure 3.14. Since lots of applications are actually scattering electromagnetic problem, we should also characterize the considered structure using scattering approach. For example, if we would like to characterize the structure in Fig. 3.14 that contains PEC ground plane, there are several possibilities of defining the cost function f_{cost}. Some of them are (the reflection coefficient of a homogeneous anisotropic layer and of the periodic metamaterial structure is denoted by Γ_{hom} and Γ_{met}, respectively):

1. Structure with PEC ground plane → phase of reflection coefficient as a function of incoming angle. The cost function is equal:

$$f_{cost} = \sum_{i=1}^{N} \left| \arg(\Gamma_{met}(\theta_i)) - \arg(\Gamma_{hom}(\theta_i)) \right| \qquad (3.24)$$

2. Structure without PEC ground plane → amplitude of reflection coefficient as a function of incoming angle. The cost function is equal:

$$f_{cost} = \sum_{i=1}^{N} \left| |\Gamma_{met}(\theta_i)| - |\Gamma_{hom}(\theta_i)| \right| \qquad (3.25)$$

3. Structure without PEC ground plane → amplitude and phase of reflection and transmission coefficients as a function of incoming angle.

$$f_{cost} = \sum_{i=1}^{N} \left| \Gamma_{met}(\theta_i) - \Gamma_{hom}(\theta_i) \right| \qquad (3.26)$$

In order to illustrate the accuracy of these methods let us consider the following examples. The first one is simple one-layer structure, of thickness 2 cm and with ground plane, which has permeability equal to 1.0, and uniaxial permittivity $\varepsilon_x = \varepsilon_z = 1.0$ and $\varepsilon_y = 0.5$ (see Figure 3.14). The working frequency is 4 GHz. Such a structure can be realized using metal strips, for example with periodicity $P_x = 3$ cm. In order to get an estimate of the strip width, we have calculated the effective constitutive parameters of a dielectric slab ($\varepsilon_r = 1.0$ in the considered case) containing the periodic strips in the middle of the structure (see Fig. 3.15). For that purpose we have developed a Moment Method code for planar periodic structure (we have named this code *pfss*, and its description is given in the Appendix of this report). From calculated reflection and transmission coefficient for normal incidence we have calculated the constitutive parameters using the method explained in section 3.2. The calculated results show that for obtaining $\varepsilon_y = 0.5$ we need to select the strip width $W = 0.9$ mm. The results also show that the strips introduce change in effective permeability, i.e. for the considered case the x-component of the $\boldsymbol{\mu}$ tensor is $\mu_x = 1.145$.
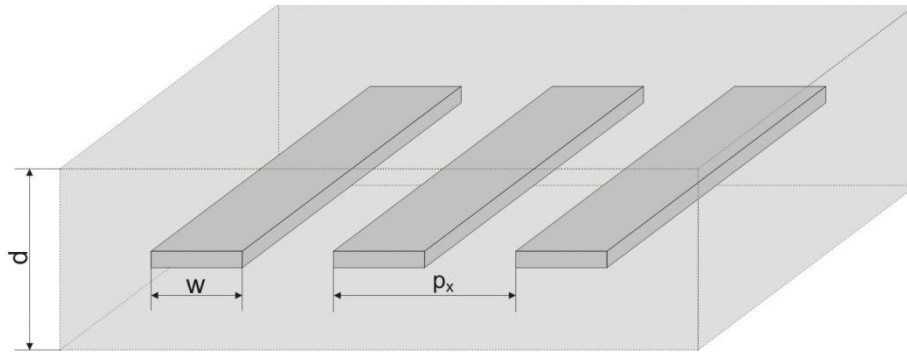
Figure 3.14. Dielectric slab with periodic metal strips
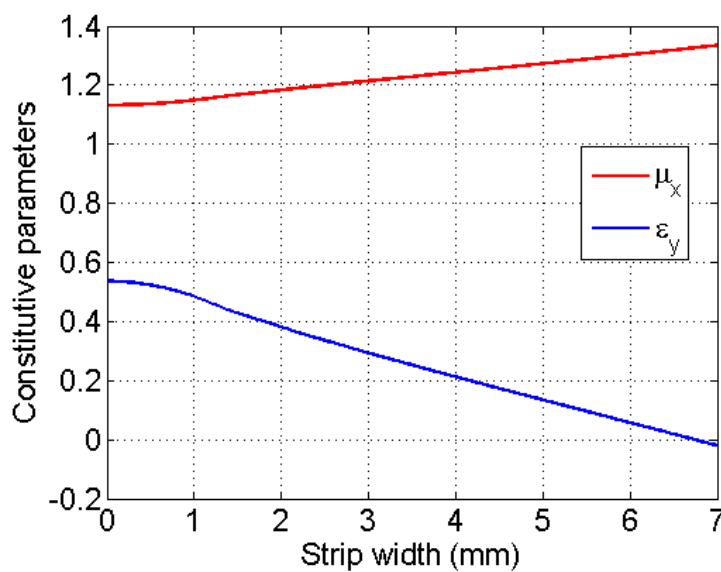
Figure 3.15. Effective constitutive parameters of a dielectric slab with periodic metal strips
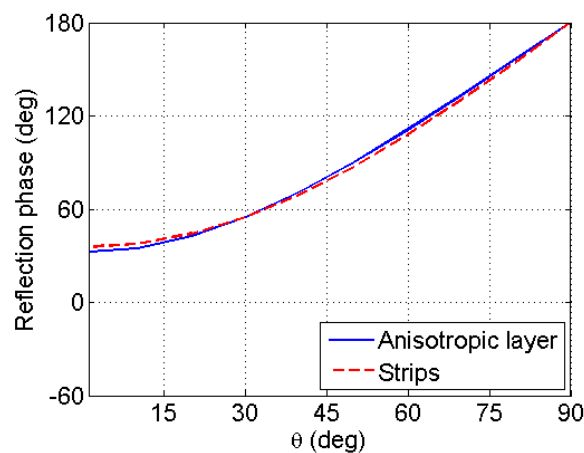
Figure 3.16. Phase of reflection coefficient of a grounded anisotropic dielectric layer and of metamaterial realization. Anisotropic layer is characterized with $\varepsilon_x = \varepsilon_z = 1.0$, $\varepsilon_y = 0.5$ and $\mu_x = 1.0$. The used cost function in optimization routine is defined by eq. (3.24). Parameters of strips are listed in Table 3.4.
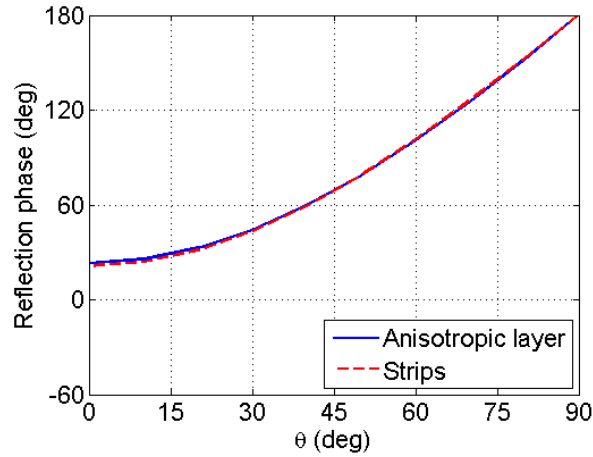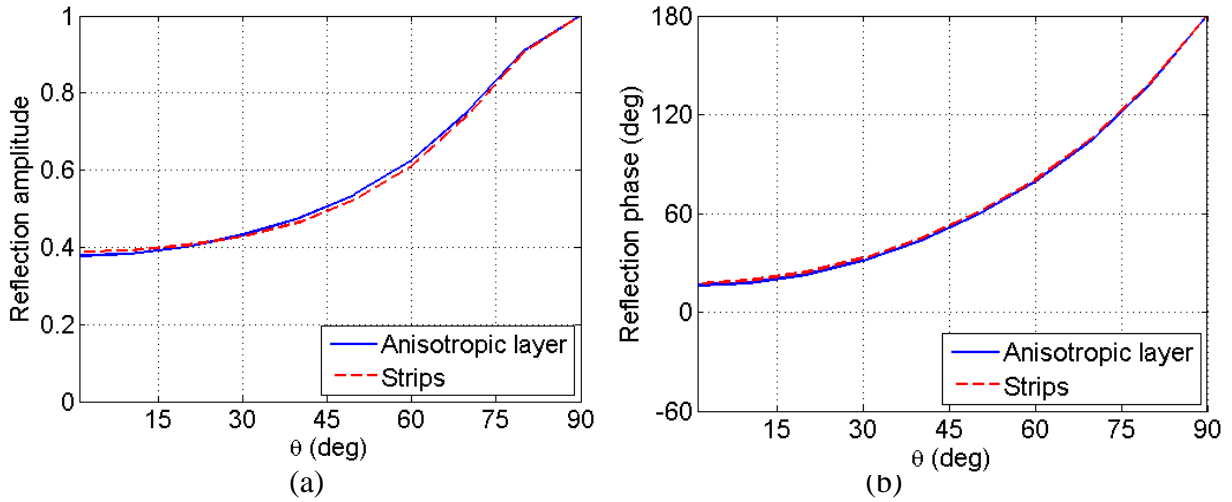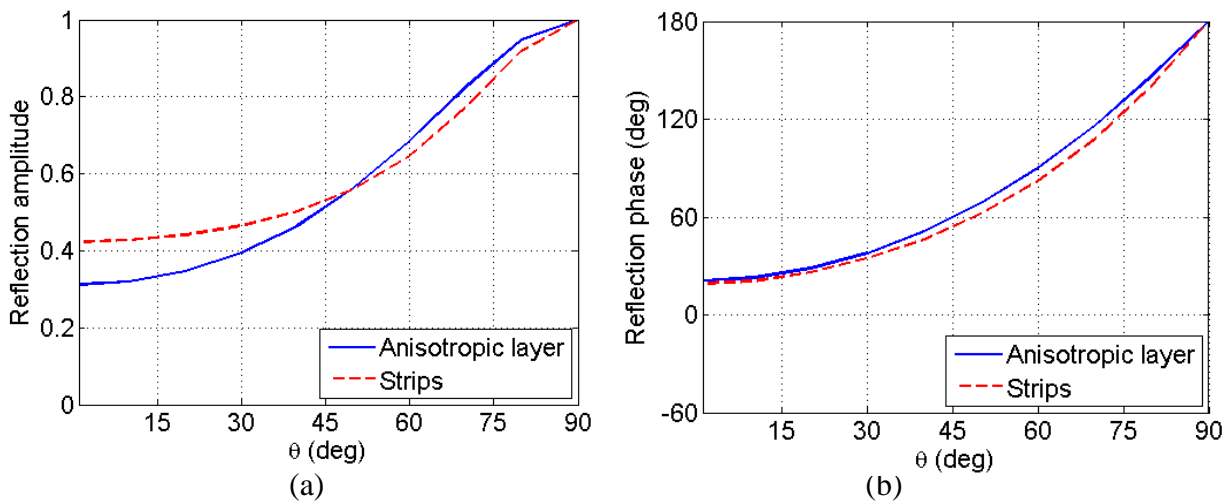
Figure 3.17. Phase of reflection coefficient of a grounded anisotropic dielectric layer and of metamaterial realization. Anisotropic layer is characterized with $\varepsilon_x = \varepsilon_z = 1.0$, $\varepsilon_y = 0.5$ and $\mu_x = 1.146$. The used cost function in optimization routine is defined by eq. (3.24). Parameters of strips are listed in Table 3.4.

(a)   (b)
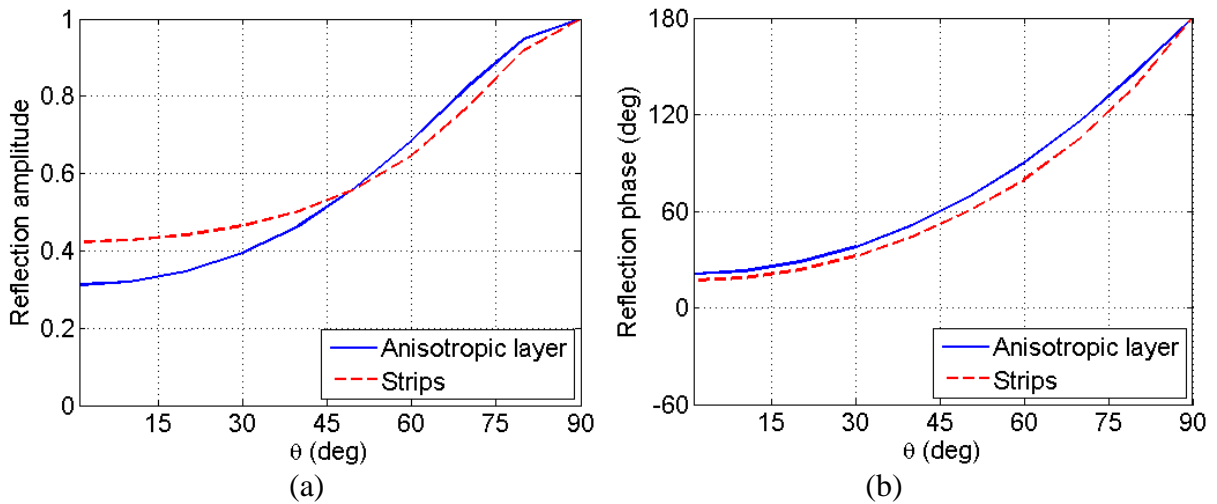
Figure 3.18. Amplitude and phase of reflection coefficient of an anisotropic dielectric layer and of metamaterial realization. Anisotropic layer is characterized with $\varepsilon_x = \varepsilon_z = 1.0$, $\varepsilon_y = 0.5$ and with $\mu_x = 1.0$. The used cost function in optimization routine is defined by eq. (3.25). Parameters of strips are listed in Table 3.4.

Figure 3.19. Amplitude and phase of reflection coefficient of an anisotropic dielectric layer and of metamaterial realization. Anisotropic layer is characterized with $\varepsilon_x = \varepsilon_z = 1.0$, $\varepsilon_y = 0.5$ and with $\mu_x = 1.146$. The used cost function in optimization routine is defined by eq. (3.25). Parameters of strips are listed in Table 3.4.
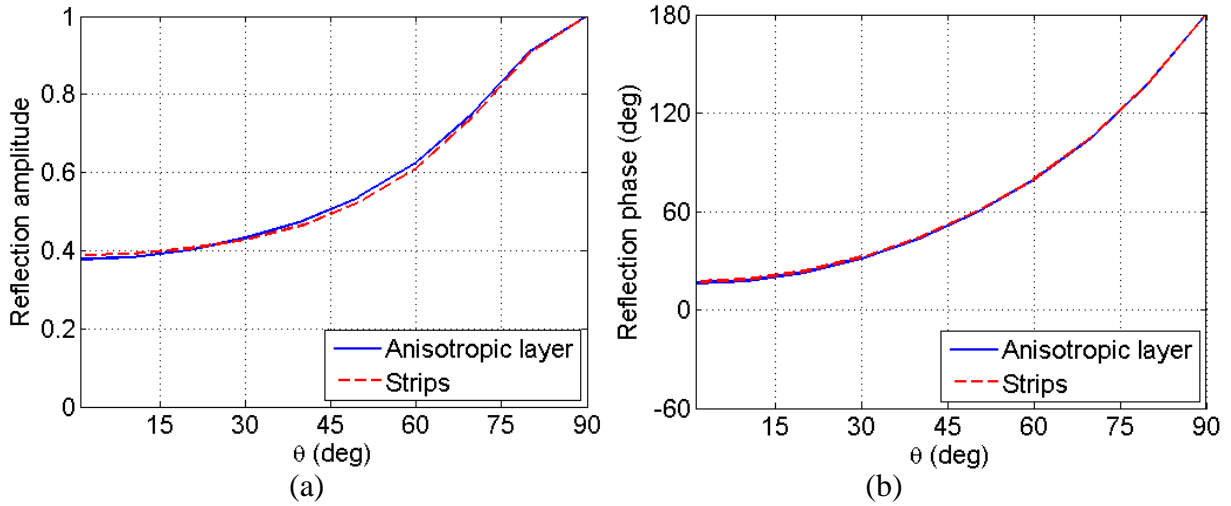

Figure 3.20. Amplitude and phase of reflection coefficient of an anisotropic dielectric layer and of metamaterial realization. Anisotropic layer is characterized with $\varepsilon_x = \varepsilon_z = 1.0$, $\varepsilon_y = 0.5$ and with $\mu_x = 1.0$. The used cost function in optimization routine is defined by eq. (3.26). Parameters of strips are listed in Table 3.4.

Figure 3.21. Amplitude and phase of reflection coefficient of an anisotropic dielectric layer and of metamaterial realization. Anisotropic layer is characterized with $\varepsilon_x = \varepsilon_z = 1.0$, $\varepsilon_y = 0.5$ and with $\mu_x = 1.146$. The used cost function in optimization routine is defined by eq. (3.26). Parameters of strips are listed in Table 3.4.
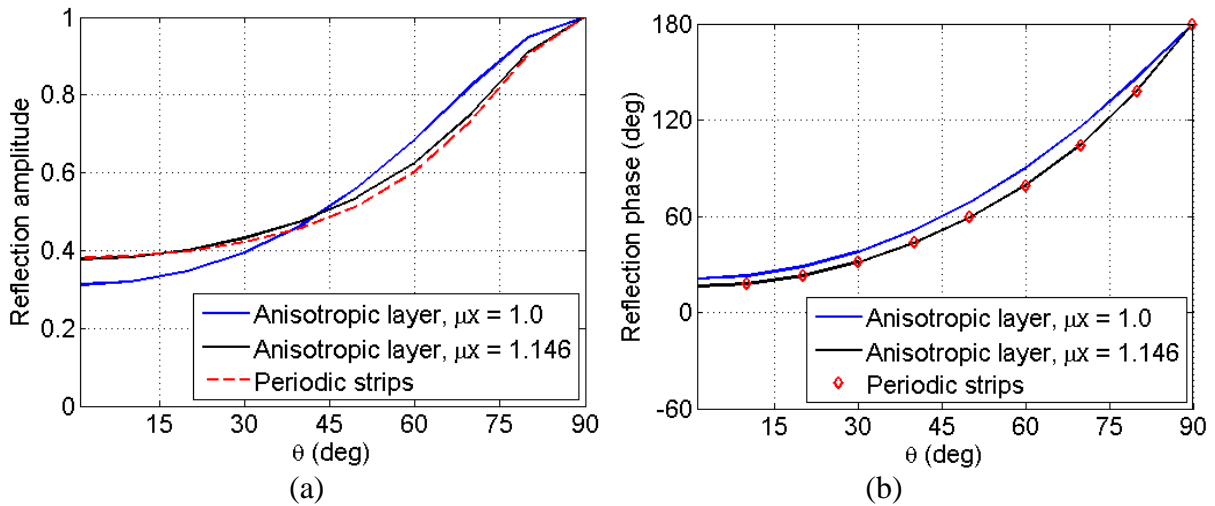

Figure 3.22. Amplitude and phase of reflection coefficient of an anisotropic dielectric layer and of metamaterial realization. Anisotropic layer is characterized with $\varepsilon_x = \varepsilon_z = 1.0$, $\varepsilon_y = 0.5$ and with $\mu_x = 1.146$. The width of the strips is determined using effective constitutive parameters approach.

TABLE 3.4. COMPARISON OF DIFFERENT REALIZATIONS OF STRIP-GRID LAYER OBTAINED USING VARIOUS OPTIMIZATION APPROACHES (CONSIDERED COST FUNCTIONS ARE DEFINED WITH EQS. (3.12) –(3.14)).

Method	Cost function	μ_x of homogeneous anisotropic structure	Optimum width of the strips (mm)	Value of effective ε_y (Figure 3.14)	Value of cost function
1	(3.12)	1.0	3.002	0.292	0.35560
1	(3.12)	1.146	0.2	0.534	0.15631
2	(3.13)	1.0	1.356	0.444	0.83416
2	(3.13)	1.146	0.986	0.485	0.09344
3	(3.14)	1.0	0.979	0.487	0.47885
3	(3.14)	1.146	1.092	0.474	0.07079
effective	-	1.0	0.9	0.5	0.89252
effective	-	1.146	0.9	0.5	0.11154

Figures 3.16 - 3.21 show the comparison of amplitude and phase of reflection coefficient of metamaterial structure obtained using three different approaches (in the first case with a PEC ground plane, so the amplitude of reflection coefficient is equal to one). Two types of quality control can be examined: similarity between reflection coefficients (as a function of incidence angle) and effective constitutive parameters of the considered metamaterial structure (when the considered metamaterial structure is not resonant the effective parameter approach gives accurate results). For that reason, for each considered case we have listed the optimized parameters, the value of the cost function and the value of effective ε_y, see Table 3.4. It can be seen that the first approach (phase of the reflection coefficient from the grounded metamaterial/anisotropic layer) gives quite good results at the first glance (see Figures 3.16 and 3.17). However, the optimized width of the strips is quite different in comparison to the value obtained by the effective parameters approach. Therefore, the first approach does not give accurate results (since the presence of the PEC plane "kills" information about the structure), so it is much better to take out the PEC ground plane (although it is present) and to consider the reflection coefficient of the structure without the ground plane.

The second approach (no PEC ground plane present and only the amplitude of reflection coefficient is considered in the definition of cost function) gives better results, i.e. more similar to the effective parameters approach. However, in this case the influence of the induced permeability ($\mu_x \neq 1.0$) is clearly seen. If we state that $\mu_x = 1.0$ (Fig. 3.18) the agreement between the amplitude of the reflected signal from two structures is not good. One can drastically improve the accuracy of the metamaterial realization simply by adding small permeability to the structure (Fig. 3.19). However, in "real" practical situations it is not obvious if we are allowed to simply add this small permeability to the designed structure.

The last approach is if the used cost function takes into account both the amplitude and the phase of the structure (Figures 3.20 and 3.21 and Table 3.4). It can be seen that the accuracy of this method is the largest (although not so different comparing to the previous case) and that the optimized width of the strips is the closest to value we would expect. Therefore, in the

rest of the report we will use the cost function defined by eq. (3.26) in the optimization process.

Final comparison gives the results for the case when we would use just effective constitutive parameters approach, see Figure 3.22 and Table 3.4. Two values of effective μ_x are considered: $\mu_x = 1.0$ and $\mu_x = 1.146$. The width of the strips is determined using effective constitutive parameters approach, i.e. the width $W = 0.9$ mm is taken from the Figure 3.15. It can be seen that there is good matching for normal incidence (almost perfect matching if we take into account that effective permeability is different from free-space for strip-loaded substrates), and that this matching is deteriorated for angles different from $\theta = 0$. If we calculate the error of this approach (i.e. the cost function using in the optimization procedure), it can be seen that this value is larger comparing to the results obtained by optimizing the strips width value, see Table 3.4.

3.4. CURVATURE EFFECTS

In the previous section we have described a design procedure in which the main step is metamaterial realization of the equivalent planar multilayer anisotropic structure. The real device will contain curved structures, so we need to transform back the planar structure. Two possibilities will be discussed in this section: conformal mapping and Bloch theory for cylindrical structures.

3.4.1. Conformal mapping

In order to take curvature effects into account we could use techniques that actually we have used for designing metamaterial devices – transformation optics. However, this procedure can lead to complicated mathematical expressions that we could evaluate only numerically. Therefore, let us consider a subgroup of transformation techniques that are suitable for this task – conformal mapping.

A function defined in the complex plane $f(z) = f(x + jy) = u(x, y) + jv(x, y)$ is conformal if it satisfies the requirements for an analytic function, i.e. Caushy-Riemann conditions:

$$\frac{\partial u}{\partial x} = \frac{\partial v}{\partial y} \quad \text{and} \quad \frac{\partial v}{\partial x} = -\frac{\partial u}{\partial y}. \tag{3.27}$$

On the other side, transformation of the area in the free-space is given by equation (3.4):

$$\boldsymbol{\mu}' = \boldsymbol{\varepsilon}' = \frac{\mathbf{A}\mathbf{A}^T}{\det \mathbf{A}}. \tag{3.28}$$

The two-dimensional conformal mapping can be expressed in three-dimensions as [33]:

$$(u, v, z) = (u(x, y), v(x, y), z) \tag{3.29}$$

By taking into account the Caushy-Riemann conditions (3.27) one can calculate Jacobian matrix:

$$\mathbf{A} = \begin{bmatrix} \partial u/\partial x & \partial u/\partial y & \partial u/\partial z \\ \partial v/\partial x & \partial v/\partial y & \partial v/\partial z \\ \partial z/\partial x & \partial z/\partial y & \partial z/\partial z \end{bmatrix} = \begin{bmatrix} \partial u/\partial x & \partial u/\partial y & 0 \\ -\partial u/\partial y & \partial u/\partial x & 0 \\ 0 & 0 & 1 \end{bmatrix} \tag{3.30}$$

The determinant |A| is equal:

$$|\mathbf{A}| = (\partial u/\partial x)^2 + (\partial u/\partial y)^2 = (\partial u/\partial x)^2 + (\partial v/\partial x)^2 \tag{3.31}$$

Therefore, the constitutive parameters of the transformed medium are equal:

$$\boldsymbol{\mu}' = \boldsymbol{\varepsilon}' = \frac{\mathbf{A}\mathbf{A}^T}{\det \mathbf{A}} = \begin{vmatrix} 1 & 0 & 0 \\ 0 & 1 & 0 \\ 0 & 0 & 1/|\mathbf{A}| \end{vmatrix} \tag{3.32}$$

In order to understand properties of the obtained transformation let us consider an example – transformation of planar layer with strips into a circular-cylindrical layer (see Figure 3.23). Let us suppose that we have already designed the metamaterial realization of anisotropic layer with permittivity smaller than one. Now we would like to see how this structure is transformed to a cylindrical layer.
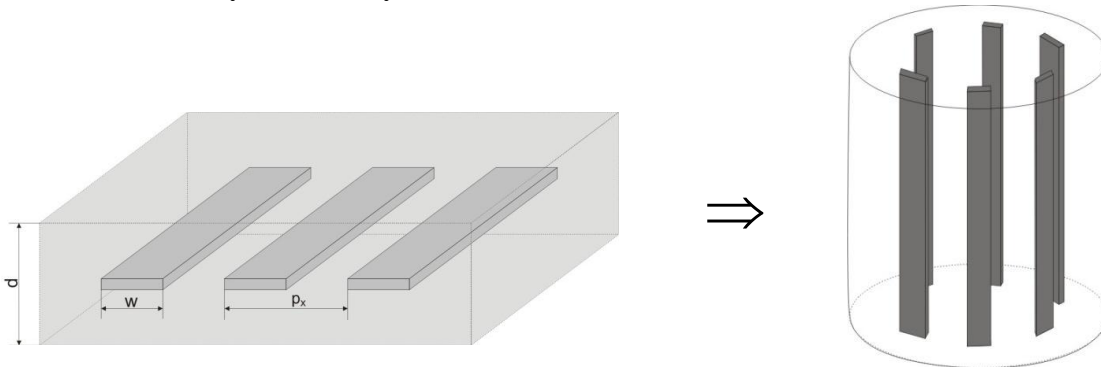
Figure 3.23. Transformation of planar to cylindrical metamaterial structure.

The conformal mapping that supports this transformation is given by ($z = x + jy$; $x = \rho_{strips} \ln(\rho)$, $y = \rho_{strips}\phi$):

$$f(z) = \exp(z/\rho_{strips}) = \exp\left([\rho_{strips}\ln(\rho) + j\rho_{strips}\phi]/\rho_{strips}\right) = \rho \cdot (\cos\phi + j\sin\phi). \tag{3.33}$$

The factor ρ_{strips} is introduced to "match" transformation from the arc length (i.e. width of the strips) to the angular coordinate. In other words, the real part of z complex variable represents the thickness of the considered layer, and the imaginary part represents the angular coordinate. The determinant of matrix **A** is equal:

$$\left|\mathbf{A}\right|(\rho,\phi) = \left(\partial u/\partial x\right)^2 + \left(\partial u/\partial y\right)^2 = \frac{1}{\rho_{strips}^2}\left(\exp(x/\rho_{strips})\right)^2 \cdot \left(\cos^2\phi + \sin^2\phi\right) = \frac{\rho^2}{\rho_{strips}^2}. \quad (3.34)$$

For example, let us consider the same strip-grid structure like in the previous section ($P_x = 3$ mm, $W = 0.9$ mm, $d = 2$ cm, $f = 4$ GHz). This structure correspond to an anistropic layer with $\varepsilon_x = \varepsilon_z = 1.0$, $\varepsilon_y = 0.5$ and $\mu_x = 1.146$. We would like to consider three cylindrical structure radii – around $0.5\,\lambda_0$, $1.0\,\lambda_0$ and $1.5\,\lambda_0$ (i.e. the number of strips in the azimuthal direction were 8, 16 and 24, respectively). Figure 3.24. shows these three cases, i.e. we compared the scattered field from a homogeneous anisotropic cylindrical layer and from the strip structure obtained by the conformal mapping. Note that only the cylindrical structure geometry is obtained using conformal mapping, and that the scattering properties of periodic cylindrical structure is calculated by in-house developed code for the analysis of cylindrical periodic structures (cylindrical FSS; description of the code is given in the Appendix). The results show excellent agreement between scattered field for structures with larger radius, and some discrepancy in the back-scattered field for the structures with small radius.
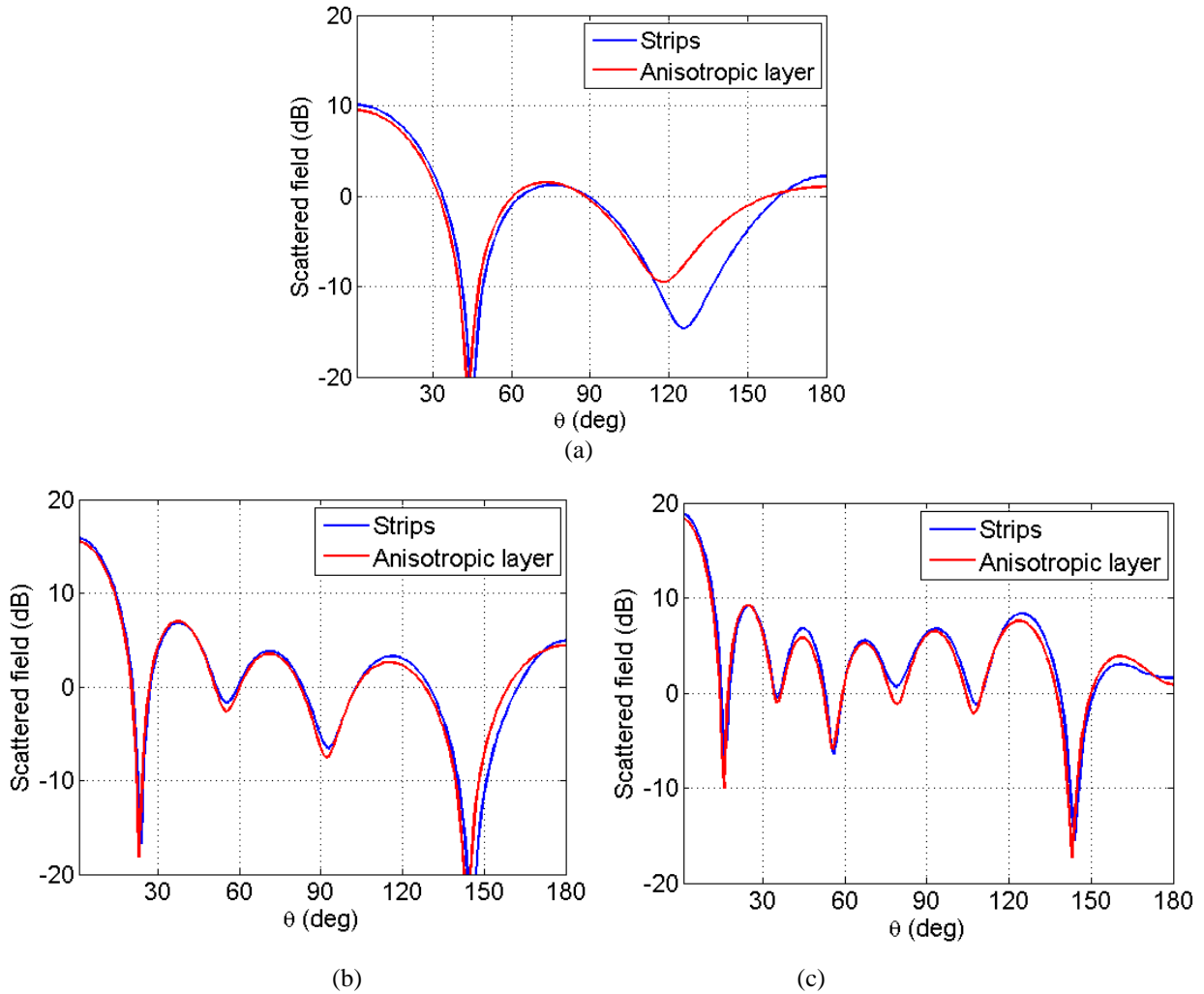
Figure 3.24. Scattered field from the periodic strip-grid structure and from the homogeneous anisotropic cylindrical shell. (a) $\rho_{strips} \cong 0.5\lambda_0$, (b) $\rho_{strips} \cong 1.0\lambda_0$, (c) $\rho_{strips} \cong 1.5\lambda_0$.

3.4.2. Bloch theory for cylindrical structures

The Bloch theory of periodic transmission lines can be extended to the cylindrical structures. The basic block of the method is a unit cell that is periodically repeated (see Figure 3.24). In our case we have quasi-periodical structure in the radial direction and periodical structure in the ϕ–direction.
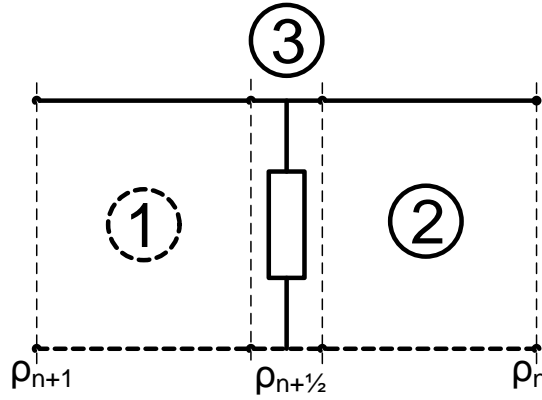
Figure 3.25. Decomposition of periodic unit cell into 3 parts.

The considered unit cell will be decomposed into 3 parts, and for each part the ABCD matrix will be determined. Then the ABCD matrix of the unit cell is equal to the product (cascade) of ABCD matrices of each part.
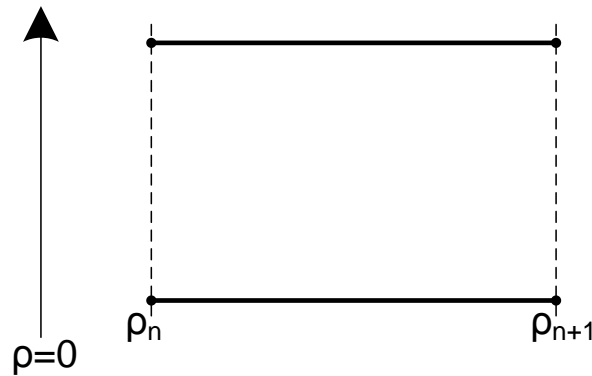
Figure 3.26. First segment of the unit cell.

The ABCD matrices describe the considered system in the following way:

$$\begin{bmatrix} U_n \\ I_n \end{bmatrix} = \begin{bmatrix} A & B \\ C & D \end{bmatrix} \begin{bmatrix} U_{n+1} \\ I_{n+1} \end{bmatrix} \tag{3.35}$$

Here subscript n represents position on the radial transmission line, i.e. n denotes the radial position ρ_n. Situation on the line is described with linear combination of two independent solutions of the Helmholtz equation. In our situation these solutions describes incoming and outgoing wave, so representation matrix for a line is:

$$\begin{bmatrix} U_n \\ I_n \end{bmatrix} = \begin{bmatrix} H_n^{(1)}(k_\rho \rho_n) & H_n^{(2)}(k_\rho \rho_n) \\ \dfrac{1}{jZ_0} H_n^{(1)}(k_\rho \rho_n)' & \dfrac{1}{jZ_0} H_n^{(2)}(k_\rho \rho_n)' \end{bmatrix} \begin{bmatrix} A_n \\ B_n \end{bmatrix} = N \begin{bmatrix} A_n \\ B_n \end{bmatrix}$$

$$\begin{bmatrix} U_{n+1} \\ I_{n+1} \end{bmatrix} = \begin{bmatrix} H_n^{(1)}(k_\rho \rho_{n+1}) & H_n^{(2)}(k_\rho \rho_{n+1}) \\ \dfrac{1}{jZ_0} H_n^{(1)}(k_\rho \rho_{n+1})' & \dfrac{1}{jZ_0} H_n^{(2)}(k_\rho \rho_{n+1})' \end{bmatrix} \begin{bmatrix} A_n \\ B_n \end{bmatrix} = M \begin{bmatrix} A_n \\ B_n \end{bmatrix}$$

(3.36)

Here A_n and B_n represents the E- and H-field, and Z_0 is the characteristic impedance of the free-space (or of the homogeneous media that fills the transmission line). From those two equations we can deduce equation for voltage and current on the line:

$$\begin{bmatrix} U_n \\ I_n \end{bmatrix} = NM^{-1} \begin{bmatrix} U_{n+1} \\ I_{n+1} \end{bmatrix},$$

(3.37)

which is equivalent to the ABCD representation, so the ABCD matrix is equal to NM^{-1}. For inverse computation we need to calculate the determinant of the matrix M. For easier computation we introduce:

$$x = k_\rho \rho_n$$
$$y = k_\rho \rho_{n+1}$$

(3.38)

$$\det M = \frac{1}{jZ_0} \ H_n^{(1)}(y) H_n^{(2)}(y)' - H_n^{(1)}(y)' H_n^{(2)}(y) \ = \frac{1}{jZ_0} \frac{-4i}{\pi k_\rho \rho_{n+1}}$$

(3.39)

Using this information we get:

$$M^{-1} = \frac{j\pi k_\rho \rho_{n+1}}{4} \begin{bmatrix} H_n^{(2)}(y)' & -jZ_0 H_n^{(2)}(y) \\ -H_n^{(1)}(y)' & jZ_0 H_n^{(1)}(y) \end{bmatrix}.$$

(3.40)

Now we have all needed expressions to determine the ABCD matrix of transmission line in the cylindrical coordinate system.

$$\begin{bmatrix} A & B \\ C & D \end{bmatrix} = NM^{-1} = \begin{bmatrix} H_n^{(1)}(x) & H_n^{(2)}(x) \\ \dfrac{1}{jZ_0} H_n^{(1)}(x)' & \dfrac{1}{jZ_0} H_n^{(2)}(x)' \end{bmatrix} \frac{j\pi y}{4} \begin{bmatrix} H_n^{(2)}(y)' & -jZ_0 H_n^{(2)}(y) \\ -H_n^{(1)}(y)' & jZ_0 H_n^{(1)}(y) \end{bmatrix} =$$

$$= \frac{j\pi y}{4} \begin{bmatrix} H_n^{(1)}(x)H_n^{(2)}(y)' - H_n^{(1)}(y)'H_n^{(2)}(x) & -jZ_0 \left(H_n^{(1)}(x)H_n^{(2)}(y) - H_n^{(1)}(y)H_n^{(2)}(x) \right) \\ \dfrac{1}{jZ_0} \left(H_n^{(1)}(x)'H_n^{(2)}(y)' - H_n^{(1)}(y)'H_n^{(2)}(x)' \right) & - \left(H_n^{(1)}(x)'H_n^{(2)}(y) - H_n^{(1)}(y)H_n^{(2)}(x)' \right) \end{bmatrix}$$

(3.41)

We can verify this matrix via the analogy with planar case. For large argument of the Hankel functions (i.e. when cylindrical structure is almost planar) we get:

$$
\begin{bmatrix} A & B \\ C & D \end{bmatrix} = \frac{j\pi y}{4}
\begin{bmatrix}
\frac{2}{\pi\sqrt{xy}} e^{jx}e^{-jy}(-j) - \frac{2}{\pi\sqrt{xy}} e^{jy}e^{-jx} j & -jZ_0 \; \frac{2}{\pi\sqrt{xy}} e^{jx}e^{-jy} - \frac{2}{\pi\sqrt{xy}} e^{jy}e^{-jx} \\
\frac{1}{iZ_0} \frac{2}{\pi\sqrt{xy}} je^{jx}e^{-jy}(-j) - \frac{2}{\pi\sqrt{xy}} je^{jy}e^{-jx}(-j) & \frac{2}{\pi\sqrt{xy}} e^{jx}e^{-jy}(-j) - \frac{2}{\pi\sqrt{xy}} e^{jy}e^{-jx} j
\end{bmatrix}
$$

$$
= \sqrt{\frac{y}{x}}
\begin{bmatrix}
\cos(x-y) & jZ_0 \sin(x-y) \\
\frac{j}{Z_0} \sin(x-y) & \cos(x-y)
\end{bmatrix}
$$

(3.42)

So for large radii the ABCD matrix of the cylindrical transmission is equivalent to the ABCD matrix of the transmission line in the Cartesian coordinate system, i.e. we have only phase shift present (and small adjustment of the amplitude since cylindrical waves decay as $1/\sqrt{\rho}$).

If the FSS admittance is known it is easy to compute the ABCD matrix. It is equal to the admittance ABCD matrix in the Cartesian coordinate system:

$$
\begin{bmatrix} A & B \\ C & D \end{bmatrix} =
\begin{bmatrix} 1 & 0 \\ Y_{FSS} & 1 \end{bmatrix}
$$

(3.43)

ABCD matrix of the unit periodic cell is equal to the product of ABCD matrices of unit cell parts. To make expressions easier to code we will introduce slightly different notation:

$$
\begin{aligned}
x &= k_\rho \rho_n \\
y &= k_\rho \rho_{n+\frac{1}{2}} \\
z &= k_\rho \rho_{n+1}
\end{aligned}
$$

(3.44)

From Figure 3.25, derivations from previous two paragraphs and using notations (3.44) we derive:

$$
\begin{bmatrix} U_n \\ I_n \end{bmatrix} = \frac{j\pi k_\rho \rho_{n+0.5}}{4}
\begin{bmatrix}
H_n^{(1)}(x)H_n^{(2)}(y)' - H_n^{(1)}(y)'H_n^{(2)}(x) & -jZ_0 \; H_n^{(1)}(x)H_n^{(2)}(y) - H_n^{(1)}(y)H_n^{(2)}(x) \\
\frac{1}{jZ_0} H_n^{(1)}(x)'H_n^{(2)}(y)' - H_n^{(1)}(y)'H_n^{(2)}(x)' & - H_n^{(1)}(x)'H_n^{(2)}(y) - H_n^{(1)}(y)H_n^{(2)}(x)'
\end{bmatrix}
\begin{bmatrix} U_{n+\frac{1}{2}} \\ I_{n+\frac{1}{2}} \end{bmatrix}
$$

$$
\begin{bmatrix} U_{n^-+\frac{1}{2}} \\ I_{n^-+\frac{1}{2}} \end{bmatrix} =
\begin{bmatrix} 1 & 0 \\ Y_{FSS} & 1 \end{bmatrix}
\begin{bmatrix} U_{n^++\frac{1}{2}} \\ I_{n^++\frac{1}{2}} \end{bmatrix}
$$

$$
\begin{bmatrix} U_{n+\frac{1}{2}} \\ I_{n+\frac{1}{2}} \end{bmatrix} = \frac{j\pi k_\rho \rho_{n+1}}{4}
\begin{bmatrix}
H_n^{(1)}(y)H_n^{(2)}(z)' - H_n^{(1)}(z)'H_n^{(2)}(y) & -jZ_0 \left(H_n^{(1)}(y)H_n^{(2)}(z) - H_n^{(1)}(z)H_n^{(2)}(y) \right) \\
\frac{1}{jZ_0} \left(H_n^{(1)}(y)'H_n^{(2)}(z)' - H_n^{(1)}(z)'H_n^{(2)}(y)' \right) & - \left(H_n^{(1)}(y)'H_n^{(2)}(z) - H_n^{(1)}(z)H_n^{(2)}(y)' \right)
\end{bmatrix}
\begin{bmatrix} U_{n+1} \\ I_{n+1} \end{bmatrix}
$$

(3.45)

To introduce even simpler notation let us introduce the following abbreviations:

$$H_n^{(1)}\ y\ = H_y^1$$
$$H_n^{(2)}\ z\ ' = \bar{H}_z^2$$
$$H_x^1 H_y^2 - H_y^1 H_x^2 = H_{xy}$$
$$H_x^1 \bar{H}_y^2 - \bar{H}_y^1 H_x^2 = \widehat{H}_{xy}$$
$$\bar{H}_x^1 \bar{H}_y^2 - \bar{H}_y^1 \bar{H}_x^2 = \bar{\bar{H}}_{xy}$$

(3.46)

The ABCD matrix of the unit cell in cylindrical coordinate system is equal:

$$
\begin{bmatrix} A & B \\ C & D \end{bmatrix} = \left(\frac{j\pi}{4}\right)^2 yz
\begin{bmatrix}
\widehat{H}_{xy}\widehat{H}_{yz} - jZ_0 Y_{FSS} H_{xy}\widehat{H}_{yz} - H_{xy}\bar{H}_{yz} \\
\dfrac{1}{jZ_0}\bar{H}_{xy}\widehat{H}_{yz} + Y_{FSS}\widehat{H}_{yx}\widehat{H}_{yz} + \dfrac{1}{Z_0}\widehat{H}_{yx}\bar{H}_{yz} \\
-jZ_0\widehat{H}_{xy}H_{yz} - Z_0^2 Y_{FSS} H_{xy}H_{yz} - jZ_0 H_{xy}\widehat{H}_{zy} \\
-\bar{H}_{xy}H_{yz} - jZ_0 Y_{FSS}\widehat{H}_{yx}H_{yz} + \widehat{H}_{zy}\widehat{H}_{yx}
\end{bmatrix}
$$

(3.47)

After grouping terms that represent elements of the ABCD matrix:

$$AL = \widehat{H}_{xy}\widehat{H}_{yz} - jZ_0 Y_{FSS} H_{xy}\widehat{H}_{yz} - H_{xy}\bar{H}_{yz}$$
$$BL = -jZ_0\widehat{H}_{xy}H_{yz} - Z_0^2 Y_{FSS} H_{xy}H_{yz} - jZ_0 H_{xy}\widehat{H}_{zy}$$
$$CL = \frac{1}{jZ_0}\bar{H}_{xy}\widehat{H}_{yz} + Y_{FSS}\widehat{H}_{yx}\widehat{H}_{yz} + \frac{1}{Z_0}\widehat{H}_{yx}\bar{H}_{yz}$$
$$DL = -\bar{H}_{xy}H_{yz} - jZ_0 Y_{FSS}\widehat{H}_{yx}H_{yz} + \widehat{H}_{zy}\widehat{H}_{yx}$$

(3.48)

we get the ABCD matrix in simplified notation:

$$
\begin{bmatrix} V_n \\ I_n \end{bmatrix} = \left(\frac{j\pi}{4}\right)^2 yz
\begin{bmatrix} AL & BL \\ CL & DL \end{bmatrix}
\begin{bmatrix} V_{n+1} \\ I_{n+1} \end{bmatrix}
$$

(3.49)

Using the Bloch Theorem in cylindrical coordinate system we can conclude that ratio of eigenvalues behaves as:

$$\frac{|\lambda(\rho_{n+1})|}{|\lambda(\rho_n)|} = \sqrt{\frac{\rho_n}{\rho_{n+1}}}$$

(3.50)

We can test that conclusion on one example. We can use SRR unit cell with $d=8$ mm from the paper [29] and for validation we have calculated eigenvalues of the above ABCD matrix, see Figure 3.27. We took the distance 1.6 cm from the origin as arefernce point and we

investigate the relative change of the eigenvalues of the ABCD matrix (we always compare eigenvalues for two neighboring ρ-coordinates). If we go further away from the origin, ratio will become more and more accurate because of the large-argument approximation.
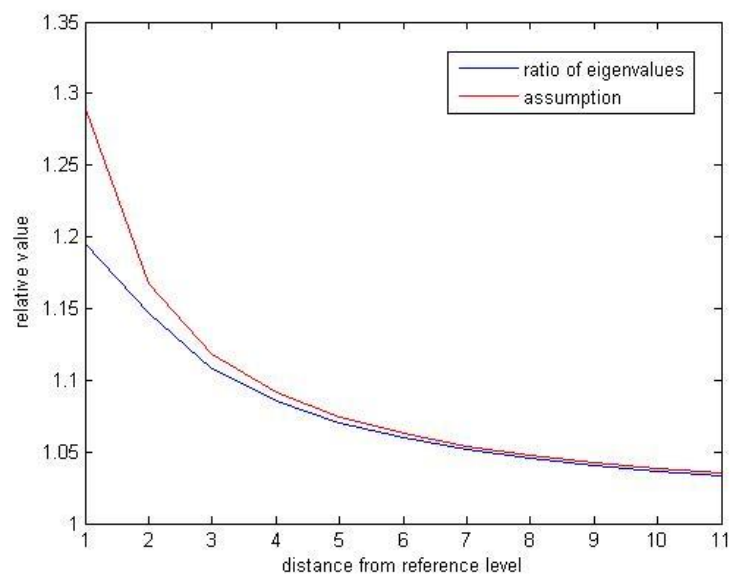
Figure 3.27. Validation of expression (3.50). Distance 1.6 cm from the origin is taken as a reference point.

The described ABCD matrix approach represent a powerful tool for analyzing multilayer periodic cylindrical structures. One just need to analyze each layer separately (more precisely one just needs to determine YFSS of each cylindrical layer with FSS), and the ABCD approach construct the solution for the multilayer case. This approach also simplifies the optimization process since it is possible to separate the original complex problem into several simpler sub-problems.

4   EXAMPLES

EXAMPLES

4.1 PERMITTIVITY TAILORING – LAYERS WITH STRIPS

The basic structure that enables permittivity values smaller than one (or even negative) are periodic wires or strips (their shape can be curved in order to obtain the desired performances). We would like to test the described design procedure on a more complex structure (comparing the one given in the previous section). Let us consider a four-layer homogeneous anisotropic structure with the following parameters (the working frequency is 4 GHz):
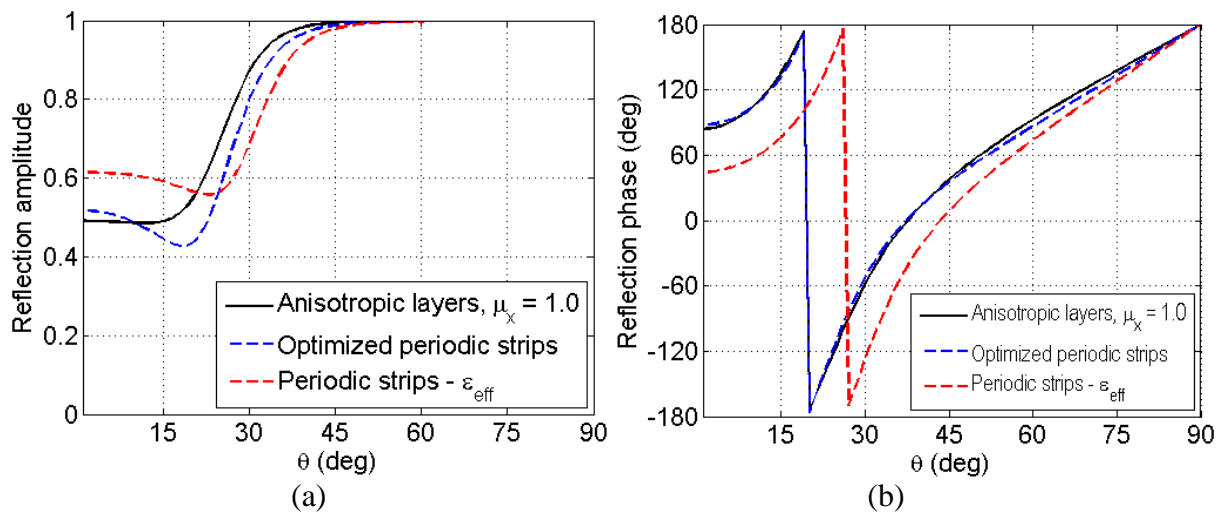
TABLE 4.1. CONSTITUTIVE PARAMETERS OF ANISOTROPIC MULTILAYER HOMOGENEOUS STRUCTURE.

| layer	thickness (cm)	permittivity
1	2	$\varepsilon_x = \varepsilon_z = 1.0, \ \varepsilon_y = 0.125$
2	2	$\varepsilon_x = \varepsilon_z = 1.0, \ \varepsilon_y = 0.25$
3	2	$\varepsilon_x = \varepsilon_z = 1.0, \ \varepsilon_y = 0.3755$
4	2	$\varepsilon_x = \varepsilon_z = 1.0, \ \varepsilon_y = 0.5$

We would like to realize such a structure using layers with strip-grids (see Fig. 4.1). Let the periodicity of the strips is $P_x = 3$ cm (like in the previous example). The parameter that we would like to determine is the width of the strips in each layer (therefore, we have an optimization problem with four unknowns). Two approaches are possible: using the design procedure that we have described in previous section, or simply to take the width that is determined for each layer by considering the effective parameters of isolated layer (i.e. the width values are determined from Figure 3.15). The results obtained by two design methods are described in Figures 4.2 and 4.3. In the optimization procedure there are two possible approaches regarding the permeability values of the equivalent homogeneous anisotropic structure: either to simply state that $\mu_x = 1.0$ (Figure 4.2) or to take expected value of the induced x-component of the permeability tensor $\mu_x = 1.2$ (Figure 4.3). It can be seen that if we include in the optimization procedure the expected induced value of the permeability tensor the obtained scattering parameters are much more close to the scattering parameters of the homogeneous anisotropic multilayer structure. Furthermore, the determined widths of the strips are much more close to the values obtained by considering effective constitutive parameters of a single-layer structure (i.e. the width is determined from Fig. 3.15). One should also notice that if we select $\mu_x = 1.0$ the widths of the strips are not monotonically decreasing, i.e. the obtained structure does not have physical picture like the case when $\mu_x = 1.2$. These results are summarized in Table 4.2.
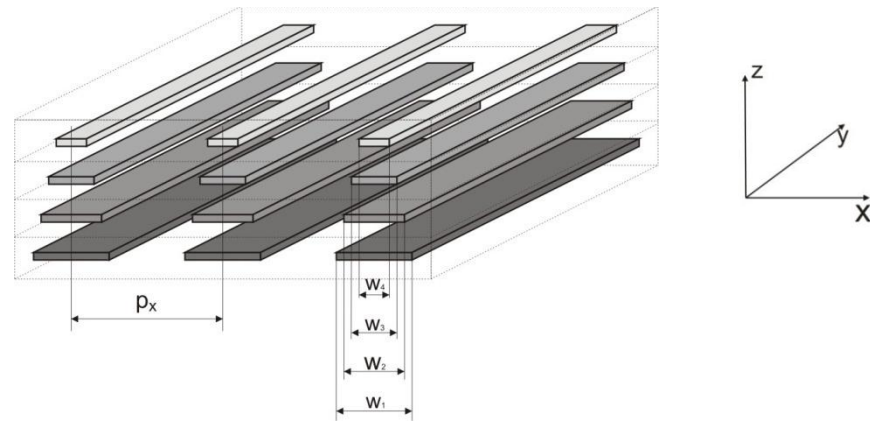
Figure 4.1. Multilayer metamaterial structure containing periodic metal strips

Figure 4.2. Amplitude and phase of reflection coefficient of an anisotropic dielectric multilayer structure and of metamaterial realization. Anisotropic layer is characterized with constitutive parameters given in Table 4.1 (permeability $\mu_x = 1.0$). The width of the strips is given in Table 4.2.
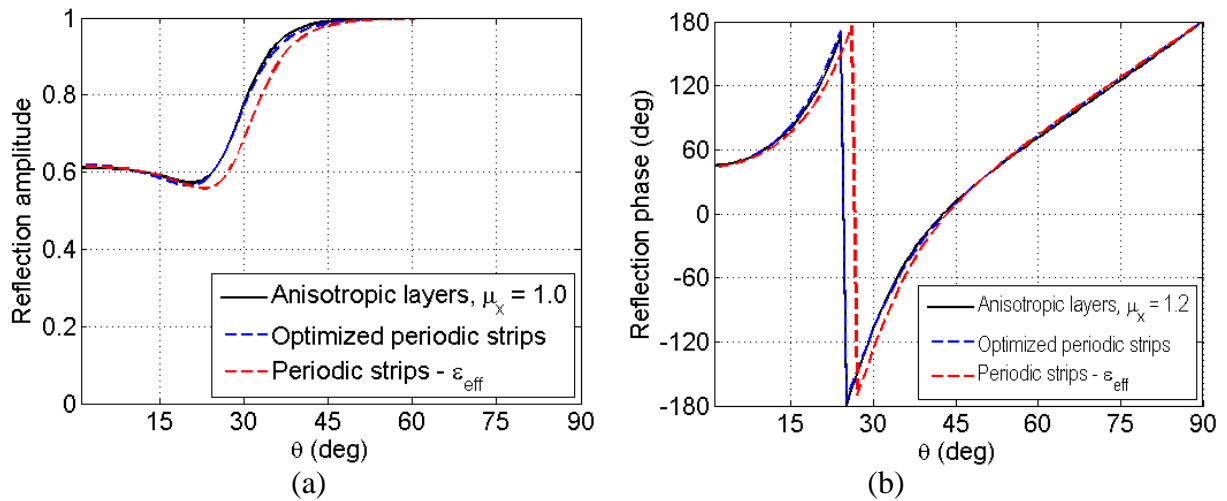
Figure 4.3. Amplitude and phase of reflection coefficient of an anisotropic dielectric multilayer structure and of metamaterial realization. Anisotropic layer is characterized with constitutive parameters given in Table 4.1 (permeability $\mu_x = 1.2$). The width of the strips is given in Table 4.2.

TABLE 4.2. COMPARISON OF DIFFERENT REALIZATIONS OF STRIP-GRID LAYER OBTAINED USING OPTIMIZATION APPROACH AND EFFECTIVE PARAMETERS APPROACH.

Method	μ_x of homogeneous anisotropic structure	Optimum width of the strips (mm)	Value of effective ε_y (Figure 3.4)	Value of cost function
optimization method	1.0	$W_1 = 2.79$ $W_2 = 5.76$ $W_3 = 2.01$ $W_4 = 2.41$	$\varepsilon_y = 0.310$ $\varepsilon_y = 0.075$ $\varepsilon_y = 0.379$ $\varepsilon_y = 0.343$	0.60819
optimization method	1.2	$W_1 = 6.36$ $W_2 = 3.00$ $W_3 = 2.84$ $W_4 = 0.67$	$\varepsilon_y = 0.029$ $\varepsilon_y = 0.292$ $\varepsilon_y = 0.306$ $\varepsilon_y = 0.536$	0.23724
effective parameters	1.0	$W_1 = 5.11$ $W_2 = 3.53$ $W_3 = 2.05$ $W_4 = 0.9$	$\varepsilon_y = 0.125$ $\varepsilon_y = 0.25$ $\varepsilon_y = 0.375$ $\varepsilon_y = 0.5$	4.33642
effective parameters	1.2	$W_1 = 5.11$ $W_2 = 3.53$ $W_3 = 2.05$ $W_4 = 0.9$	$\varepsilon_y = 0.125$ $\varepsilon_y = 0.25$ $\varepsilon_y = 0.375$ $\varepsilon_y = 0.5$	0.72906

Here we will mention just one possible application of such structures. In some cases we would like to make the radiation of basic antennas (like dipoles) more directive. That can be made by placing a layer that has permittivity smaller than one in front of the non-directive

antenna (see Fig. 4.4). In this example we will place the four-layer metamaterial structure from Fig. 4.3 (and Table 4.2) in front of a dipole antenna, i.e. this multilayer structure will act as a collimating lens. The parameter of interest is radiation pattern in H-plane, see Fig. 4.5. It can be seen that we managed to obtain the directive pattern, and that practically there is no difference in results obtained using homogeneous anisotropic structure and real metamaterial periodic structure. Reflections from the metamaterial planar lens introduce the losses of 2 dB in the main beam in the main beam direction, but this can be improved with a careful design.
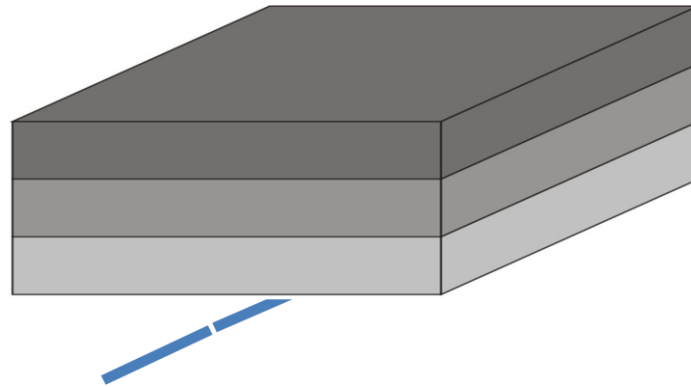
Figure 4.4. Dipole antenna with planar metamaterial lens.
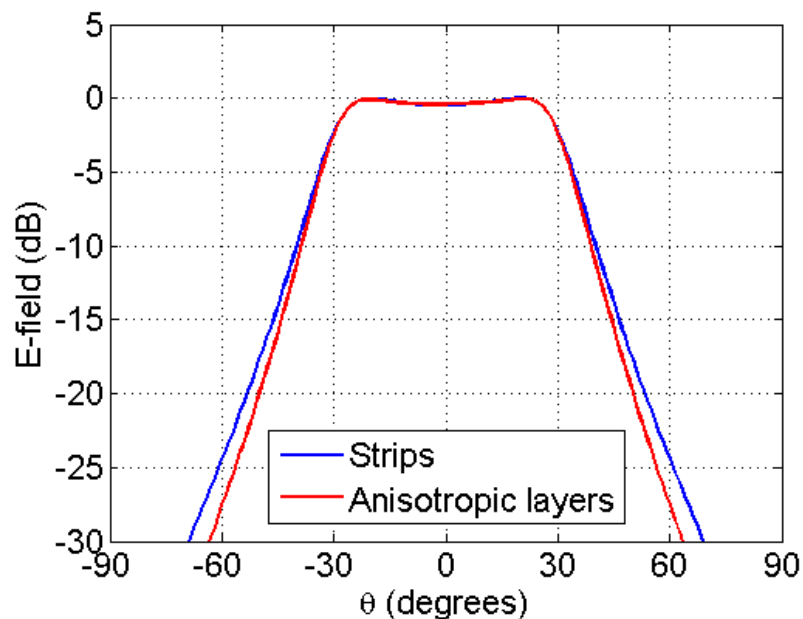
Figure 4.5. H-plane radiation pattern of a dipole antenna with planar metamaterial lens.

4.2 PERMEABILITY TAILORING
– LAYERS WITH SPLIT-RING RESONATORS

Split-ring resonators (SRRs) are usually used when permeability with negative or close to zero values is needed. The main disadvantage of SRR elements is their resonant behavior. In other words, the negative and near-to-zero values of permeability appear for frequency in the vicinity of the resonant frequency (more precisely, for frequencies larger than resonant frequency). This resonant behavior makes practical designs very difficult. As it is shown in previous chapter the bandwidth of such structures is very narrow. Even if we are „satisfied" with narrow bandwidth it is still extremely hard to design some practical structure. The main reason again lies in the resonant behavior and non-perfectness of all electromagnetic solvers (including the commercial ones). This non-perfectness is shown, for example, in the shift of calculated resonant frequency (disadvantage of all commercial solvers), which is very critical when designing metamaterial structures. Furthermore, due to non symmetry of the structure, bianisotropy effects are induced, i.e. the constitutive relations are now

$$\mathbf{D} = \boldsymbol{\varepsilon} \cdot \mathbf{E} + \boldsymbol{\xi} \cdot \mathbf{H}$$
$$\mathbf{B} = \boldsymbol{\zeta} \cdot \mathbf{E} + \boldsymbol{\mu} \cdot \mathbf{H}$$

(4.1)

This resonant and bianisotropy behavior of SRRs makes extraction of effective parameters extremely difficult. With the described method of extraction from the reflection and transmission coefficients of normal incident plane wave, we actually extract each the parameter twice (see Table 3.3). The agreement between the extracted parameters for two different excitation direction indicate us what is the accuracy of the proposed method. For example, let us try to extract the constitutive parameters from the SRR structure from Figure 4.6. The parameters of the structure are: a = 5.25 mm, g = d = 0.125 mm, w = 3.75 mm. The most important components of the constitutive parameters are μ_{yy} (the negative or near-to-zero permeabilty that we want to obtain) and ε_{zz}. Note that H_y is inducing an electric dipole in the z-direction, and E_z is inducing a magnetic dipole in the y-direction (therefore, these two components are strongly coupled). Figures 4.7 – 4.9 shows the extracted effective parameters obtained by CST Microwave studio, and Figure 4.10 the effective permeability obtained by in-house moment method program. The attempt to extract the effective parameters had lead to the following conclusions:

(1) The method of extraction of parameters is not accurate close to the resonant frequency.. It can be seen that all three considered components of effective constitutive parametsres (μ_{yy}, ε_{zz}. and ε_{xx}) strongly depends on the method of extraction around the resonant frequency (i.e. in the frequency range of interest). This effect is mostly due to bianisotropy nature of SRRs. However, even if we take bianisotropy into account (see [29]) the retrieval method is still not accurate around the resonant frequency.

(2) The calculated resonant frequency depends on the selected electromagnetic solver. In order to illustrate that we have analyzed the same structure with the in-house developed electromagnetic solver based on the Moment Method. Figure 4.10 shows the extracted values of μ_{yy}. It can be seen that the extracted curve has the same shape like for the results obtained by CST Microwave Studio, but the resonant frequency is more than 1 GHz lower. This (unknown) shift of the resonant frequency is disadvantage of all nowadays electromagnetic solvers, and only the measurements can show how large is that difference.

(3) There are strong mutual coupling effects between the layers with SRR elements. To illustrate this effect let us consider 4-laer structure consisting of identical SRR elements (the unit cell therefore contains 4 cubes from the Figure 4.11). It can be seen that the mutual coupling effects are extremely strong around the resonant frequency, and that it is not possible to say what are the values of the equivalent effective parameters for frequencies around the resonant frequency. Such strong effects are not present when building layers from non-resonant elements (or from resonant elements with different enough resonant frequency). To illustrate that we have considered 4-layer structure of strip grids (of identical period and strip width; the period P_x was 30 mm, the layer thickness d was 30 mm and the width of the strips W was 0.9 mm). It can be see that there is almost no difference of extracted effective parameters for one-layer and four-layer structures, except around resonant frequencies of a Fabry-Perot resonator built from partly reflective mirrors (i.e. partly reflective periodic structures). Therefore, in practical metamaterial designs the resonant elements should be avoided (if possible).
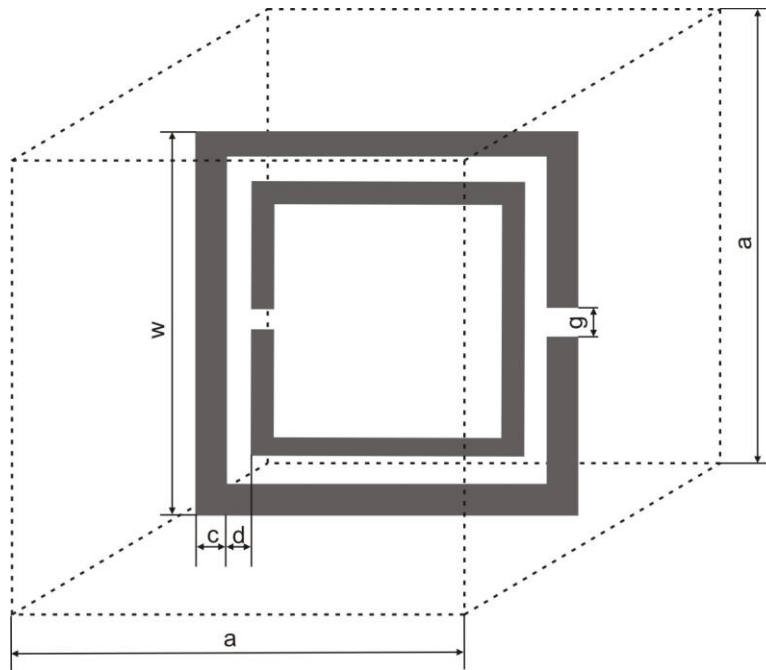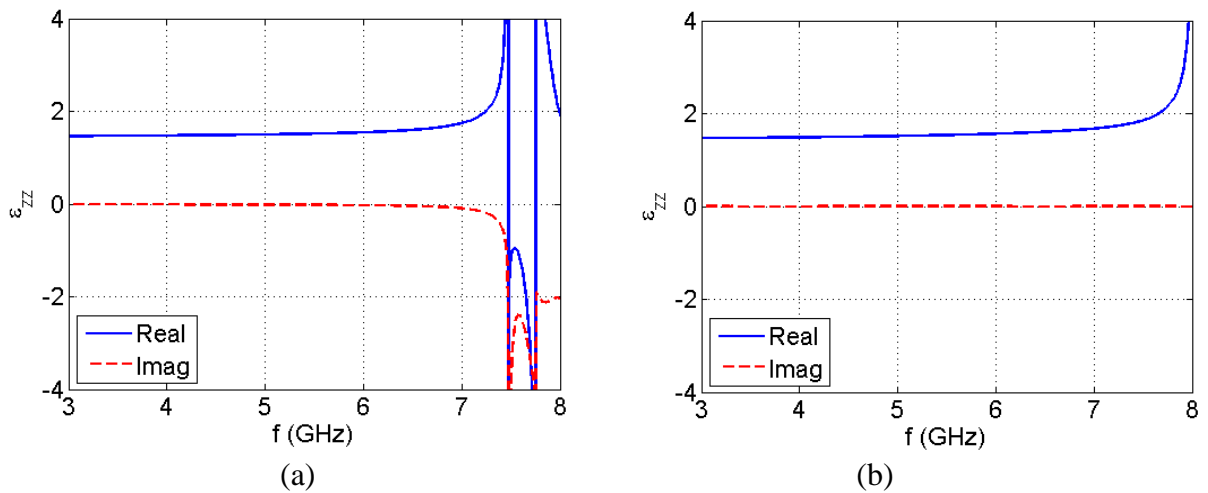

Figure 4.6. Sketch of the unit cell of split-ring structure.

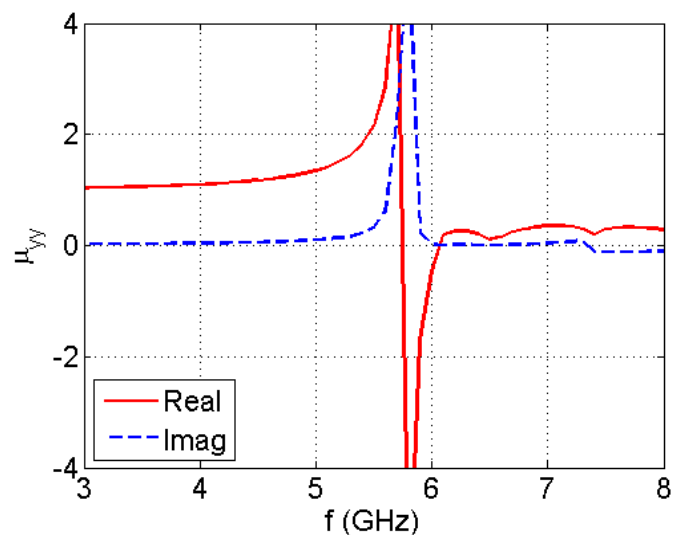(a)   (b)
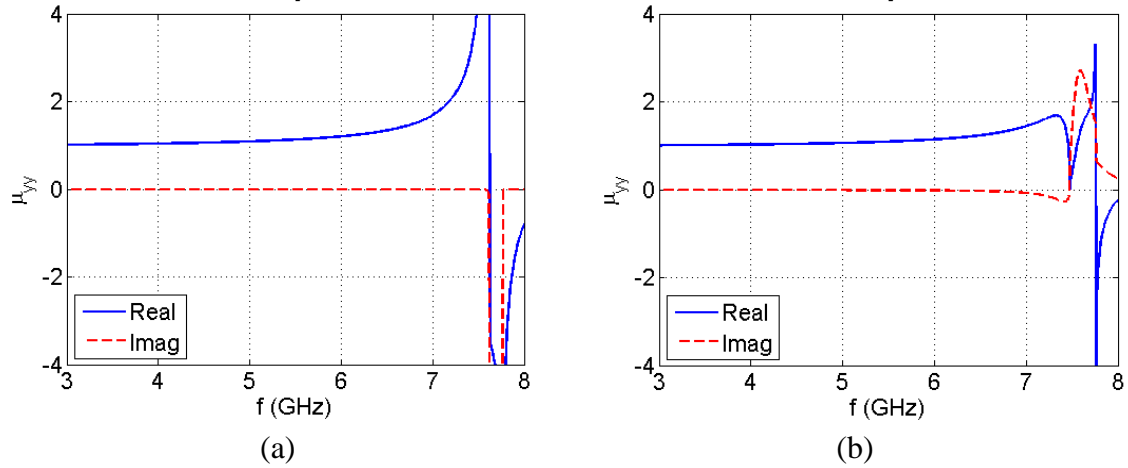
Figure 4.7. Extracted μ_{yy} for the structure in Fig. 4.6; (a) TE2 way, (b) TM1 way of retrieval of effective parameters (definitions are given in Fig. 3.10 and Table 3.3).
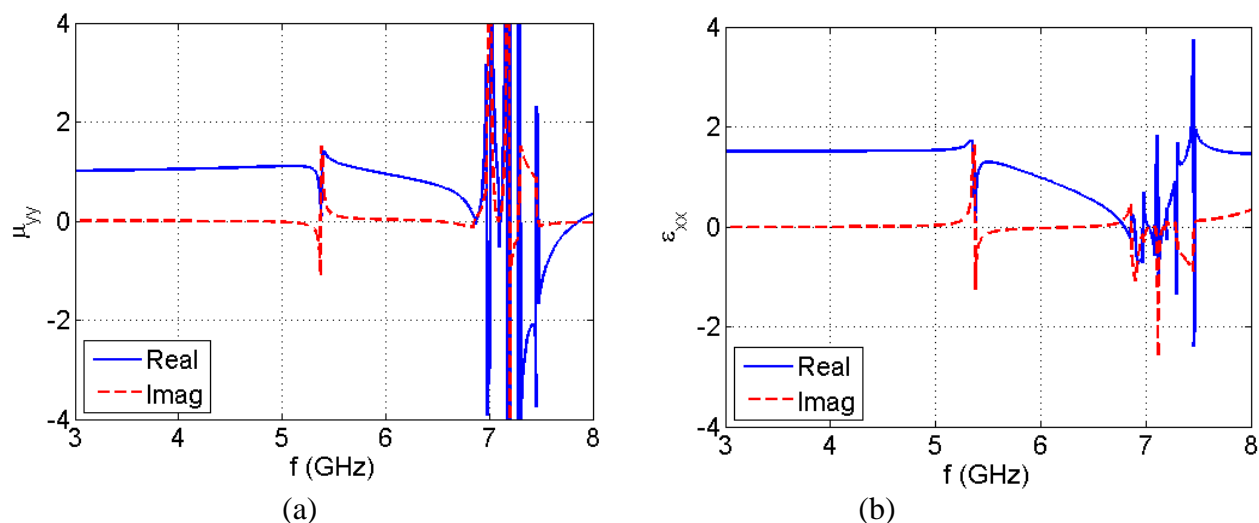

(a)   (b)
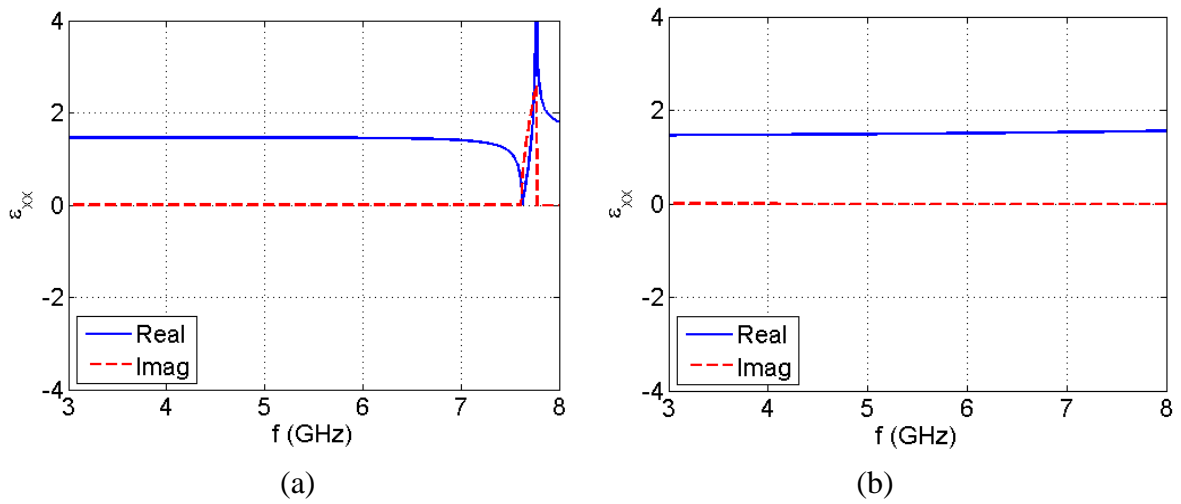
Figure 4.8. Extracted ε_{xx} for the structure in Fig. 4.6; (a) TM1 way, (b) TE3 way of retrieval of effective parameters (definitions are given in Fig. 3.10 and Table 3.3).
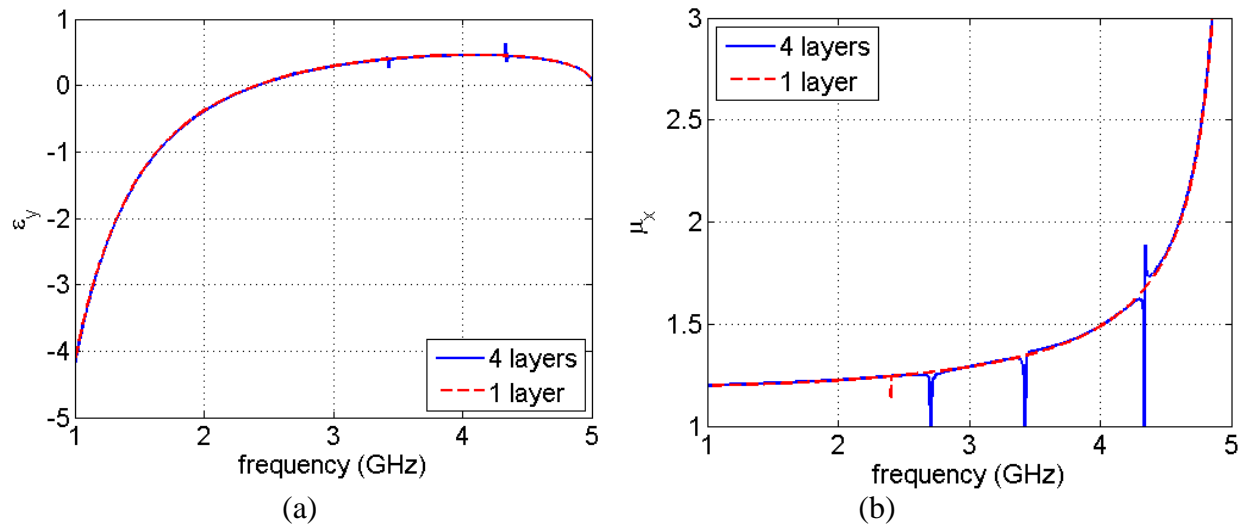

(a)   (b)

Figure 4.9. Extracted ε_{zz} for the structure in Fig. 4.6; (a) TE2 way, (b) TM3 way of retrieval of effective parameters (definitions are given in Fig. 3.10 and Table 3.3).

Figure 4.10. Extracted μ_{yy} of the structure in Fig. 4.6 obtained by the Moment Method.

Figure 4.11. Extracted μ_{yy} of the4-layer structure in Fig. 4.6; (a) TE2 way, (b) TM1 way of retrieval of effective parameters (definitions are given in Fig. 3.10 and Table 3.3).

Figure 4.12. Extracted μ_{yy} of the strip-grid 4-layer structure in Fig. 4.6; (a) TM1 way, (b) TE3 way of retrieval of effective parameters (definitions are given in Fig. 3.10 and Table 3.3).

4.3 ROTATORS OF POLARIZATION

In this section we will give an example of designing metamaterial device that cannot be realized using effective constitutive parameters, but that can be designed using reflection and transmission coefficients approach.

Rotators of polarization and polarizers find their applications in microwave systems, where it is required to change the polarization of an electromagnetic wave. It is very well known that a periodic structure of parallel wires or strips can rotate plane of polarization of a linearly polarized wave by a desired angle over a broad frequency range. In order to obtain a high accuracy with this design in a broad frequency range, and improve the transmission coefficient at the same time, it is necessary to use a great number of screens. That automatically means significantly increase in both the polarizer thickness and weight of the system. Utilizing a smaller amount of screens the change from linear to elliptical or circular polarization is observed in higher frequency bands [35].

Our realizations will be made from multilayered thin screens that are two dimensional periodic structures with period much smaller than the wavelength (therefore is called metamaterial structure). Different geometries for unit cell realizations will be considered. Unit cell will be made from two separated surfaces. One will be at the edge, and second will be in the middle of the cell. Idea is to discretely rotate the middle part of unit cell in separated screens. After several steps screens elements will be rotated for 90 degrees. So, at the front side element is oriented in one direction and on the back side element is oriented perpendicular to the first direction. It is reasonable to expect that in some frequency range the designed device works as a rotator. All realizations are simulated in CST Microwave Studio.

1st design

As a first design we considered a slot in the middle of the patch which is surrounded by the free space. There is a cascade of 7 thin screens and slot is rotated by 15 degrees between screens in negative direction. System is excited by a plane wave orthogonally to the surface of the system.
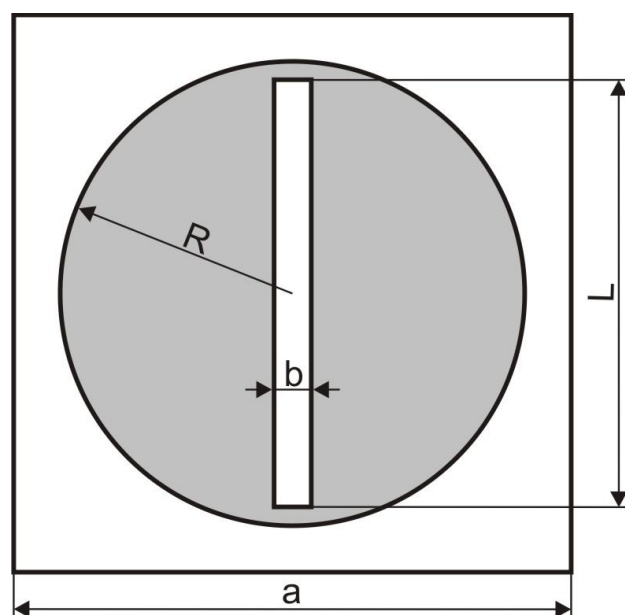

Figure 4.13. 1st design: slot in a patch, a=10 mm, L=8 mm, R=4.5 mm, b=1mm

This unit cell doesn't have a load (metal insert) in the slot so we cannot expect resonant behavior in the frequency range of interest. In all other realizations an inverted geometry will be used.
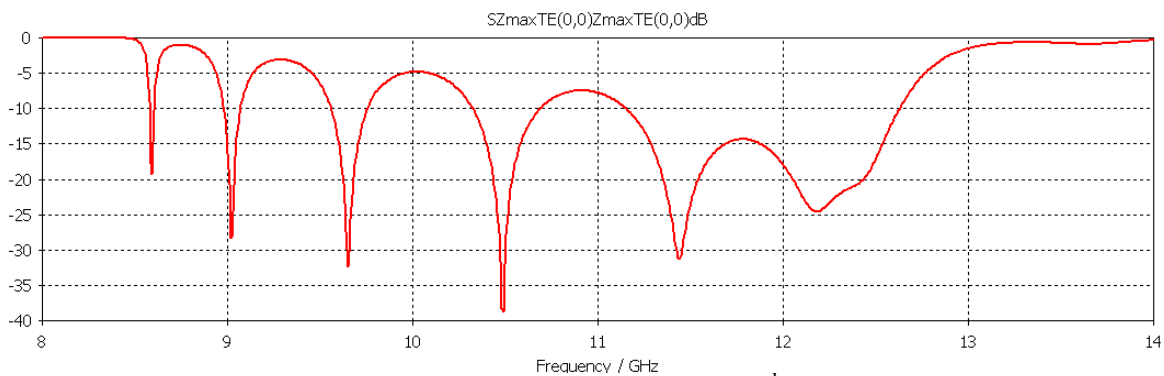
2nd design

This realization is a complementary structure to the previous design. From the Babinet principle we can expect broader bandwidth (frequency range with S_{11} below -10 dB). Starting geometry is equal to the starting geometry in previous realization (a=10 mm, L=8 mm, R=4.5 mm, b=1mm).
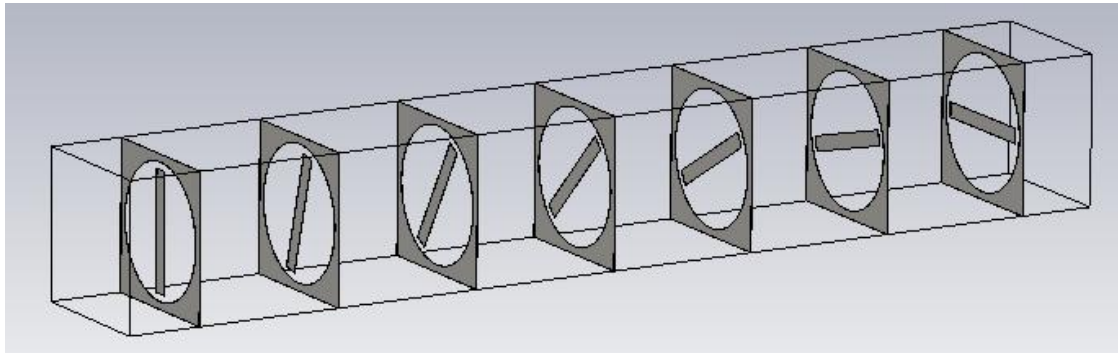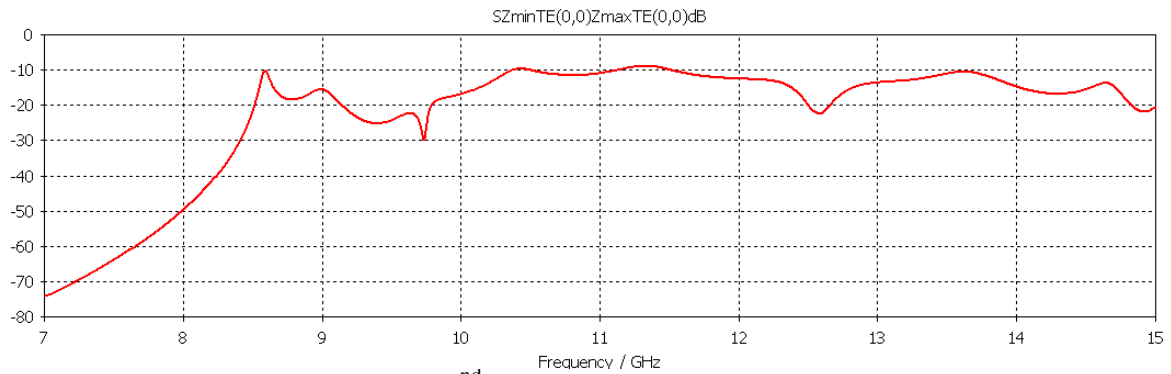

Figure 4.14. System with rotating effect
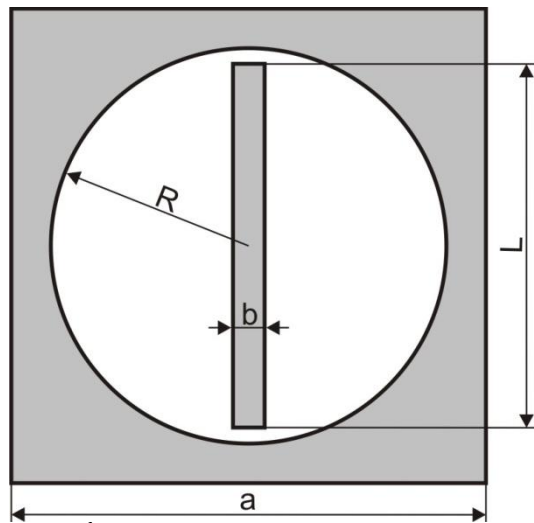
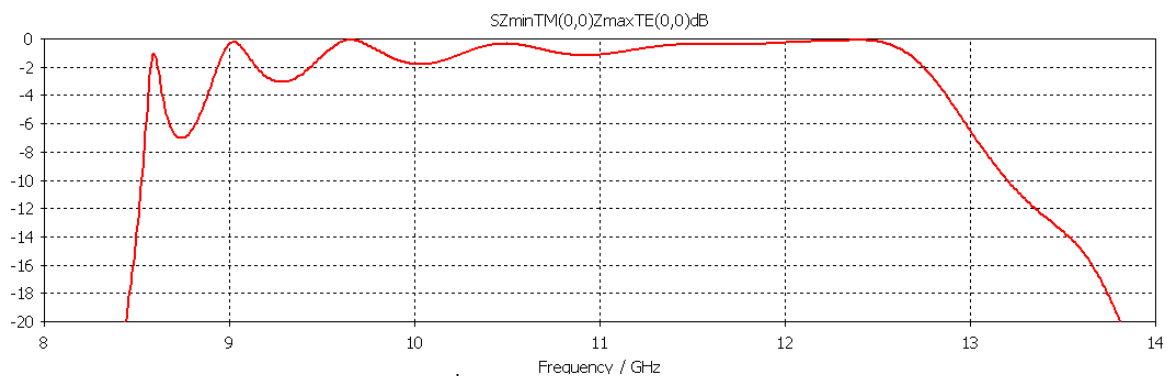**Figure 4.15.** 2nd design: dipole in a slot surrounded by metal
(a=10 mm, L=8 mm, R=4.5 mm, b=1 mm)


Figure 4.16. S_{11} parameter of the 2nd design

Figure 4.17. S_{21} parameter of the 2nd design, coupling between TE input and output waves

Figure 4.18. S_{21} parameter of the 2nd design, coupling between TE input and TM output wave

First geometry have bandwidth of approximately 1 GHz (between 11.5 and 12.5 GHz), and in that range cross-coupling S_{21} coefficient (TE input plane wave and TM output plane wave) is below -2dB. In that range 2nd design behaves as an excellent rotator.

If we want rotator in lower frequency range we have to increase the unit cell size. Also, we can change the cell geometry (and keep the same outer cell dimensions), and by changing the geometry parameters try to change frequency range of interest. First idea is to reduce distance between neighboring screens. In Figures 4.19 and 4.20 results for several screen distances are shown.
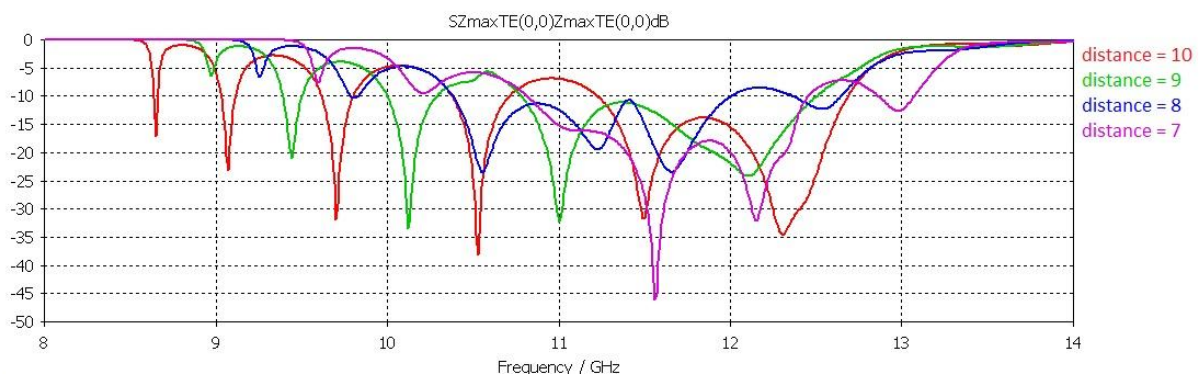
Figure 4.19. S_{11} parameter as a function of distance between neighboring screens
(distance is 10mm, 9 mm, 8 mm and 7 mm, respectively)
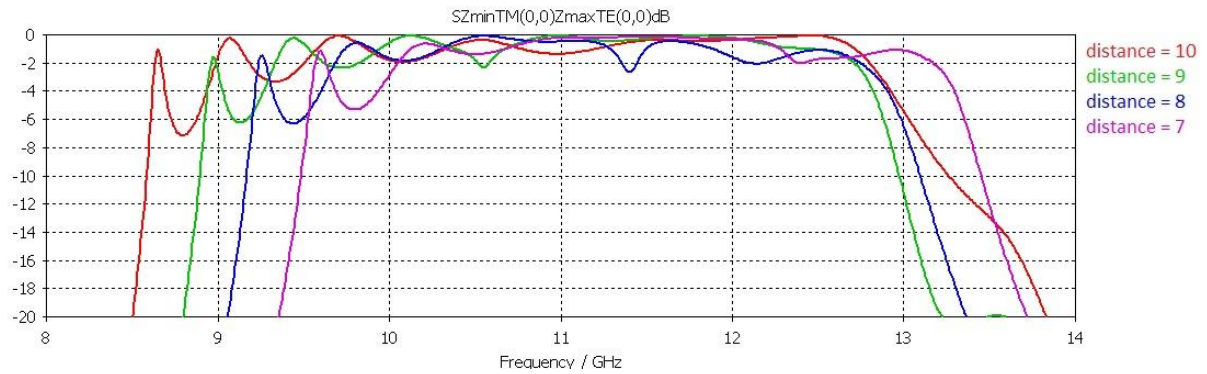
Figure 4.20. S21 parameter as a function of distance between neighboring screens (coupling between TE input and TM output wave; distance is 10mm, 9 mm, 8mm and 7 mm)

With smaller distance between screens realization becomes more compact, and also the working frequency is shifted to the lower frequencies. Second idea is to increase dipole length *L*. With larger middle metal element capacitance between edge and middle element is also increased and shift to the lower frequencies is expected. As it can be seen in Figures 4.21 and 4.22, the operating frequency is shifted from 11 GHz to 10 GHz, and the bandwidth is also increased from 1 GHz to almost 1.5 GHz.
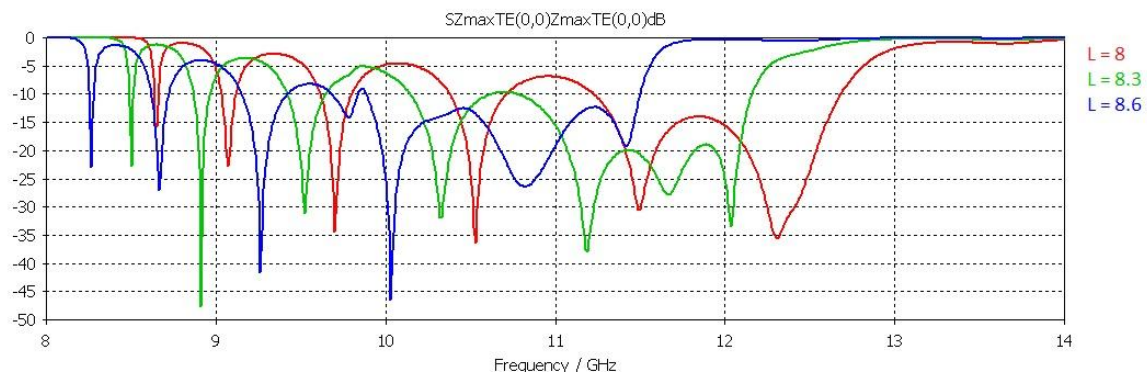
Figure 4.21. S_{11} parameter as a function of dipole length (*L*=8 mm, 8.3 mm and 8.6 mm)
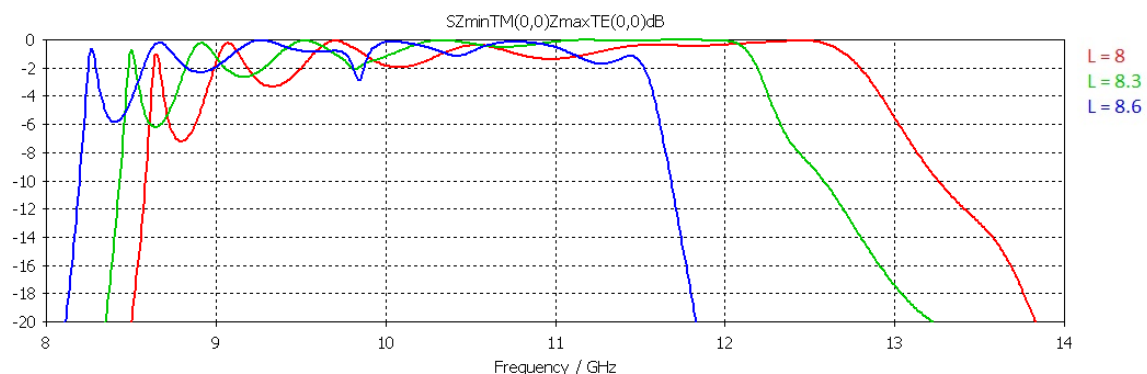
Figure 4.22. S_{21} parameter as a function of dipole length (coupling between TE input and TM output wave; *L*=8 mm, 8.3 mm and 8.6 mm)

3rd design

In order to increase capacitance some changes in the middle element geometry could be made. Idea is to increase contact surface between element and edge, and by that to increase capacitance between load and surrounding metal. Therefore, we have added an arch to the dipole. By changing the parameters g, r and ß we can affect that capacitance.
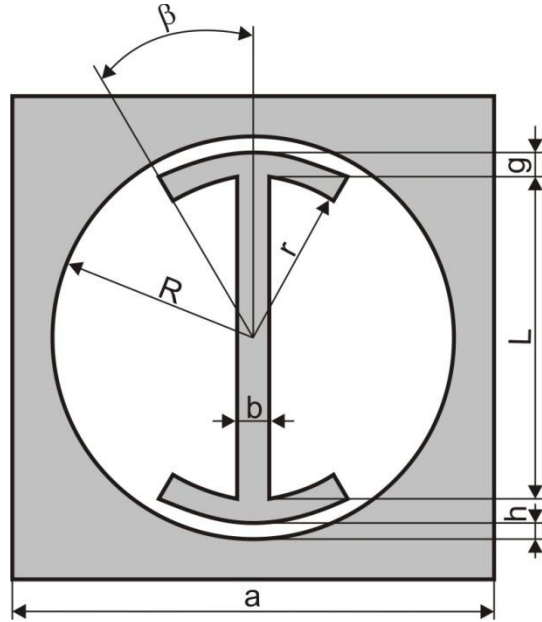
Figure 4.23. 3rd design: dipole in the slot surrounded with metal. An arch at the top and bottom of dipole are introduced to increase capacitance (g=0.2,ß=45)
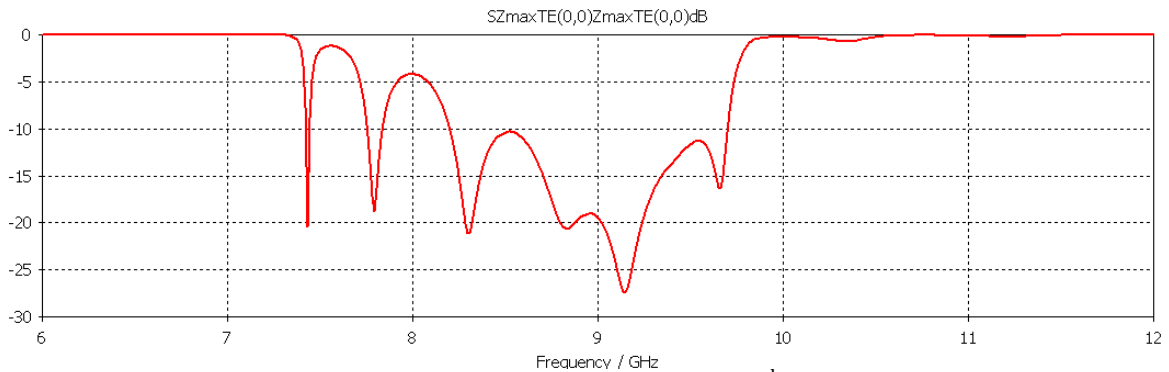
Figure 4.24. S$_{11}$ parameter of the 3rd design
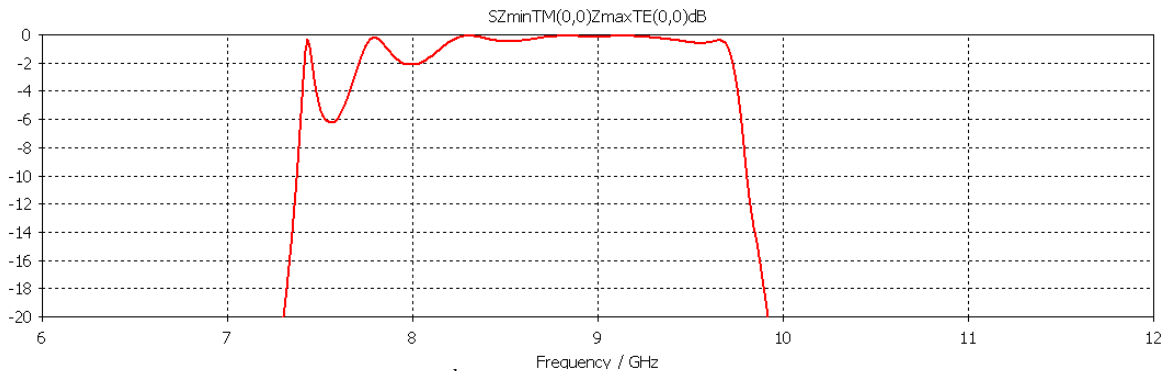
Figure 4.25. S$_{21}$ parameter of the 2nd design, coupling between TE input and TM output wave

In this realization there is a shift of the working frequency to the lower frequencies because of increased capacitance between the dipole element and surrounding metal. If we reduce distance between layers from 10 mm to 8 mm we get S_{11} which is unusable in practice.
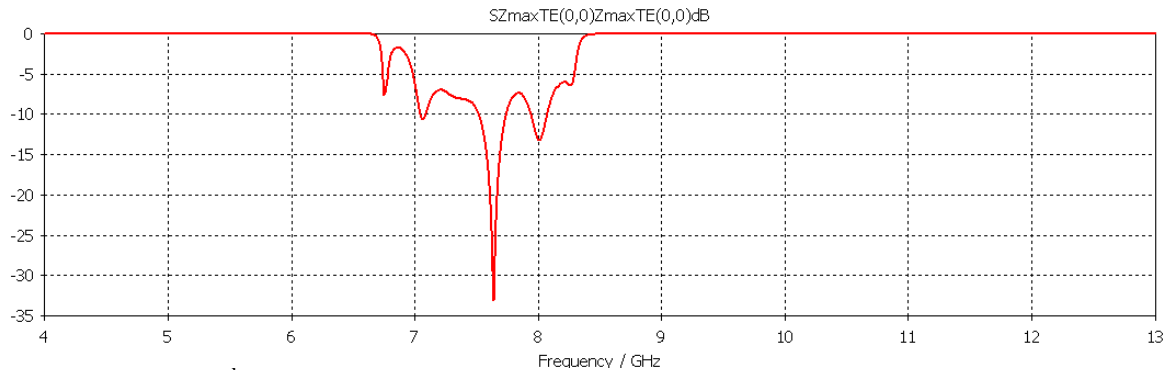
Figure 4.26. 3rd design: S_{11} parameter for structure with 8 mm distance between layers

First idea how to improve the design is to increase parameter *g* (Fig. 4.23). Increasing the g distance between arch and surounding metal is decreased and capacitance is increased. We can expect shift to the lower frequencies.
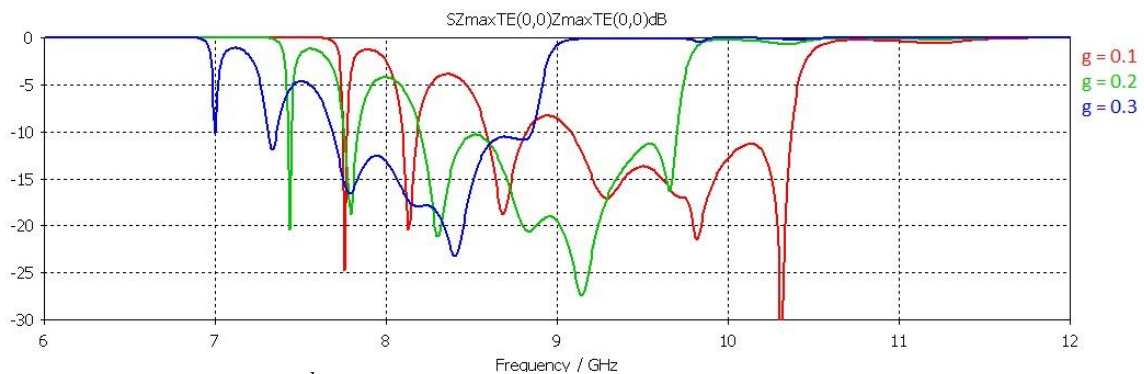
Figure 4.27. 3rd design: S_{11} parameter for g=0.1 mm, 0.2 mm and 0.3 mm.
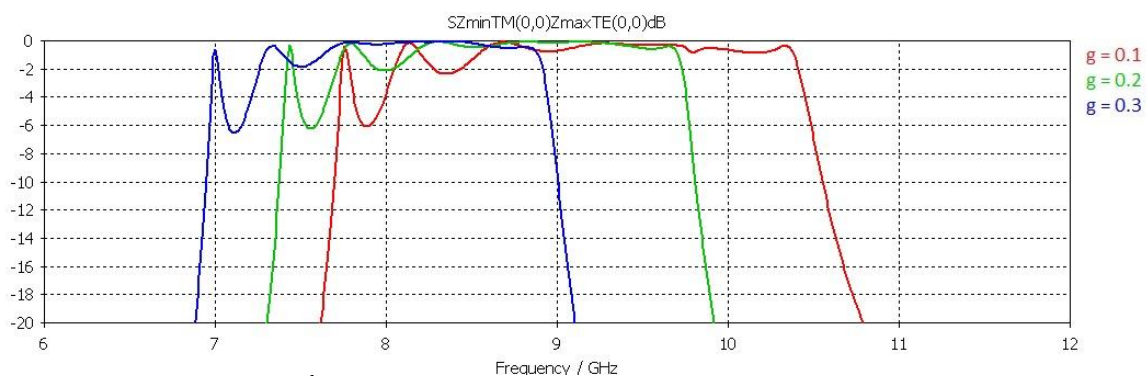
Figure 4.28. 3rd design: S_{21} parameter for g=0.1 mm, 0.2 mm and 0.3 mm; coupling between TE input and TM output wave is considered.

By increasing angle ß the length of coupling arc between middle dipole element and metal surface is increased. Accordingly, one can expect increase of the capacitance and shift of the working frequency to the lower frequencies.
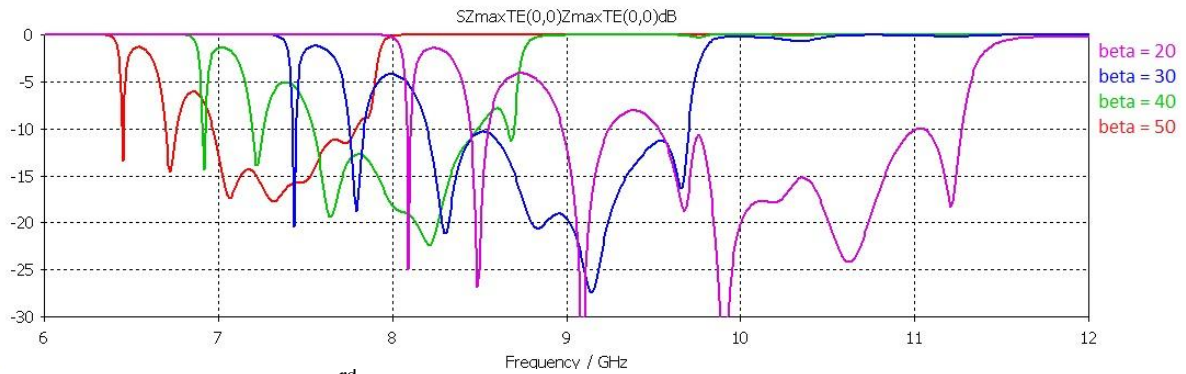
Figure 4.29. 3rd design: S$_{11}$ parameter for ß = 20°, 30°, 40° and 50°
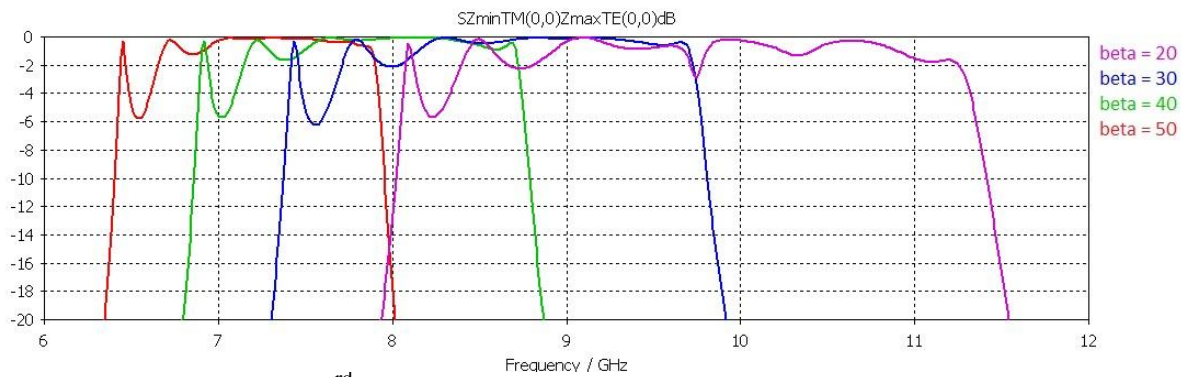
Figure 4.30. 3rd design: S$_{21}$ parameter for ß = 20°, 30°, 40° and 50°; coupling between TE input and TM output wave is considered.

4th design

The basic idea of the 4th design is to combine two orthogonal loads from the 3rd design. By this maybe it will be possible to increase capacitance and get lower resonant frequency, and maybe it will be possible to obtain polarizing effect.
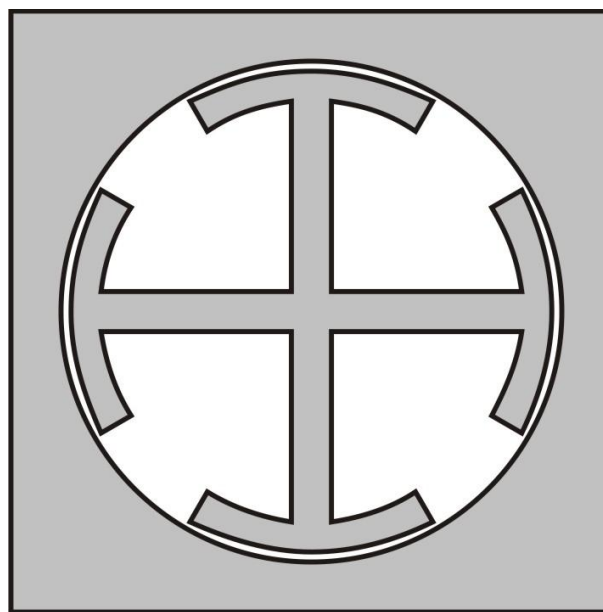
Figure 4.31. Double cross geometry
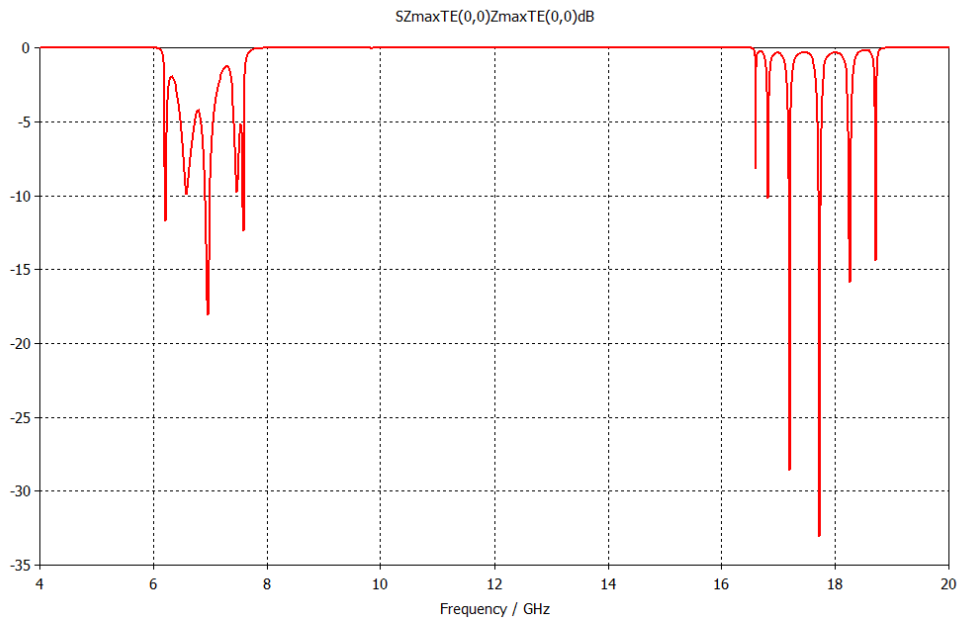
Figure 4.32. 4th design: S_{11} parameter

All parameters in simulation are the same as the basic parameters in third realization. As we can see in Figure 4.32 this structure is useless. Almost all energy of incident wave is reflected, i.e. it is not possible to use this structure as a polarization rotator or a polarizer.

CONCLUSIONS

Conclusions

Metamaterial-based cloaks have recently been proposed to prevent scattering of electromagnetic waves, i.e. to render objects invisible. The design of cloaks is usually done using transformation electromagnetics, i.e. the designed structure is described is terms of space-varying permeability and permittivity tensors. However, at least some of the elements of the constitutive tensors should have close-to-zero values (either relative permeability or permittivity). Since such materials do not exist in nature one should realize them using metamaterial approach – by developing an appropriate periodic structure with period smaller than wavelength. There is still a big gap between the wishes – desired permeability and permittivity distribution – and reality – the real electromagnetic parameters of different metamaterial structures. The purpose of this project is to make a step in filling this gap.

Metamaterial structures are extremely complicated to design. They consist of a large number of unit cells with geometry that is varying along the considered structure. Due to complexity it is not possible to design them without good strategy (i.e. we cannot simply use optimization possibilities of some commercial electromagnetic solver). Therefore, we proposed a procedure for designing metamaterial-based devices. The procedure starts with the ideal design obtained using some physical method like transformation electromagnetics. The ideal design contains layers of homogeneous anisotropic materials that cannot be found in nature. Therefore, we need to search for metamaterial realization of such complex multilayer structure. In order to do that in an efficient way, we propose an intermediate step in which an equivalent planar anisotropic multilayer structure is defined and which is realized using metamaterial approach. The main reason for introducing an intermediate step is that planar periodic structures can be rapidly analyzed (and designed) using most of the commercial electromagnetic solvers since we need to design only a unit cell. After designing an equivalent planar structure, we need to go back and map (i.e. to curve) the structure to the desired shape. In order to do that we considered an efficient approach based on conformal mapping.

We have also investigated methods dealing with the problem of how to electromagnetically characterize metamaterial structures. The first idea is to determine effective constitutive parameters either form the analysis process or from measurement results. However, these methods have serious drawbacks if the considered structure is resonant, like split-ring resonators. In that case it is not possible to determine effective constitutive parameters around the resonant frequency (unfortunately, at the same time this is the frequency range of interest). Therefore, we propose to use reflection and transmission coefficients for characterization of the considered structure, which (in connection with the optimization routine) represent a powerful tool for designing metamaterial structures.

We have also investigated the method that can simply transform the auxiliary planar structure into a desired shape. It is shown that conformal mapping can be used for this purpose resulting in accurately determined scattering properties of the final structure. We have also investigated the extension of the Bloch theory for multilayer planar periodic structure. The extension to cylindrical structures represents an accurate method for determining properties of circular-cylindrical multilayer periodic structures.

Finally, as a support to this investigation we have developed several algorithms and programs. First, we have extended the previously developed G1DMULT algorithm to include calculation of Green's functions of anisotropic multilayer structures (the G1DMULT algorithm calculates Green's functions of planar, cylindrical and spherical multilayer structures). Furthermore, we have developed programs for analyzing planar and cylindrical periodic structures. The programs are based on the Moment Method approach, and their main purpose is fast and accurate analysis of specific periodic structures.

As a short summary, the purpose of this report is to help researchers in understanding where the critical points when designing metamaterial structures are, and to propose an efficient and successful designing procedure of metamaterial-based devices. We sincerely hope that we have managed to give contribution in that direction.

APPENDIX

APPENDIX

A.1 DESCRIPTION OF G1DMULT ALGORITHM

The algorithm G1DMULT calculates spectral-domain Green's functions of planar, circular cylindrical and spherical multilayer structures (see [37] for details). The algorithm will be explained for the planar case. The 3D elements are replaced by equivalent or physical current excitations of electric and magnetic type, which then are Fourier transformed. In the planar case we use the two-dimensional Fourier transformation in the x and y directions, defined by

$$\widetilde{f}(k_x,k_y,z) = \int_{-\infty}^{\infty}\int_{-\infty}^{\infty} f(x,y,z)e^{jxk_x}e^{jyk_y}\,dxdy \tag{A.1}$$

By this Fourier transformation, the 3D excitations are transformed into harmonic current sheets. If the source is infinitely thin in z direction, we get one discrete current sheet per source, otherwise we get a continuous distribution of current sheets in z-direction. Each current sheet excites two plane waves, one propagating upwards and one propagating downwards. The presence of the multilayer structure will cause a number of transmitted and reflected waves in each layer, with variation $e^{-jk_x x}$ and $e^{-jk_y y}$ in the x- and y-directions. Notice that all the waves have the same field variation in the x- and y-directions for all layers, which is a consequence of the boundary conditions. Therefore, only the field variation in the direction perpendicular to the boundaries is unknown, so we have a harmonic one-dimensional (1D) field problem. In this way the spectral domain problem is interpreted as a 1D spatial domain problem consisting of the 1D multilayer structure and harmonic 1D sources in the form of current sheets.

The algorithm G1DMULT is based on subdividing the spatial harmonic problem into one equivalent problem per layer, where the field in each region is formulated as the field radiated by equivalent currents at the layer boundaries. For example, the E-field in the layer j is expressed as

$$\widetilde{\mathbf{E}}_j = \widetilde{\mathbf{G}}_{EJ}^{\text{hom}}\widetilde{\mathbf{J}}_{j-1} + \widetilde{\mathbf{G}}_{EJ}^{\text{hom}}\widetilde{\mathbf{J}}_{j} + \widetilde{\mathbf{G}}_{EM}^{\text{hom}}\widetilde{\mathbf{M}}_{j-1} + \widetilde{\mathbf{G}}_{EM}^{\text{hom}}\widetilde{\mathbf{M}}_{j} + \widetilde{\mathbf{G}}_{EJ}^{\text{hom}}\widetilde{\mathbf{J}}_{j}^{exci} + \widetilde{\mathbf{G}}_{EM}^{\text{hom}}\widetilde{\mathbf{M}}_{j}^{exci} \tag{A.2}$$

where $\widetilde{\mathbf{J}}_j$ and $\widetilde{\mathbf{M}}_j$ are equivalent electric and magnetic current sheets at boundary j, $\widetilde{\mathbf{J}}_j^{exci}$ and $\widetilde{\mathbf{M}}_j^{exci}$ are excitation electric and magnetic currents in layer j (if any), and $\widetilde{\mathbf{G}}^{\text{hom}}$ is the Green's function of the homogeneous problem. By using $\widetilde{\mathbf{J}}_j = \pm \hat{z} \times \widetilde{\mathbf{H}}_j$ and $\widetilde{\mathbf{M}}_j = \mp \hat{z} \times \widetilde{\mathbf{E}}_j$ eq. (A.2) can be expressed in terms of the unknown tangential E- and H-fields $\widetilde{\mathbf{E}}_j$ and $\widetilde{\mathbf{H}}_j$ at the boundary j between layers j and $j+1$ and known excitation currents.

The boundary conditions that the tangential E- and H- fields are continuous at the layer boundaries give 4 linear equations per boundary. The tangential E- and H-fields are evaluated by solving the system of $4(N_{layer}-1)$ equations with $4(N_{layer}-1)$ unknowns, where N_{layer} is the number of layers in the multilayer structure. After they have been determined, the total E- and H-fields at any desired z-location can be found by using the equivalent problem formulation.

The core problem in the formulation is to calculate the E- and H- fields due to a harmonic current sheet in a homogeneous region. The two subroutines G1DJ and G1DM which calculate these fields (G1DJ for electric source and G1DM for magnetic source) are the only part of the routine which depend on whether we consider a planar, circular cylindrical or spherical geometry, and they represent the only difference between the three versions of the G1DMULTroutine. In the planar case, the electromagnetic field excited by a current sheet is equal:

$$
\tilde{\mathbf{E}} = \begin{cases} -\dfrac{k}{2k_z}\left[\eta\tilde{\mathbf{J}}-\left(\eta\tilde{\mathbf{J}}\cdot\hat{k}^{+}\right)\hat{k}^{+}\right]e^{-jk\hat{k}^{+}\cdot\mathbf{r}} & z>0 \\[4mm] -\dfrac{k}{2k_z}\left[\eta\tilde{\mathbf{J}}-\left(\eta\tilde{\mathbf{J}}\cdot\hat{k}^{-}\right)\hat{k}^{-}\right]e^{+jk\hat{k}^{-}\cdot\mathbf{r}} & z<0 \end{cases}
\tag{A.2}
$$

$$
\eta\tilde{\mathbf{H}} = \begin{cases} \dfrac{k}{2k_z}\left[\eta\tilde{\mathbf{J}}\times\hat{k}^{+}\right]e^{-jk\hat{k}^{+}\cdot\mathbf{r}} & z>0 \\[4mm] \dfrac{k}{2k_z}\left[\eta\tilde{\mathbf{J}}\times\hat{k}^{-}\right]e^{+jk\hat{k}^{-}\cdot\mathbf{r}} & z<0 \end{cases}
\tag{A.3}
$$

where $\hat{k}^{+}=(k_x\hat{x}+k_y\hat{y}+k_z\hat{z})/k$ and $\hat{k}^{-}=(k_x\hat{x}+k_y\hat{y}-k_z\hat{z})/k$. In the cylindrical case, the electromagnetic field excited by a current tube is equal :

(a) from z-directed current tube

$$
\tilde{E}_z(\rho,n,k_z) = -\frac{\pi\eta}{2}\frac{k_\rho^2}{k}\rho_s \ \ \tilde{J}_z(n,k_z) \ \cdot \begin{cases} H_n^{(2)}(k_\rho\rho_s) \ \ J_n(k_\rho\rho) & \rho\le\rho_s \\ J_n(k_\rho\rho_s) \ \ H_n^{(2)}(k_\rho\rho) & \rho\ge\rho_s \end{cases}
\tag{A.4}
$$

$$
\tilde{H}_z(\rho,n,k_z) = 0
\tag{A.5}
$$

(b) from ϕ-directed current tube

$$
\tilde{E}_z(\rho,n,k_z) = \frac{\pi\eta}{2}\frac{nk_z}{k} \ \ \tilde{J}_\phi(n,k_z) \ \cdot \begin{cases} H_n^{(2)}(k_\rho\rho_s) \ \ J_n(k_\rho\rho) & \rho\le\rho_s \\ J_n(k_\rho\rho_s) \ \ H_n^{(2)}(k_\rho\rho) & \rho\ge\rho_s \end{cases}
\tag{A.6}
$$

$$
\tilde{H}_z(\rho,n,k_z) = -\frac{j\pi}{2}k_\rho\rho_s \ \ \tilde{J}_\phi(n,k_z) \ \cdot \begin{cases} H_n^{(2)'}(k_\rho\rho_s) \ \ J_n(k_\rho\rho) & \rho\le\rho_s \\ J_n^{'}(k_\rho\rho_s) \ \ H_n^{(2)}(k_\rho\rho) & \rho\ge\rho_s \end{cases}
\tag{A.7}
$$

The other field components are calculated using the following expressions:

$$\tilde{E}_\rho = -j\frac{k_z}{k_\rho^2}\frac{\partial \tilde{E}_z}{\partial \rho} - \eta\frac{nk}{k_\rho^2\rho}\tilde{H}_z \tag{A.8.a}$$

$$\tilde{E}_\phi = -\frac{nk_z}{k_\rho^2\rho}\tilde{E}_z + j\eta\frac{k}{k_\rho^2}\frac{\partial \tilde{H}_z}{\partial \rho} \tag{A.8.b}$$

$$\tilde{H}_\rho = \frac{1}{\eta}\frac{nk}{k_\rho^2\rho}\tilde{E}_z - j\frac{k_z}{k_\rho^2}\frac{\partial \tilde{H}_z}{\partial \rho} \tag{A.8.c}$$

$$\tilde{H}_\phi = -j\frac{1}{\eta}\frac{k}{k_\rho^2}\frac{\partial \tilde{E}_z}{\partial \rho} - \frac{nk_z}{k_\rho^2\rho}\tilde{H}_z \tag{A.8.d}$$

More details about the G1DMULT algorithm can be found in [37].

A.2 GREEN'S FUNCTIONS OF ANISOTROPIC PLANAR STRUCTURE

Let $E, H : \mathbb{R}^3 \to \mathbb{C}^3$ represents electric and magnetic field respectively. Components of mentioned fields will be annotated $E_x = \hat{x} \cdot E$ where hat over x means unit vector in x direction. In the case of partial derivation over some variable, notation will be slightly changed. Component mark in that case will be in superscript, and derivative mark will be in subscript $E_y^x = \partial_y \; E_x \;\; = \partial_y \; \hat{x} \cdot E \;\;$. Fourier transform will be annotated with hat over function. In this appendix next definition of Fourier transform will be used:

$$
\hat{E} \; k_x, k_y, z \;\; = \int_{\mathbb{R}^2} E \; x, y, z \;\; e^{-jk_x x} e^{-jk_y y} dx dy
$$

$$
E \; x, y, z \;\; = \frac{1}{2\pi^2} \int_{\mathbb{R}^2} \hat{E} \; k_x, k_y, z \;\; e^{jk_x x} e^{jk_y y} dk_x dk_y
$$

(A.9)

A2.1 Case 1: Source with direction orthogonal to the axis of anisotropy

In the first case current is orthogonal to the axis of anisotropy. Permeability and permittivity will be diagonal matrices with same entry at *xx* and *yy* places, and different at *zz*. Because the axis of anisotropy is in the *z* direction, all other field components can be described over *z* components of electromagnetic field. Therefore, the idea is to find differential equations for *z* component of electric and magnetic field. Permeability and permittivity looks like:

$$
\mu = \begin{pmatrix} \mu_x & 0 & 0 \\ 0 & \mu_x & 0 \\ 0 & 0 & \mu_z \end{pmatrix} \quad \varepsilon = \begin{pmatrix} \varepsilon_x & 0 & 0 \\ 0 & \varepsilon_x & 0 \\ 0 & 0 & \varepsilon_z \end{pmatrix}
$$

(A.10)

In considered situation excitation current will have only *x* and *y* components:
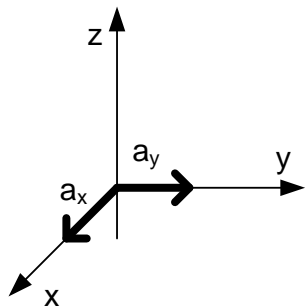
$$
J = \begin{pmatrix} a_x \delta(x, y, z) \\ a_y \delta(x, y, z) \\ 0 \end{pmatrix}
$$

From Maxwell equations:

$$
\nabla \times E = -i\omega\mu_0\mu H
$$

$$
\nabla \times H = i\omega\varepsilon_0\varepsilon E
$$

(A.11)

we get set of equations for electric field:

$$\nabla \times \ \mu^{-1}\nabla \times E \ - k_0^2 \varepsilon E = 0, \quad k_0^2 = \omega^2 \mu_0 \varepsilon_0 \tag{A.12}$$

Because axis of anisotropy is z axis, we only need equation for z component (third equation):

$$E_{zx}^x - E_{xx}^z - E_{yy}^z + E_{zy}^y - k_0^2 \mu_x \varepsilon_z E_z = 0 \tag{A.13}$$

Using the Gauss law for electrical field $div \ \varepsilon_0 \varepsilon E \ = 0$ we get equation which connects all three components of electric field:

$$\varepsilon_x E_x^x + \varepsilon_y E_y^y + \varepsilon_z E_z^z = 0 \tag{A.14}$$

From that equation we can express:

$$E_x^x + E_y^y = -\frac{\varepsilon_z}{\varepsilon_x} E_z^z \tag{A.15}$$

From equations (1) and (2) we can express equation for z component of electric field:

$$E_{xx}^z + E_{yy}^z + \frac{\varepsilon_z}{\varepsilon_x} E_{zz}^z + k_0^2 \mu_x \varepsilon_z E_z = 0 \tag{A.16}$$

Using the duality theorem we can get equation for z component of magnetic field:

$$H_{xx}^z + H_{yy}^z + \frac{\mu_z}{\mu_x} H_{zz}^z + k_0^2 \varepsilon_x \mu_z H_z = 0 \tag{A.17}$$

This equation is partial differential equation in all three space variables. That equation is not standard Helmholtz equation because it contains different constants multiplying second derivative of field component. The idea is to use Fourier transformation over x and y variables and transform equations (3) and (4) into ordinary differential equations over variable z:

$$-k_x^2 \hat{E}_z - k_y^2 \hat{E}_z + \frac{\varepsilon_z}{\varepsilon_x} \hat{E}_{zz}^z + k_0^2 \mu_x \varepsilon_z \hat{E}_z = 0 \tag{A.18}$$

This is equivalent to Helmholtz equation for the z component of electrical field:

$$\hat{E}_{zz}^z + k_E^2 \hat{E}_z = 0 \quad k_E^2 = k_0^2 \mu_x \varepsilon_x - \frac{\varepsilon_x}{\varepsilon_z} \beta^2 . \tag{A.19}$$

From the duality theorem we get:

$$\hat{H}_{zz}^z + k_H^2 \hat{H}_z = 0 \quad k_H^2 = k_0^2 \mu_x \varepsilon_x - \frac{\mu_x}{\mu_z} \beta^2 , \tag{A.20}$$

where $\beta^2 = k_x^2 + k_y^2$.

Two independent solutions of the Helmholtz differential equation are combinations of complex exponentials. From the Silver-Muller radiation condition we know that solutions have this form:

$$\hat{E}_z\left(k_x, k_y, z\right) = \begin{cases} Ae^{-jk_E z}, z > 0 \\ Be^{jk_E z}, z < 0 \end{cases} \qquad \hat{H}_z\left(k_x, k_y, z\right) = \begin{cases} Ce^{-jk_H z}, z > 0 \\ De^{jk_H z}, z < 0 \end{cases} \tag{A.21}$$

All other components of electric and magnetic field will be expressed over z components. From transformed Ampere and Faraday law we can express other field components in the form of Helmholtz equation with nonzero right side:

$$\begin{aligned}
k_0^2 \mu_x \varepsilon_x \hat{E}_x + \hat{E}_{zz}^x &= \omega \mu_0 \mu_x k_y \hat{H}_z + jk_x \hat{E}_z^z \\
k_0^2 \mu_x \varepsilon_x \hat{E}_y + \hat{E}_{zz}^y &= -\omega \mu_0 \mu_x k_x \hat{H}_z + jk_y \hat{E}_z^z \\
k_0^2 \mu_x \varepsilon_x \hat{H}_x + \hat{H}_{zz}^x &= jk_x \hat{H}_z^z - \omega \varepsilon_0 \varepsilon_x k_y \hat{E}_z \\
k_0^2 \mu_x \varepsilon_x \hat{H}_y + \hat{H}_{zz}^y &= jk_y \hat{H}_z^z + \omega \varepsilon_0 \varepsilon_x k_x \hat{E}_z
\end{aligned} \tag{A.22}$$

From the general form of solution for z components of electric and magnetic field, and from above equations we can find expressions for all other components:

$$\begin{aligned}
\hat{E}_x &= \frac{\omega \mu_0 \mu_z k_y}{\beta^2} \hat{H}_z + \frac{jk_x \varepsilon_z}{\varepsilon_x \beta^2} \hat{E}_z^z \\[2mm]
\hat{E}_y &= -\frac{\omega \mu_0 \mu_z k_x}{\beta^2} \hat{H}_z + \frac{jk_y \varepsilon_z}{\varepsilon_x \beta^2} \hat{E}_z^z \\[2mm]
\hat{H}_x &= \frac{jk_x \mu_z}{\mu_x \beta^2} \hat{H}_z^z - \frac{\omega \varepsilon_0 \varepsilon_z k_y}{\beta^2} \hat{E}_z \\[2mm]
\hat{H}_y &= \frac{jk_y \mu_z}{\mu_x \beta^2} \hat{H}_z^z + \frac{\omega \varepsilon_0 \varepsilon_z k_x}{\beta^2} \hat{E}_z
\end{aligned} \tag{A.23}$$

Boundary conditions for our situations are:

$$\begin{aligned}
\hat{H}_x^+ - \hat{H}_x^- &= a_y \\
\hat{H}_y^+ - \hat{H}_y^- &= -a_x \\
\hat{E}_{x,y}^+ - \hat{E}_{x,y}^- &= 0
\end{aligned} \tag{A.24}$$

By fulfilling the boundary conditions we get coefficients for the z components of electric and magnetic field:

$$C = D = \frac{\mu_x}{2k_H \mu_z}\left(k_x a_y - k_y a_x\right) \tag{A.25}$$

$$B = -A = \frac{k_x a_x + k_y a_y}{2\omega \varepsilon_0 \varepsilon_z} \tag{A.26}$$

A2.2 Case 2: Source with direction parallel to the axis of anisotropy

In the second case the source current is parallel with the axis of anisotropy. Permeability and permittivity will be diagonal matrices with same entry at *xx* and *zz* place, and different at *yy*. Since the axis of anisotropy is in the *y* direction, all other field components can be described over *y* field components. Permeability and permittivity tensors look like:

$$\mu = \begin{pmatrix} \mu_x & 0 & 0 \\ 0 & \mu_y & 0 \\ 0 & 0 & \mu_x \end{pmatrix} \qquad \varepsilon = \begin{pmatrix} \varepsilon_x & 0 & 0 \\ 0 & \varepsilon_y & 0 \\ 0 & 0 & \varepsilon_x \end{pmatrix} \tag{A.27}$$

In the described situation current will have only *y* component of the source:

$$J = \begin{pmatrix} 0 \\ a_y \delta(x,y,z) \\ 0 \end{pmatrix} \tag{A.28}$$

Since the source current is in the *y* direction, magnetic field in *y* direction is equal to zero. Because of that all other components of electric and magnetic field could be expressed over *y* component of electric field. From set of equations (A.22) we use only the second equation (equation for *y* component):

$$E^z_{yz} - E^x_{yx} - E^y_{xx} - E^y_{zz} - k_0^2 \mu_x \varepsilon_y E_y = 0 \tag{A.29}$$

Gauss Law gives us equation which connects all electric field components, and with that equation we find final equation for y component of electric field:

$$E^y_{xx} + \frac{\varepsilon_y}{\varepsilon_x} E^y_{yy} + E^y_{zz} + k_0^2 \mu_x \varepsilon_y E_y = 0 \tag{A.30}$$

In spectral domain we get Helmholtz equation:

$$\hat{E}^y_{yy} + k_y^2 \hat{E}_y = 0 \quad k_y^2 = k_0^2 \mu_x \varepsilon_x - \frac{\varepsilon_x}{\varepsilon_y} \beta^2 \tag{A.31}$$

where: $\beta^2 = k_x^2 + k_y^2$.

Solution of that equation have a form:

$$\hat{E}_y \left(k_x, y, k_z \right) = \begin{cases} A e^{-jk_y y}, y > 0 \\ B e^{jk_y y}, y < 0 \end{cases} \qquad \hat{H}_y \left(k_x, y, k_z \right) = 0 \tag{A.32}$$

All other components of electric and magnetic field will be expressed over y components. From transformed Ampere and Faraday law we can express other field components in the form of Helmholtz equation with nonzero right side:

$$
\begin{aligned}
k_0^2 \mu_x \varepsilon_x \hat{E}_x + \hat{E}_{yy}^x &= jk_x \hat{E}_y^y \\
k_0^2 \mu_x \varepsilon_x \hat{E}_z + \hat{E}_{yy}^z &= jk_z \hat{E}_y^y \\
k_0^2 \mu_x \varepsilon_x \hat{H}_x + \hat{H}_{yy}^x &= \omega \varepsilon_0 \varepsilon_x k_z \hat{E}_y \\
k_0^2 \mu_x \varepsilon_x \hat{H}_z + \hat{H}_{yy}^z &= -\omega \varepsilon_0 \varepsilon_x k_x \hat{E}_y
\end{aligned}
\tag{A.33}
$$

From the general form of solution for y components of electric and magnetic field, and from above connection equations we can find expressions for all other components:

$$
\begin{aligned}
\hat{E}_x &= \frac{jk_x \varepsilon_y}{\varepsilon_x \beta^2} \hat{E}_y^y \\[2mm]
\hat{E}_z &= \frac{jk_z \varepsilon_y}{\varepsilon_x \beta^2} \hat{E}_y^y \\[2mm]
\hat{H}_x &= \frac{\omega \varepsilon_0 \varepsilon_y k_z}{\beta^2} \hat{E}_y \\[2mm]
\hat{H}_z &= -\frac{\omega \varepsilon_0 \varepsilon_y k_x}{\beta^2} \hat{E}_y
\end{aligned}
\tag{A.34}
$$

In the considered situation there are only two undetermined coefficients. They can be determined using definition of equivalent magnetic current:

$$
M_{eq} = \varepsilon^{-1} \frac{j}{\omega \varepsilon_0} \nabla \times J
\tag{A.35}
$$

In our case electric current source has only y component, which is transformed with Fourier transform into:

$$
\hat{M}_{eq} = \varepsilon^{-1} \frac{j}{\omega \varepsilon_0}
\begin{pmatrix}
-ik_z a_y \\
0 \\
ik_x a_y
\end{pmatrix}
\tag{A.36}
$$

We will use only two boundary conditions:

$$
\begin{aligned}
\hat{H}_x^+ - \hat{H}_x^- &= 0 \\
\hat{E}_z^+ - \hat{E}_z^- &= -\hat{M}_x
\end{aligned}
\tag{A.37}
$$

From those two boundary conditions and from definition of equivalent magnetic current we find undetermined coefficients:

$$
A = B = -\frac{\beta^2}{\omega \varepsilon_0 \varepsilon_y k_y} a_y \; .
\tag{A.38}
$$

A3. GREEN'S FUNCTIONS OF ANISOTROPIC CYLINDRICAL STRUCTURES

In the considered case permeability and permittivity tensors will be diagonal matrices with the same entry at $\rho\rho$ and $\phi\phi$ place, and with different entry at zz. Because the axis of anisotropy is in the z direction, all other field components can be described over z components of electromagnetic field. Permeability and permittivity tensors looks like:

$$\mu = \begin{pmatrix} \mu_\rho & 0 & 0 \\ 0 & \mu_\rho & 0 \\ 0 & 0 & \mu_z \end{pmatrix} \quad \varepsilon = \begin{pmatrix} \varepsilon_\rho & 0 & 0 \\ 0 & \varepsilon_\rho & 0 \\ 0 & 0 & \varepsilon_z \end{pmatrix} \tag{A.39}$$

In the considered situation the source current will have only z component:

$$J = \hat{z} I_z \frac{\delta(\rho - d)}{2\pi\rho} \tag{A.40}$$

Starting equations are:

$$\nabla \times \ \mu^{-1}\nabla \times E \ - k_0^2 \varepsilon E = 0, \quad k_0^2 = \omega^2 \mu_0 \varepsilon_0$$
$$div(\varepsilon E) = 0 \tag{A.41}$$

From the definition of nabla operator in the cylindrical coordinate system we get equation for z component of electric field:

$$-\Delta_{\rho\phi} E_z - \frac{\varepsilon_z}{\varepsilon_\rho} \frac{\partial^2 E_z}{\partial z^2} - k_0^2 \mu_\rho \varepsilon_z E_z = 0 \tag{A.42}$$

Δ represents Laplace operator over ρ and ϕ variables. For the reason of easier computation some abbreviations will be used. Laplace operator will be decomposed into two operators.

$$-\Delta_{\rho\phi} = A_\rho + \frac{1}{\rho^2} A_\phi \tag{A.43}$$

The idea is to use the Fourier transformation over two variables to transform the considered partial differential equation into an ordinary differential equation. The differential operator A_ϕ will be transformed into multiplication with a constant. Our cylinder is infinitely long in the z direction and 2π periodic in ϕ variable. Because of that the ordinary Fourier transform in z direction will be used:

$$\hat{u} \ k_x \ = \int_{\mathbb{R}} u \ x \ e^{-jk_x x} dx$$
$$u \ x \ = \frac{1}{2\pi} \int_{\mathbb{R}} \hat{u} \ k_x \ e^{jk_x x} dk_x \tag{A.44}$$

In ϕ variable the ordinary Fourier series will be applied:

$$a_n = \frac{1}{\sqrt{2\pi}} \int\limits_0^{2\pi} f(x)e^{-jnx}dx$$

$$f(x) = \frac{1}{\sqrt{2\pi}} \sum_{n=-\infty}^{\infty} a_n e^{jnx}$$

(A.45)

Using this two transformations we get an ordinary differential equation in ρ variable:

$$\frac{1}{\rho}\frac{\partial}{\partial\rho}\left(\rho\frac{\partial\hat{E}_z^n}{\partial\rho}\right) + \left(\lambda^2 - \frac{n^2}{\rho^2}\right)\hat{E}_z^n = 0 \text{ with } \lambda^2 = k_0^2\mu_\rho\varepsilon_z - \frac{\varepsilon_z}{\varepsilon_\rho}k_z^2 \qquad \text{(A.46)}$$

This is the Bessel equation of order n. Solution of this equation is coefficient $\hat{E}_z^n$ in Fourier expansion of E_z field component. Physical conditions that we have to satisfy are:

$$\lim_{\rho\to\infty}\hat{E}_z^n(\rho,k_z) < \infty \qquad\qquad \lim_{\rho\to 0}\hat{E}_z^n(\rho,k_z) = 0 \qquad \text{(A.47)}$$

Because of condition (A-47) solution will be represents with Bessel function inside cylinder and with outgoing Hankel function outside cylinder with radius d.

$$\hat{E}_z^n\left(\rho,k_z\right) = \begin{cases} A_n J_n(\lambda\rho) & ,\rho < d \\ B_n H_n^{(2)}(\lambda\rho), & \rho > d \end{cases} \qquad \hat{H}_z^n\left(\rho,k_z\right) = \begin{cases} C_n J_n(\lambda\rho) & ,\rho < d \\ D_n H_n^{(2)}(\lambda\rho), & \rho > d \end{cases} \qquad \text{(A.48)}$$

From Maxwell equations, from two-dimensional Fourier transformation, and by using notation $\Omega = k_0^2\mu_\rho\varepsilon_\rho - k_z^2$ we get:

$$\hat{E}_\rho^n = \frac{\omega\mu_0\mu_\rho n}{\Omega}\frac{1}{\rho}\hat{H}_z^n + \frac{jk_z}{\Omega}\frac{\partial\hat{E}_z^n}{\partial\rho}$$

$$\hat{E}_\phi^n = \frac{j\omega\mu_0\mu_\rho}{\Omega}\frac{\partial\hat{H}_z^n}{\partial\rho} - \frac{nk_z}{\Omega}\frac{1}{\rho}\hat{E}_z^n$$

$$\hat{H}_\rho^n = \frac{jk_z}{\Omega}\frac{\partial\hat{H}_z^n}{\partial\rho} - \frac{\omega\varepsilon_0\varepsilon_\rho n}{\Omega}\frac{1}{\rho}\hat{E}_z^n$$

$$\hat{H}_\phi^n = -\frac{nk_z}{\Omega}\frac{1}{\rho}\hat{H}_z^n - \frac{j\omega\varepsilon_0\varepsilon_\rho}{\Omega}\frac{\partial\hat{E}_z^n}{\partial\rho}$$

(A.49)

Boundary conditions in the considered situation are:

$$
\begin{aligned}
\hat{H}^n_\phi \Big|_{d^+} - \hat{H}^n_\phi \Big|_{d^-} &= \hat{J}^n_z \\
\hat{H}^n_z \Big|_{d^+} - \hat{H}^n_z \Big|_{d^-} &= 0 \\
\hat{E}^n_\phi \Big|_{d^+} - \hat{E}^n_\phi \Big|_{d^-} &= 0 \\
\hat{E}^n_z \Big|_{d^+} - \hat{E}^n_z \Big|_{d^-} &= 0
\end{aligned}
\tag{A.50}
$$

By using the boundary conditions in cylindrical coordinate system, Wronskian for Bessel functions, definition of other field components over z components and solution for the z component of electric and magnetic field we get expressions for coefficients in the considered expansion:

$$
\begin{aligned}
\hat{E}^n_z \; \rho, k_z &= -\frac{\Omega \pi d}{2\omega \varepsilon_0 \varepsilon_\rho} \hat{J}^n_z
\begin{cases}
H^{(2)}_n(\lambda d) J_n(\lambda \rho), \rho < d \\
J_n(\lambda d) H^{(2)}_n(\lambda \rho), \rho > d
\end{cases} \\
\hat{H}^n_z \; \rho, k_z &= i\frac{\Omega \pi d^2 \lambda}{2nk_z}
\begin{cases}
H^{(2)}_n(\lambda d)' J_n(\lambda \rho), \rho < d \\
J_n(\lambda d)' H^{(2)}_n(\lambda \rho), \rho > d
\end{cases}
\end{aligned}
\tag{A.51}
$$

By using the definition of inverse Fourier transform over ρ and ϕ variables we get the final solution:

$$
E_z(x,y,z) = \frac{1}{2\pi} \int_{-\infty}^{\infty} \left(\frac{1}{\sqrt{2\pi}} \sum_{n=-\infty}^{\infty} \hat{E}^n_z \; \rho, k_z \; e^{jn\phi} \right) e^{jk_z z} dk_z
\tag{A.52}
$$

A.4 DESCRIPTION OF MOMENT METHOD PROGRAM FOR ANALYZING PLANAR AND CIRCULAR-CYLINDRICAL PERIODIC STRUCTURES

Periodic strips can be accurately analyzed by expanding the unknown currents on metal patterns in basis functions, and by using MoM to numerically determine the amplitudes of the basis functions. We formulate an integral equation by stating that the tangential electric field is zero at the metal surface, i.e. $\hat{n} \times \left[\mathbf{E}^{inc} + \mathbf{E}^{scat} \right] = 0$. Since the structure is periodic the electromagnetic field excited by the currents is in the form of the Floquet modes, and the currents on different metal patterns are identical except for a linear phase difference equal to the considered harmonic variation of the incident field.

The problem is solved in the spectral domain. In the planar case, we use a two-dimensional Fourier transformation in the directions in which the structure is periodic (i.e. x- and y-directions) and in the cylindrical case we use a Fourier transformation in a axial z direction and a Fourier series in a circumferential ϕ direction. The scattered field $\mathbf{E}^{scat}$ can be expressed in terms of the spectral domain dyadic Green's function $\tilde{\mathbf{G}}$ and the Fourier transform of the current on one metal pattern, according to

$$\mathbf{E}^{scat}(u_n, u_o, u_l) = \frac{1}{P_o P_p} \sum_{m=-\infty}^{\infty} \sum_{l=-\infty}^{\infty} \tilde{\mathbf{G}}(u_n, k_o^m, k_p^l \,|\, u'_n) \cdot \tilde{\mathbf{J}}(k_o^m, k_p^l) e^{-jk_o^m u_o} e^{-jk_p^l u_p} \tag{A.53}$$

$$k_o^m = \frac{2m\pi}{P_o} + k_o^{inc}, \qquad k_p^l = \frac{2l\pi}{P_p} + k_p^{inc} \tag{A.54}$$

where k_o^{inc} and k_p^{inc} are the propagation constants of the incident wave in two orthogonal directions across the metal pattern (i.e. o and p directions), P_o and P_p are the periodicity of the unit cell in o and p directions, and ' denotes the source coordinates. The spectral domain Green's function $\tilde{\mathbf{G}}$ is calculated by the G1DMULT routine. The integral equation is transformed into a matrix equation by using the MoM where the test functions are the same as the basis functions (Galerkin's method), and the inner product is taken across the central unit cell. The expression for the elements of the MoM matrix is derived from eq. (A.53), and the expression for the elements of the voltage vector is obtained by integrating the product of the test function and the incident field component parallel to the test function. The elements of the impedance matrix and the excitation vector are

$$Z_{ij} = \frac{1}{P_o P_p} \sum_{m=-\infty}^{\infty} \sum_{l=-\infty}^{\infty} \tilde{\mathbf{J}}(-k_o^m, -k_p^l) \, \tilde{\mathbf{G}}(u_n, k_o^m, k_p^l \,|\, u'_n) \cdot \tilde{\mathbf{J}}(k_o^m, k_p^l) \tag{A.55}$$

$$V_i = \tilde{\mathbf{J}}(-k_o^{inc}, -k_p^{inc}) \cdot \mathbf{E}(u'_n, u'_o = 0, u'_p = 0) \tag{A.56}$$

where conveniently we choose that the u'_o and u'_p coordinates of the center of the metal pattern are zero. In the planar case, the quantities in eqs. (A.53)-(A.56) are:

$$u_n = z, \quad u_o = x, \quad u_p = y \tag{A.57}$$

In the cylindrical case, the incident plane wave is expanded as

$$E_z^{inc} = E_0 \sin\theta^{inc} \cos\alpha^{inc} \cdot \sum_{n=-\infty}^{\infty} j^n J_n(k_0\rho\sin\theta^{inc})e^{-jn(\phi-\phi^{inc})}e^{jzk_0\cos\theta^{inc}} \qquad (A.58)$$

where J_n is the nth-order Bessel function of the first kind, the polarization angle α^{inc} is the angle the incident electric field makes with the plane of incidence, and θ^{inc} and ϕ^{inc} are angles of incidence measured, respectively, from the z-axis and x-axis in the xy plane. The scatterer has the following symmetry: by rotating the scatterer by $2\pi/N_\phi$ where N_ϕ is the number of unit cells in ϕ direction, we get the same structure. Thus we expand the fields in Floquet modes in ϕ direction where for every component of the incident field in eq. (A.58) the strips excite fields which have the same phase variation between the centers of the strips as the incident cylindrical wave. In this case the scattered field due to the incident wave with $\exp(-jn\phi)$ variation is also given by eq. (A.53) with

$$u_n = \rho, \quad u_o = \phi, \quad u_p = z \qquad (A.59)$$

and

$$k_o^{inc} = n, \quad k_p^{inc} = -k_z^{inc} = -k_0\cos\theta^{inc}. \qquad (A.60)$$

BIBLIOGRAPHY

Bibliography

[1] L.S. Dollin, "On the possibility of comparison of three-dimensional electromagnetic systems with nonuniform anisotropic filling," *Izv. VUZov Radiofizika*, **Vol. 4**, No. 5, pp. 964-967, 1961.

[2] P.-S. Kildal, A. A. Kishk, A. Tengs, "Reduction of forward scattering from cylindrical objects using hard surfaces", *IEEE Trans. on Antennas and Propagation.,* **Vol. AP-44**, pp. 1509-1520, Nov. 1996.

[3] M. Kerker, "Invisible bodies," *J. Opt. Soc. Am.,* **Vol. 65,** pp. 376-379, Apr. 1975.

[4] A. Alu, N. Engheta, "Achieving transparency with plasmonic and metamaterial coatings," *Phys. Rev. E,* **Vol. 72***, 016623, 2005; Erratum, **Vol. 73**, 019906, 2006.

[5] A. Alu, N. Engheta, "Plasmonic materials in transparency and cloaking problem: mechanism, robustness, and physical insights," *Opt. Express*, **Vol. 15**, pp. 3318-3332, Feb. 2007.

[6] B. Edwards, A. Alu, M. G. Silveirinha and N. Engheta, "Experimental verification of plasmonic cloaking at microwave frequencies with metamaterials," Physical Review Letters, **Vol. 103**, 153901, 2009.

[7] W. K. Kahn and H. Kurss, "Minimum-scattering antennas," *IEEE Trans. on Antennas and Propagation,* **Vol. AP-13,** pp. 671–675, Sep. 1965.

[8] N.G. Alexopoulos and N.K. Uzunoglu, "Electromagnetic scattering from active objects: invisible scatterers," *Appl. Opt.* **Vol. 17, pp.** 235–239, Jan. 1978.

[9] J. B. Pendry, D. Schurig, D. R. Smith, "Controlling electromagnetic fields", *Science,* **Vol. 312,** pp. 1780-1782, June 2006.

[10] U. Leonhardt, "Optical conformal mapping and dielectric invisibility devices," *Science*, **vol. 312**, pp. 1777-1780, June 2006.

[11] D. Schurig, J. B. Pendry, and D. R. Smith, "Calculation of material properties and ray tracing in transformation media," *Opt. Express*, **Vol. 14**, pp. 9794-9804, Oct. 2006.

[12] G. W. Milton, M. Briane, and J. R. Willis, "On Cloaking for elasticity and physical equations with a transformation invariant form," *New Journal of Physics*, **Vol. 8**, 248, Oct. 2006.

[13] A. D. Yaghjian and S. Maci, "Alternative Derivation of Electromagnetic Cloaks and Concentrators," *New Journal of Physics*, **Vol. 10**, 115022, Nov. 2008; Corrigendum *New Journal of Physics*, **Vol. 11**, 039802, 2009.

[14] D.-H. Kwon, and D. H. Werner, "Transformation electromagnetics: An overview of theory and applications," *IEEE Trans. on Antennas and Propagation Magazine,* **Vol. 52,** pp. 24-46, Feb. 2010.

[15] N. B. Kundtz, D. R. Smith and J. B. Pendry, "Electromagnetic design with transformation optics," *Proceedings of the IEEE*, Vol. 99, pp. 1622-1633, Oct. 2011.

[16] D. Schurig, J. J. Mock, B. J. Justice, S. A. Cummer, J. B. Pendry, A. F. Starr, D. R. Smith, "Metamaterial electromagnetic cloak at microwave frequencies", *Science,* **Vol. 314**, pp. 977-980, Nov. 2006.

[17] W. Cai, U. K. Chettiar, A. V. Kildishev, V. M. Shalaev, "Optical cloaking with non-magnetic metamaterials", *Nature photonics,* **Vol. 1**, pp. 224-227, Apr. 2007.

[18] B. Kanté, A. de Lustrac, J.-M. Lourtioz, and S. N. Burokur, "Infrared cloaking based on the electric response of split ring resonators," *Opt. Express*, **Vol. 16**, pp. 9191-9198, (2008).

[19] B. Kanté, D. Germain, and A. de Lustrac, „Experimental demonstration of a nonmagnetic metamaterial cloak at microwave frequencies," *Phys. Rev.* B, Vol. **80,** 201104, 2009.

[20] N. Kundtz, D. Gaultney, and D. R. Smith, "Scattering cross-section of a transformation optics-based metamaterial cloak," *New J. Phys*. **Vol. 12**, 043039, 2010.

[21] P. Alitalo, F. Bongard, J.-F. Zürcher, J. Mosig, and S. Tretyakov, "Experimental verification of broadband cloaking using a volumetric cloak composed of periodically stacked cylindrical transmission-line networks," *Appl. Phys. Lett.,* **Vol. 94**, 014103, Jan. 2009.

[22] S. Tretyakov, P. Alitalo, O. Luukkonen, and C. Simovski, "Broadband electromagnetic cloaking of long cylindrical objects," *Phys. Rev. Lett.,* **Vol. 103**, 103905, Sep. 2009.

[23] S. Hrabar, "Waveguide experiments to characterize the properties of SNG and DNG metamaterials", chapter 3 in N. Engheta and R. Ziolkowsky (Ed.), *Metamaterials: Physics and Engineering Explorations,* John Wiley and IEEE, 2006.

[24] E. S. Palencia, "Non-Homogeneous Media and Vibration Theory", Lecture Notes in Physics, Springer, 1980.

[25] C. R. Simovski, "Material Parameters of Metamaterials (a Review)", Optics and Spectroscopy, 2009, Vol. 107, No. 5, pp. 726–753.

[26] X. Chen, B. Wu, J. A. Kong, T. M. Grzegorczyk, "Robust method to retrieve the constitutive effective parameters of metamaterials", Physical Review E 70, 016608, 2004.

[27] D. R. Smith, D. C. Vier, Th. Koschny, C. M. Soukoulis, "Electromagnetic parameter retrieval from inhomogeneous metamaterials", Physical Review E 71, 036617, 2005.

[28] D. M. Pozar, "Microwave Engineering", Wiley, 2004.

[29] X. Chen, B. Wu, J. A. Kong, T. M. Grzegorczyk, "Retrieval of the effective constitutive parameters of bianisotropic metamaterials", Physical Review E 71, 046610, 2005.

[30] R. E. Collin, "Foundations for Microwave Engineering", McGraw-Hill Publishing Co, 1992.

[31] E. Martini, G. M. Sardi, S. Maci, "Extraction of equivalent constituent parameters in FSS-Based volumetric metamaterials", Interim Report #2, University of Siena, Department of Information Engineering, 2010.

[32] G. M. Sardi, "Homogenization techniques for metamaterials realized by multilayer planar periodic surfaces", Ph.D Thesis University of Siena, Department of Information Engineering, 2012.

[33] J. P. Turpin, A. T. Massoud, J. P. Pingjuan, L. Werner and D. H. Werner, "Conformal mapping to achieve simple material parameters for transformation optics devices," Optics Express, Vol. 18, pp. 244-252, 2009.

[34] A. Kitagawa, J. Sakai, "Bloch theorem in cylindrical coordinates and its application to a Bragg fiber", Physical Review A 80, 033802, 2009.

[35] R. Lech, M. Mazur, J. Mazur, "Analysis and Design of a Polarizer Rotator System", IEEE Transactions on Antennas and Propagation, Vol. 56, pp. 844 – 847, Mar. 2008.

[36] B. A. Munk, "Frequency Selective Surfaces" Wiley-Interscience, 2000.

[37] Z. Sipus, P. S. Kildal, R. Leijon, and M. Johansson, "An algorithm for calculating Green's functions for planar, circular cylindrical and spherical multilayer substrates," ACES Journal, Vol. 13, pp. 243-254, Nov. 1998.

[38] Z. Sipus, "Analysis of planar and circular cylindrical multilayer structures with application to soft and hard surfaces" Ph. D. Thesis Department of Microwave Technology, Chalmers, Goeteborg, Sweden, 1997.

[39] J. Rauch, "Partial Differential Equations", Graduate Texts in Mathematics, Springer, 1997.

[40] D.G.Dudley, "Mathematical Foundations for Electromagnetic Theory," Wiley-IEEE Press, 1997.